

UNIVERSITÉ DU QUÉBEC

THÈSE PRÉSENTÉE À
L'UNIVERSITÉ DU QUÉBEC À CHICOUTIMI
COMME EXIGENCE PARTIELLE
DU DOCTORAT EN INGÉNIÉRIE

Par
Changiz Tavakoli Zaniani

DYNAMIC MODELING OF AC ARC DEVELOPMENT ON
ICE SURFACES

MODÉLISATION DYNAMIQUE DU DÉVELOPPEMENT DE
L'ARC ÉLECTRIQUE À LA SURFACE DE LA GLACE
EN COURANT ALTERNATIF

NOVEMBRE 2004



Mise en garde/Advice

Afin de rendre accessible au plus grand nombre le résultat des travaux de recherche menés par ses étudiants gradués et dans l'esprit des règles qui régissent le dépôt et la diffusion des mémoires et thèses produits dans cette Institution, **l'Université du Québec à Chicoutimi (UQAC)** est fière de rendre accessible une version complète et gratuite de cette œuvre.

Motivated by a desire to make the results of its graduate students' research accessible to all, and in accordance with the rules governing the acceptance and diffusion of dissertations and theses in this Institution, the **Université du Québec à Chicoutimi (UQAC)** is proud to make a complete version of this work available at no cost to the reader.

L'auteur conserve néanmoins la propriété du droit d'auteur qui protège ce mémoire ou cette thèse. Ni le mémoire ou la thèse ni des extraits substantiels de ceux-ci ne peuvent être imprimés ou autrement reproduits sans son autorisation.

The author retains ownership of the copyright of this dissertation or thesis. Neither the dissertation or thesis, nor substantial extracts from it, may be printed or otherwise reproduced without the author's permission.

Abstract

Overhead lines generally pass over a variety of regions encompassing different kinds of physical terrain, climatic conditions and characteristic environments. High voltage outdoor equipment is thus subject to various forms and degrees of constraint. The most salient among these are recognized to be several types of pollution and the atmospheric icing of insulators.

Studying and understanding arc initiation and propagation is a fundamental aspect of designing weatherproof outdoor insulation suitable for use in cold climate regions. Such a research will tend to contribute to the appropriate design and manufacture of insulators able to withstand the wear and tear resulting from cold climate conditions.

Within the scope of this study, the development of a self-consistent dynamic model will be discussed for application to AC voltage in order to simulate arc behavior on ice-covered insulator surfaces. The model considers the arc as time-dependent impedance constituted of a resistance in series with an inductance. The arc resistance throughout the period of arc propagation is determined by using Mayr's equation. The unbridged ice layer is replaced with an equivalent resistance, where the surface conductivity is calculated by taking the effect of melting water into account. A comprehensive flowchart was established to model the propagation stage of arc. The flowchart incorporates a tentative explanation for the flashover phenomenon on iced insulators. The model responds to the variation of a number of major parameters, namely, insulator length, applied water conductivity, and insulator diameter. Several experiments were carried out on a simplified cylindrical model, as well as on a standard post insulator unit, so as to corroborate the simulation results. Various insulator lengths and applied water conductivities were investigated in the experiments. The model in question was verified against the experimental results, and the simulated results reflect the effects of all the major parameters in a consistent manner. The model was found to be reliable in predicting the major variables of the arc propagation phenomenon such as critical flashover voltage, arc current, and propagation velocity within a certain range of parameters.

RÉSUMÉ

Les lignes aériennes de transport d'énergie électrique, parcourent de longues distances et traversent en général des régions très différentes de par leur relief (topographie du terrain, altitude, *etc.*), leur climat (température, pression, vent, *etc.*), leur environnement (zones industrielles, régions côtières, *etc.*). De ce fait, les équipements de transport d'énergie électrique sont exposés à diverses formes et degrés de contraintes. Parmi celles-ci, la pollution et le givrage atmosphérique des isolateurs sont reconnues comme étant les facteurs majeurs à l'origine des défauts enregistrés sur les lignes aériennes.

Dans ce contexte, l'amélioration de la connaissance des processus physiques fondamentaux à l'origine de l'initiation de l'arc électrique est nécessaire si l'on veut augmenter la fiabilité du transport d'énergie électrique par voie aérienne dans les régions froides. Ces investigations contribueront à la conception et à la fabrication appropriée d'isolateurs adaptées aux régions froides.

Dans le cadre de cette étude, un modèle dynamique auto cohérent en courant alternatif sera présenté et discuté dans le but de simuler et de prédire le comportement de l'arc électrique à la surface d'isolateurs recouverts de glace. Ce modèle considère l'arc comme une impédance variable dans le temps, constituée d'une résistance en série avec une inductance. La résistance de l'arc durant la période de propagation, est déterminée en utilisant l'équation de Mayr. La couche résiduelle de glace non encore franchie par l'arc est remplacée par une résistance équivalente dont la conductivité surfacique est calculée en tenant compte de l'effet de l'eau de fonte. Un organigramme exhaustif a été établi pour modéliser les deux dernières étapes de la propagation de l'arc, à savoir l'établissement d'un arc partiel suivi de sa propagation. Cet organigramme incorpore une tentative d'explication du phénomène de contournement des isolateurs recouverts de glace. Le modèle répond à la variation d'un certain nombre de paramètres principaux, à savoir, la longueur de l'isolateur, la conductivité de l'eau de congélation appliquée, et le diamètre de isolateur. Plusieurs expériences ont été effectuées sur un modèle cylindrique simplifié, ainsi que sur une unité d'isolateur de poste standard, afin de corroborer les résultats de simulation. Plusieurs longueurs d'isolateur et conductivités d'eau de congélation ont été considérées au cours des expériences. Le modèle en question a été comparé aux résultats expérimentaux, et les résultats simulés reflètent d'une façon cohérente les effets de tous les paramètres principaux. Le modèle s'est avéré fiable en prévoyant les variables principales du phénomène de propagation d'arc telles que la tension critique de contournement, le courant d'arc, et la vitesse de propagation dans une certaine marge des paramètres.

Acknowledgment

مَنْ عَلَّمَنِي حَرْفًا صِرْتُ لَهُ عَبْدًا
بِسْمِ اللَّهِ

This work was carried out within the framework of the NSERC/Hydro-Quebec/UQAC Industrial Chair on Atmospheric Icing of Power Network Equipment (CIGELE) and the Canada Research Chair, tier 1, on Engineering of Power Network Atmospheric Icing (INGIVRE) at the University of Quebec in Chicoutimi.

I would like to take this opportunity to convey my grateful recognition to all of my professors during all stages of my academic education. Particularly, I would like to express my deepest gratitude to my director of studies, Prof. M. Farzaneh, for his supervision, presence, patience, and support during the entire project; and my co-director, Prof. A. Béréal, for precious discussions and guidance.

I am also grateful to Dr. J. Zhang for the valuable advice and worthwhile discussions and help, and Dr. A. Karev for his professional advice and encouragement. I would also like to thank Mme M. Sinclair for her precious efforts and editorial help, whose help was invaluable in making my text legible.

I should also remember of all my dear friends who their supports and encouragements gave me the strength to pass the hard time. Particularly, I would like to name MM. Hossein Hemmatjou, Ping Fu, Fredy Marino, H. R. Nikanpour, ...

Finally, I want to express my gratitude and respect to Dr. Issouf Fofana, for not only his scientific, but also human qualities. I am especially thankful to him for his sincere and unsparing support, which were essential in realizing this project.

This work is offered to all my professors, all my friends, all the members of my family, to my dears Mazyar, Maral, Kamyar, Noura and

*to the pain of my father,
to the love of my sisters,
to the hands of my mother...*

TABLE OF CONTENTS

CHAPTER 1	
INTRODUCTION	1
1.1 Overview.....	2
1.2 Objectives of the Thesis.....	7
1.3 Statement of Originality.....	8
1.4 Outline of Thesis Structure.....	9
CHAPTER 2	
REVIEW OF LITERARUE ON	
EFFECTS OF ICE ON HIGH VOLTAGE INSULATORS	10
2.1 Introduction.....	11
2.2 Types of Ice.....	13
2.3 Creating Ice Artificially in the Laboratory.....	14
2.4 Insulator Performance under Icing Conditions.....	16
2.4.1 Air Gaps and Partial Arcs.....	18
2.4.2 Effect of Various Parameters.....	20
2.4.2.1 <i>Dry Arcing Distance</i>	20
2.4.2.2 <i>Applied Water Conductivity</i>	20
2.4.2.3 <i>The Type of Voltage Applied</i>	21
2.4.2.4 <i>Ice Type and Wind</i>	22
2.4.2.5 <i>Ice Thickness</i>	23
2.4.2.6 <i>Air Pressure</i>	24
2.4.2.7 <i>Supplementary Parameters</i>	25
2.5 Recapitulation of Main Points.....	25

CHAPTER 3	
REVIEW OF LITERATURE ON	
SURFACE FLASHOVER MODELING	27
3.1 Basic Model.....	29
3.1.1 Arc Models.....	30
3.1.1.1 Ayrton's Equation.....	30
3.1.1.2 The Gopal and Rao Model.....	34
3.1.1.3 The Cassie-Francis and Mayr Equations.....	34
3.1.1.4 LTE and Saha's Equation.....	36
3.1.1.5. The Elenbaas-Heller Equation.....	38
3.1.1.6 Numerical Solution.....	41
3.1.2 Resistance of the Conductive Surface.....	43
3.1.2.1 Form Factor Concept.....	43
3.1.2.2 Circular Disc Model.....	44
3.1.2.3 The Wilkins Equations.....	44
3.1.2.4 Plane Model.....	46
3.1.2.5 Dry and Polluted Band Impedance.....	47
3.2 Static Modeling.....	48
3.2.1 DC Static Models.....	48
3.2.2 AC Static Models.....	54
3.3 Dynamic Modeling.....	55
3.3.1 Arc Elongation Mechanism.....	57
3.3.2 Arc Velocity Models.....	59
3.3.2.1 The Al-Baghdadi Model.....	59
3.3.2.2 The Tominaga Model.....	59
3.3.2.3 The Jolly et al. Model.....	60
3.3.2.4 Arc Mobility Model.....	60
3.3.2.5 The Gallimberti Model.....	61
3.3.2.6 Rahal's Model.....	61
3.3.2.7 The Alston et al. Model.....	62
3.3.2.8 The Fofana et al. Model.....	62
3.3.3 Propagation Criterion.....	63
3.3.3.1 The Hampton Model.....	63
3.3.3.2 The Hesketh Criterion.....	64
3.3.3.3 The Wilkins Criterion.....	64
3.3.3.4 The Anjana et al. Criterion.....	65
3.3.3.5 Ghosh et al. Model.....	65
3.3.4 Dynamic Models.....	65
3.3.4.1 The Jolly et al. Model.....	65
3.3.4.2 The Rizk Model.....	66
3.3.4.3 The Anjana et al. Model.....	67
3.3.4.4. The Sundararajan et al. Model.....	68
3.3.4.5 The Dhahbi and Bérroual Model.....	68
3.3.4.6 The Farzaneh et al. Model for Iced Insulators.....	69
3.4 Recapitulation of Main Points.....	77

CHAPTER 4	
AC ARC PROCESS AND MODELING	
ON THE SURFACE OF ICE ACCUMULATED	
ON INSULATORS	79
4.1 The Flashover Process.....	80
4.2 Basic Model.....	84
4.3 Simulation Method.....	87
4.3.1 Simulation of the Second Stage.....	87
4.3.2 Simulation of the Third Stage.....	89
4.4 Circuit Elements.....	94
4.4.1 Ice Resistance.....	95
4.4.2 Arc Inductance.....	99
4.4.3 Capacitance.....	99
4.4.4 Arc Resistance.....	100
4.5 Arc Velocity and Propagation Criterion.....	103
4.6 Recapitulation of Main Points.....	104
CHAPTER 5	
DESCRIPTION AND IMPLEMENTATION OF	
EXPERIMENTS	105
5.1 Test Facilities.....	107
5.1.1 High Voltage Equipment.....	107
5.1.2 Climate Room.....	108
5.1.3 Physical Objects.....	109
5.1.4 Data Acquisition System.....	110
5.1.5 High-Speed Camera.....	113
5.2 Test Procedure.....	115
5.3 Test Results.....	117
5.3.1 Flashover Results.....	120
5.3.2 Effects of Initial Air Gap Length.....	125
5.3.3 Current and Voltage Curves.....	126
5.3.4 Arc Length Observations.....	128
5.4 Recapitulation of Main Points.....	131

CHAPTER 6	
TEST DATA ANALYSIS AND NUMERICAL SIMULATIONS	132
6.1 Pre-flashover Stage Simulation.....	133
6.2 Heat Dissipation Rate Calculations.....	144
6.3 Calculation of Flashover Voltage	148
6.3.1 Comparison of the Model and Experiments.....	148
6.3.2 Present Model and Experiments Performed by Other Researchers..	151
6.3.2.1 <i>Cylinder and Post Insulator</i>	152
6.3.2.2 <i>IEEE Standard String Insulators</i>	154
6.4 Simulation of the Propagation Stage	158
6.4.1 Arc Current Comparison.....	158
6.4.2 Propagating Arc.....	162
6.4.2.1 <i>Arc Current</i>	163
6.4.2.2 <i>Arc Velocity</i>	165
6.4.2.3 <i>Arc Resistance per Unit</i>	167
6.4.2.4 <i>Arc Temperature</i>	169
6.4.2.5 <i>E-I Arc Characteristics</i>	172
6.5 Recapitulation of Main Points.....	174
CHAPTER 7	
CONCLUSIONS AND RECOMMENDATIONS	175
7.1 Concluding Remarks.....	176
7.2 Future Trends.....	180
REFERENCES.....	183

LIST OF FIGURES

Figure	Title	Page
2.1	Dry ice formed on a short suspension insulator string [138].	15
2.2	Wet-grown ices on a chain insulator [138].	16
2.3	Air gaps formed during accumulation of ice [31].	19
3.1	The Obenaus model.	30
3.2	Effect of the variation in n .	33
3.3	Effect of the variation in A .	33
3.4	Temperature dependence of the electrical conductivity of nitrogen plasma at atmospheric pressure [119].	39
3.5	The dependence $\lambda_{\mathcal{T}}$ as a function of temperature [119].	40
3.6	Variations of central temperature and voltage of arc versus time for a 1.5 A mercury arc [95].	42
3.7	Form Factor plotted against creeping distance for a cap and pin insulator [22].	43
3.8	Disc insulator model as studied by McElroy [143].	44
3.9	The Wilkins model for flashover of a polluted strip [142].	45
3.10	Cap-and-pin insulator and its plane model [149].	46
3.11	Plate model and pollution band, (a) near HV, and (b) near ground electrodes [102].	47
3.12	Typical arc and uniform conductive layer resistances in a given arc length.	50
3.13	Typical arc and uniform conductive layer resistances for a variety of arc lengths.	50
3.14	Critical arc voltage and length.	51
3.15	Arc characteristics for a narrow-strip polluted band using Wilkins' equation.	52
3.16	Arc characteristics for a wide-strip polluted band using Wilkins' equation.	53
3.17	General flowchart of a dynamic model.	56
3.18	Wilkins' proposed mechanism of elongation [141].	58
3.19	Equivalent circuit used by D. C. Jolly <i>et al.</i> , for arc propagation modeling [82].	66
3.20	Equivalent circuit used for arc propagation modeling [24].	69
3.21	Equivalent circuit used for modeling arc propagation on iced surfaces [39].	70

Figure	Title	Page
3.22	Comparison between the measured and computed positive arc velocity.	73
3.23	Comparison between the measured and computed negative arc velocity.	73
3.24	Comparison between the measured and computed leakage currents of the positive arc.	74
3.25	Comparison between the measured and computed leakage currents of the negative arc.	74
3.26	Comparison between the critical voltages measured under DC+ for various arcing distances and those computed from the model.	75
3.27	Comparison between the critical voltages measured under DC- for various arcing distances and those computed from the model.	75
3.28	Comparison between the critical voltages measured under DC+ and those computed from the model.	76
3.29	Comparison between the critical voltages measured under DC- with those computed from the model.	76
4.1	Different stages of arc development on an ice-covered insulator.	82
4.2	Figure 4.2 Transformation of discharge to arc during return stroke.	85
4.3	Principal model of arc propagation on an ice-covered insulator surface.	86
4.4	Air conductivity as a function of air temperature [99].	88
4.5	Flowchart of AC modeling.	93
4.6	A rectangular conductive layer in the presence of an arc.	95
4.7	Different Wilkins' equations for a resistance of a given specimen.	98
4.8	Capacitance of the rod and finite plane geometry [56].	100
5.1	Climate room.	109
5.2	Cylindrical model used for experiments.	110
5.3	Post insulator unit.	110
5.4	Main program menu.	111
5.5	Test data loading menu.	112
5.6	DAQ period of program.	112
5.7	Data analysis program session.	113
5.8	Schematic diagram of test circuit.	114
5.9	Complete samples of ice and initial air gap, before applying the voltage.	114
5.10	Ice geometry immediately after flashover.	119

Figure	Title	Page
5.11	Flashover test results for $L = 40$ cm on a cylindrical insulator and different applied water conductivities.	121
5.12	Flashover test results for $L = 80$ cm on a cylindrical insulator and different applied water conductivities.	122
5.13	Flashover test results for $L = 54$ cm on a post insulator and different applied water conductivities.	123
5.14	Flashover test results for $L = 103$ cm on a post insulator and different applied water conductivities.	124
5.15	Comparison of different flashover results for different initial air gap lengths, and different applied water conductivities, σ_w .	126
5.16	Typical current and voltage signals.	127
5.17	Typical current and voltage signals for a flashover test.	128
5.18	Arc behavior, before and in the period of flashover for a 40 cm length cylindrical insulator and applied water conductivity of $100 \mu\text{S/cm}$.	130
6.1	Arc current during second stage for iced cylinder and $L = 40$ cm.	137
6.2	Arc current during second stage for iced cylinder and $L = 80$ cm.	138
6.3	Arc current during the second stage for tested post insulator and $L = 54$ cm.	139
6.4	Arc current during the second stage for tested post insulator and $L = 103$ cm.	140
6.5	Effect of applied water conductivity, σ_w , on typical arc current cycle.	141
6.6	Effect of ice width, w , on typical arc current cycle.	142
6.7	Effect of insulator length, L , on typical arc current cycle.	143
6.8	Effect of variations in L_{arc0} on the calculation of flashover voltage.	146
6.9	Effect of variation of T on the calculation of flashover voltage.	147
6.10	Flashover results for a 40-cm iced cylinder and different applied water conductivities with 13.6% accuracy.	148

Figure	Title	Page
6.11	Flashover results for an 80-cm iced cylinder and different applied water conductivities with 8.9% accuracy.	149
6.12	Flashover results for a 54-cm post insulator and different applied water conductivities with 8.1% accuracy.	149
6.13	Flashover results for a 103-cm post insulator and different applied water conductivities with 10.3% accuracy.	150
6.14	Flashover results for a 30-cm iced cylinder and various applied water conductivities.	152
6.15	Flashover results for applied water conductivity of $80 \mu\text{S}/\text{cm}$ and different cylinder lengths.	153
6.16	Calculated and experimental critical voltages of 1 to 6 units of IEEE standard strings for $w = 46.2 \text{ cm}$ and $\sigma_w = 80 \mu\text{S}/\text{cm}$.	155
6.17	Calculated and experimental critical voltages for 5 units of IEEE standard insulators and different applied water conductivities.	156
6.18	Calculated and experimental critical voltages of 5 units of IEEE standard insulator strings and different ice widths.	157
6.19	Experimental and calculated last quarter cycle of the current for an iced cylinder.	160
6.20	Experimental and calculated last quarter cycle of the current for a post insulator.	161
6.21	Arc current for different simulation series.	164
6.22	Arc velocities for different simulation series.	166
6.23	Arc resistances per unit for different simulation series.	168
6.24	Arc temperatures for different simulation series.	171
6.25	$E-I$ arc characteristics for different simulation series.	173

LIST OF TABLES

Table	Title	Page
2.1	Characteristics of ice-formation on structures.	14
2.2	Conditions favoring the formation of various types of ice.	14
2.3	Maximum withstand stress of a short string of IEEE standard insulators under wet- grown ice.	22
2.4	E_{WS} of insulators covered with ice grown in wet and dry regimes.	22
3.1	Constants and exponents used by different investigators.	32
5.1	Ice-making specifications.	108
5.2	Minimum flashover voltages (kV) for cylinder and post insulator.	125
5.3	Flashover results for a 40 cm cylinder and longer initial air gap in kV.	125
6.1	Values of P_0 obtained by comparing experimental results with those of simulations.	144
6.2	Simulation input data.	146
6.3	Test settings for different series of simulation.	162

LIST OF ABBREVIATIONS AND SYMBOLS

AC	Alternative current
CIGELE	NSERC/Hydro-Quebec/UQAC Industrial Chair on Atmospheric Icing of Power Network Equipment
DC	Direct current
DC+	Positive direct current
DC-	Negative direct current
$E - I$	Voltage gradient-current
HV	High Voltage
IEC	International Electrotechnical Commission
INGIVRE	Canada Research Chair, tier 1, on Engineering of Power Network Atmospheric Icing
IEEE	Institute of Electrical and Electronics Engineers
KVL	Kirchhoff's Voltage Law
LTE	Local Thermodynamic Equilibrium
NaCl	Sodium Chloride
PID	Proportional Integral Differential
UQAC	University of Quebec in Chicoutimi
$V-I$	Voltage – Current
A	Arc gradient constant
b	Arc re-ignition component
C	Capacitance
C_p	Air specific heat
E_{arc}	Arc voltage gradient
E_{pr}	Electric field in the vicinity of the arc foot.

E_{WS}	Maximum withstand stress
G	Arc conductance per unit
h	Conductive layer thickness
h_P	Planck's constant
I	Current
I_{arc}	Arc current
I_c	Critical arc current
K	Arc re-ignition constant
k	Arc current density
K_B	Boltzmann constant
L	Arcing distance (insulator length)
L_{arc}	Arc inductance
l_{arc}	Arc inductance per unit
n	Arc gradient component
n_e	Number of electrons
P	Air pressure
P_0	Heat conduction loss rate
q	Charge per unit length of the arc
r	Arc radius
R_{arc}	Arc resistance
r_{arc}	Arc resistance per unit
R_{ice}	Ice bulk resistance
r_{ice}	Ice bulk resistance per unit
R_p	Pollution resistance
r_p	Pollution resistance per unit
S	Heat flux potential
T	Arc temperature
t	Time
U	Radiation loss rate
v	Arc velocity
V_{ap}	Applied voltage

V_{arc}	Arc voltage
V_b	Breakdown voltage
V_c	Critical flashover voltage
V_e	Electrode voltage drop
V_{MF}	Minimum flashover voltage
V_{WS}	Maximum withstand voltage
W	Internal energy stored in the arc channel
w	Conductive layer width
x	Axial arc length
x_c	Critical arc length
γ_s	Surface conductivity
κ	Air thermal diffusivity
λ	Air thermal conductivity
μ	Arc mobility
ρ	Air density
σ	Air conductivity
σ_w	Applied water conductivity
τ	Arc time constant
Δt	Duration of propagation

CHAPTER 1

INTRODUCTION

CHAPTER 1

INTRODUCTION

1.1 Overview

Damage to electrical network equipment due to accreted ice and snow is considerable in many cold climate regions [9, 61, 76 and 86]. A part of this damage is mechanical [65, 90, 124 and 140]. The heavy weight of ice and snow, combined often with wind, contributes sometimes to deforming structures to an extreme degree [65, 90 and 140]. A decrease in the electrical performance of high voltage equipment is a further consequence of atmospheric icing [19, 42, 46, 91, 98 and 125]. A number of major power failures as a result of flashover on ice-covered insulators have been reported worldwide [9, 14, 54, 61, 76, 77, 86, 98 and 103]. The insulating performance of ice-covered equipment depends mainly on numerous parameters. Not only the type and meteorological nature of the deposit and climatic characteristics, but also insulator geometry and the type of applied voltage have an effect on equipment performance [20, 32-35, 46, 87 and 129].

The study and understanding of arc initiation and propagation in the presence of ice, is a fundamental aspect of insulator studies. Predicting the incidence of flashover on ice-covered insulators may be considered an essential factor in insulator design. This

type of research is also helpful in modeling and manufacturing the right kind of insulator for use in cold climate regions [44].

Valuable work accomplished by many researchers has already been contributed in the domain of modeling and understanding of polluted and/or iced insulators [1, 3, 22, 28, 36, 40, 64, 69, 70, 118, 122 and 149]. Despite numerous similarities between the mechanism of the flashover phenomenon on polluted and iced insulators, these two circumstances are not totally identical [52]. The most acceptable hypothesis for arc propagation on polluted surfaces is based on the heating of the overlying resistive surface which results from the current flowing through it, leading to the formation of dry bands [22]. In this case, it is considered that the surface of the insulator is covered with a conductive layer. The low voltage-drop along the high conductive surface provides enough field strength along the dry bands [70]. Each dry band becomes short-circuited locally by a partial discharge which is immediately transformed into an arc [22 and 70]. The consecutive dry band formation, up to a certain length, leads to a sudden flashover under a number of other assumptions [81]. In spite of the applicability of this proposed theory for arc propagation under DC or impulse voltage, the flashover mechanism of AC applied voltage is considered to be more complex than indicated [122 and 142]. The weakness and re-ignition of the arc after each voltage peak cannot, however, be fully explained by this hypothesis. In spite of this, a few models present several theories for an AC propagating arc [22, 97 and 121]. Most of these models make use of the same DC method of applied voltage to analyze the phenomenon under AC voltage and consider that flashover occurs in a single cycle [3, 22 and 142].

There is a certain amount of similarity in the nature of arc initiation and its maintenance under iced and polluted conditions, although the arc propagation on a wet

conductive electrolyte surface, such as a water film on ice deposits, cannot be explained using the same hypothesis of dry arcing zones. For this reason, the entire mechanism of arc motion on ice-covered surfaces requires particular study and attention.

In order to further knowledge and understanding of discharge initiation on an iced insulator surface and its development into a flashover arc, a research program was set up under the auspices of the NSERC / Hydro-Quebec / UQAC Industrial Chair on Atmospheric Icing of Power Network Equipment (CIGELE) and Canada Research Chair, tier 1, on Engineering of Power Network Atmospheric Icing (INGIVRE) at Université du Québec à Chicoutimi. A considerable quantity of theoretical and experimental research work has been published on this subject, to date [30, 34-41 and 46]. Studies of the effects of different climatic parameters and insulator geometry, as well as insulator voltage type, have been carried out based on a wide variety of experiments [30, 41, 46 and 92]. The results show the inevitable influence of several ice-accretion parameters in diminishing the maximum withstands voltage of high voltage equipment [30, 41 and 46]. The type of precipitation involved was found to be one of the salient parameters [46]. This factor itself is influenced by the prevailing ambient air conditions including temperature, wind velocity, and droplet size [46]. The flashover voltage is also dependent on the conductivity of applied water which provides the conductive surface during arc initiation, maintenance and propagation [30 and 46]. Research in this field also includes recording and studying the first few nanoseconds of arc initiation and its propagation on different ice-covered surface materials under impulse voltage [10]. The potential distribution of real-shape ice-covered insulators of different geometries was also examined [138]. A predictive static model for the estimation of critical flashover voltage was originally established within the same

context and was applied to the different types of voltage such as AC and DC [13, 17, 47, 52 and 146-148].

The above-mentioned model has proved to be of signal usefulness in predicting the critical flashover voltage of ice-covered insulators, although several questions still remain unanswered. Static models are not structured in such a way as to provide the time-dependent evolution of such parameters as current or resistance of the components. The major purpose of these types of models is the determination of the critical flashover voltage, rather than the dynamic evolution of various parameters during different phases of the flashover phenomenon.

By contrary, dynamic models are capable of calculating and predicting the time-dependent evolution of the main parameters of the arc. Based on an appropriate physical theory of the total discharge process, dynamic modeling can contribute to a better understanding of the detailed phenomena involved in the whole range of discharge mechanisms. By comparing the results of the simulation with those of experiments, it will become possible to accept or reject the physical hypothesis used. This thesis is also submitted with the intention of providing a fresh perspective and contributing an innovative approach to the entire process.

An adequate dynamic model should take into account all the major parameters which influence the flashover phenomena. These parameters include ice type and characteristics, freezing water conductivity and insulator geometry. Although, the observation of the arc behavior of insulators under DC and impulse applied voltages is usually worthwhile from a physical point of view, but because of the general use of AC source voltages in high voltage networks, a predictive model for AC voltage would be even more useful from an engineering point of view.

Arcing phenomena may be deemed a blend of a variety of aspects, including chemical, mechanical and electrical properties [119]. Despite the complexity of the mechanisms involved in surface discharge or arc phenomena, many simplifying assumptions must be made in order to render mathematical modeling possible. Several models have been presented over the years to explain the mechanism of a propagating discharge channel both in air and on insulating surfaces [70, 118 and 142], although not all the pertinent aspects of such a dynamic phenomenon have been discovered yet. The complexity of icing and melting periods tends to cause even more uncertainty in obtaining a perfect model which would cover all eventualities. Several of the surrounding parameters, such as wind velocity, air temperature and water droplet characteristics, influence the type of ice formed. A comprehensive dynamic model, beyond providing the representative elements for the arc and ice, needs to be accompanied by the corresponding chronological correlatives. In this regard, arc velocity is a major link. Several models in the literature have thus far been presented to simulate the propagation velocity of the discharge in air, and a number of these models determine the same parameter for insulating surfaces. Most of the models are, however, empirical and have not yet been explained by any physical facts. Choosing a suitably accurate formula for the velocity has usually been a major difficulty in this type of research. Another main item in dynamic modeling is selecting a suitable propagation criterion. As regards the nature of this type of modeling, dynamic simulations must also deal with all of the time steps in the process.

1.2 Objectives of the Thesis

Generally speaking, the objective of this type of research study is to improve our knowledge on the physical phenomena involved in ice-covered insulator flashover phenomenon, through a systematic study (experimental and theoretical) of the mechanisms, associated with each development stage of an electric discharge, where for each mechanism, mathematical models should be elaborated. From these elementary models, a complete model, able to simulate the temporal behavior of propagating arc will be elaborated. In the long term, these studies will allow us to identify the best way of the reliability optimization and design of the insulators. The new insulator concept could support in an innovating way the quality and the reliability of the electrical power distribution.

As regards, specific objectives of this project are:

- To develop a dynamic model for a propagating AC arc on an iced surface, using electrical circuit concept,
- To translate the associated physical phenomena into mathematical equations, to be used in the electrical circuit,
- To present a method of simulation through a flowchart capable of predicting and determining the variations in some macroscopic parameters such as leakage current and propagating velocity, over time, during the arc propagation stage on an ice-covered insulating surface under AC applied voltage. This dynamic procedure should take into account major parameters

which influence the phenomenon. These parameters include applied water conductivity, insulator length and insulator radius.

- Experimental validation and adjustment of model parameters on a simple cylinder and a short post insulator.

1.3 Statement of Originality

As will be appeared later on the text, in the review of the literature, to the best of our knowledge there is no any dynamic model able to predict and simulate the temporal evolution of the flashover main parameters as arc current and velocity on ice-covered insulator surfaces under AC applied voltage. An all-exclusive model should take into account all the influent parameters and be able to predict main variables of the phenomena and then the resulting data of the model should be verified against experimental results; even thought the existence of a few dynamic models which were presented to describe the arc behavior on polluted surfaces, such a model has not been created yet. In order to realize this study, a new exploratory hypothesis for flashover phenomena was proposed and based on that, a complete new flowchart was established to determine the desired variables. The model results were justified by comparison of the experimental results performed within the thesis and of other researchers. The model not only predicts the variation of the arc parameters over the time, but also is accurate in critical flashover calculating.

1.4 Outline of Thesis Structure

This dissertation introduces and discusses the different aspects of dynamic arc modeling on ice-covered insulator surfaces, as follows:

- Chapter 1 introduces the problem of insulator flashover and atmospheric icing, and also provides a brief review of the literature;
- Chapter 2 reviews the problematic of atmospheric icing on electrical networks;
- Chapter 3 describes arc modeling on resistive surfaces and provides the main relationships and methods involved;
- Chapter 4 discusses the basis of arc modeling on iced insulator surfaces is in, and an entirely new dynamic model is introduced for the prediction of different propagating arc variables such as velocity and current. In order to adjust the model and validate the simulation results, the need for several series of flashover tests is justified in this chapter;
- Chapter 5 presents the experimental setting and results;
- Chapter 6 provides the comparison of the simulation results with those of the experiments; and finally;
- Chapter 7 describes the conclusions of this project and also recommends future directions for project research and development.

CHAPTER 2

REVIEW OF LITERATURE ON EFFECTS OF ICE ON HIGH VOLTAGE INSULATORS

CHAPTER 2

REVIEW OF LITERATURE ON EFFECTS OF ICE ON HIGH VOLTAGE INSULATORS

2.1 Introduction

In most cold climate regions, transmission line towers and HV substations are subjected to seasonal icing and snowfall [54 and 77]. The resulting ice and snow accretion increases the weight of the line cables and conductors as well as wind load, sometimes leading to mechanical damage [140]. Also, ice and snow accretion on a string of insulators decreases their insulating performance [46]. The power outages caused by flashover on ice- or snow-covered insulators have been reported in many northern countries including Canada [19, 45, 87 and 104], China [139], Great Britain [62], Norway [53 and 54], Finland [83], and Japan [98].

The level of transmission-line voltage is being increased regularly to parallel the increase in the consumption of electrical energy. This situation has become a subject of prime importance in current research into insulator flashover phenomena.

As a general rule, the flashover process on ice-covered insulators includes the following stages: first, several violet arcs appear across the air gaps, or ice-free zones; second, one of the arcs then propagates along the ice surface forming a white arc; and, later, when the white arc reaches a certain length, flashover suddenly occurs [40]. Methods designed to mirror this process as it develops on polluted insulators were

frequently used in the past to investigate the mechanism of flashover on ice-covered insulators, as well [17, 47, 50-52 and 146-148]. It will be observed, however, that flashover along ice-covered insulators, when compared with flashover on polluted surfaces, presents different degrees of complexity in various ways:

- The freezing processes influence the type of ice formed [46].
- There are two discharge surfaces for ice-covered insulators: the outer ice surface and the interface between the ice and the insulator, as compared to only one surface for polluted insulators [147]. Flashover along the interface between ice and insulator was frequently observed in laboratory investigations [147].
- The surface and bulk conductivities of ice are influenced by a number of parameters such as surrounding air temperature, applied water conductivity, type of ice formation, and the icing process [46].
- The ice layer which forms on the insulator is relatively thick in contrast with air-polluted surfaces, which are often covered with a thin layer of pollution [32 and 101].

In addition to this, several factors influencing the flashover on ice surfaces should be taken into account, including applied water conductivity, voltage type, arcing distance, and ice-covered surface uniformity [46]. The statistical aspect should also be considered, in view of the fact that flashover voltage is a statistical variable characterized by significant dispersion even under seemingly controlled conditions. Due to a number of physical phenomena and electrical factors acting simultaneously on individual super-cooled drops and droplets, the possibilities for determining such ice

characteristics as density, structure, and shape are fairly limited. The same goes for the amount of ice accreted on high-voltage equipment, weather conductors or insulators, and so forth. In this regard, very few data are accessible in the presently available literature. Climate room experiments, which always involve conductors and insulators submitted to high voltage, show that density and other ice characteristics may be altered under energizing conditions [30]. The phenomena caused by ice or snow accretion on power network equipment, and their consequences, are divided into two main categories [40]. The electrical category only will be introduced and discussed further on in the text.

2.2 Types of Ice

Most investigators tend to subdivide ice and snow into two categories: wet and dry [20]. A number of factors may have an influence on the type of ice accreted [20, 78, 89 and 113]. Such factors include the temperatures of the insulator surface, water droplets and ambient air, as well as the parameters of wind velocity and droplet size [20, 78, 89 and 113]. Dry ice, of a relatively low density, whether hard rime or soft rime forms at a low droplet size and the temperature below zero [20], on the other hand, wet ice or glaze, which is the most dangerous type of ice from an electrical point of view [29 and 45], tends to grow in the presence of a surface water film [20]. The density of the glaze produced is relatively high, of about 0.9 g/cm^3 [20]. The names of different types of ice and the general atmospheric characteristics favorable to the formation each type is shown in Tables 2.1 [20] and 2.2 [46].

Table 2.1 Characteristics of ice-formation on structures.

Type of Ice	Density (g/cm ³)	Appearance	Shape
Glaze	0.8 to 0.9	transparent and clear	cylindrical icicles
Hard Rime	0.6 to 0.8	opaque	eccentric pennants into the wind
Soft Rime	< 0.6	white and opaque	feathery and granular

Table 2.2 Conditions favoring the formation of various types of ice.

Type of Ice	Air Temperature (°C)	Wind Speed (m/s)
Glaze	0 to -3	1 to 20
Hard Rime	-3 to -15	5 to 20
Soft Rime	-5 to -25	5 to 20

2.3 Creating Ice Artificially in the Laboratory

Being able to produce ice in the laboratory provides greater scope for the study of and research into the mechanism of flashover. The use of a climate room makes it possible to produce ice year-round independently of the seasons. Experiments may be carried out under a variety of controlled circumstances and climatic conditions in this facility.

For insulator flashover tests, ice in the laboratory is produced under both wet and dry regimes [44, 46 and 116]. In a dry regime, ice is accumulated as a result of small water-droplet (15 μm) spray which turns to ice immediately upon impact on the surface [30 and 43]. A surface temperature below 0°C will ensure the instant thermal equilibrium between ice deposits and the ambient air, where the heat disturbance results from the impact of water droplets and forced convection [43]. When dry ice is

produced, it has a low density of about 0.4 to 0.6 g/cm³ similar to natural light ice and it is opaque in appearance [30] (cf. Fig. 2.1).



Figure 2.1 Dry ice formed on a short suspension insulator string [138].

Wet-grown ice is produced by water droplets (50 to 80 μm) which are bigger than those observed during the formation of low density ice [30 and 43]. These water droplets are not in a frozen state before impacting the surface of the insulator in air and they reach the insulator in a liquid form. As a result, ice will accrete between the skirts of the insulator in the form of icicles. The density of this type of ice will be approximately 0.9 g/cm³ for the icicles and about 0.87 g/cm³ for the ice deposit on the surface of the insulator [30 and 43]. The color and transparency of the ice in this regime depend on the presence of air bubbles in the ice which has the appearance of atmospheric glaze [30] (cf. Fig. 2.2).

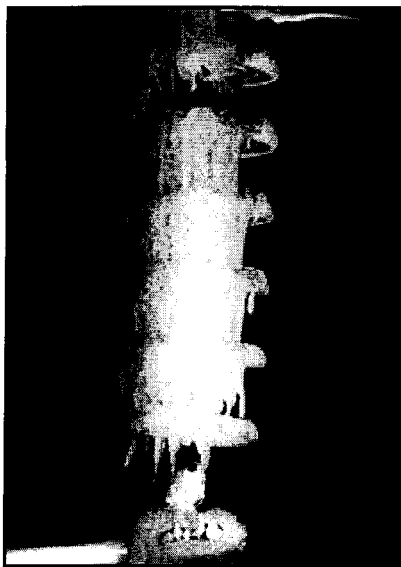


Figure 2.2 Wet-grown ices on a chain insulator [138].

In the laboratory ice-making, the maximum rate of ice accumulation, both wet-grown and dry-grown, may be achieved when wind velocity, air temperature and liquid water content are 3.3 m/s, $-12\text{ }^{\circ}\text{C}$, and 6.8 g/m^3 , respectively [30 and 43].

2.4 Insulator Performance under Icing Conditions

The discussion of this topic touches on several studies carried out regarding ice accretion on high-voltage *conductors*, and includes a description of a number of parameters related to this topic [18, 40 and 126]. These parameters are the appearance of an electric field and its effects on ice accretion, the structural parameters of ice, the influence of transmitted current, effects of ionic wind, and several other associated parameters [40]. It should be noted, however, that this discussion will address insulators, rather conductors, from now on.

The uniformity of the ice accreted on the insulator surfaces is one of the main parameters which influence the electrical performance of the insulator itself [71 and 72]. This ice is not usually uniform, and also several air gaps occurring on the sections of the insulator under observation are due to the complexity of the ice formation process under an applied electrical field [40, 44, 71 and 72]. These gaps are produced as a result of the heat dissipating from partial arcs during the icing period (cf. 2.4.1), as well as ice-shedding during and after this stage [138].

The flashover phenomenon is generally preceded by the formation of a water film on the surface of the ice [40, 45 and 84]. The appearance of this water film may be due to an increase in the ambient temperature or it may be a result of melting ice due to partial arcs and corona [86]. Considering that the volume conductivity of ice is low and may be negligible [12 and 49], this water film is the main carrier of the leakage current [17, 52 and 146]. The high conductivity of this layer implies that the applied electrical field will mainly drop along the above-mentioned air gaps [138]. Since, in most of the cases, the total length of the gaps is much less than the total length of the insulator, relatively strong partial arcs may appear. Several small violet arcs along the air gaps provide more heat to melt more ice thereby increasing the quantity and area of the water film on the surface. From this point onward, the heating effect due to burning arcs is more dominant than the effect of the ambient temperature. Occasionally, the ice will remain on the surface of the insulator and may produce enough water for surface conductivity to reach a critical level. Such a situation depends on the type and thickness of the ice and the adhesive forces between the inner surface of the ice and the outer surface of the insulator. Consequently, small arcs gather together to form a white arc,

where the leakage current is estimated to be around 25 mA maximum [71]. This stage can lead to flashover under certain conditions.

Thus, it is clear that a variety of factors can affect the flashover phenomenon. The parameters involved are related to the ambient conditions and ice formation characteristics; as well as to the type and manner of applying the voltage and carrying out the tests. Insulator shape and configuration can also modify the experimental results.

Further discussion and experimental results will be presented further on the text. The effects of the above-mentioned parameters on flashover performance are subject to experimental methods in each individual circumstance and are, therefore, only to be compared in each specific situation and should not be used for general comparison.

2.4.1 Air Gaps and Partial Arcs

Earlier studies have shown the presence of partial arcs along the air gaps of iced insulators [40, 44, 71 and 72]. These air gaps are the part of the insulator which is not covered with ice. Observation has shown that the creation of these air gaps begins at the outset of the ice accumulation period on the insulator surface [138]. During this period, the icicles grow between the insulator skirts by elongation, and each process is complete upon reaching the next skirt. When the icicle length comes within a certain distance of the next skirt, an electric arc appears between the tips of the icicles and the insulator skirt immediately below due to the presence of high water film conductivity. The appearance of partial arcs halts further elongation of the icicles and may even melt them. This process is the basis of air-gap making and, when the accumulation is terminated, a careful examination of the ice surface shows the presence of air gaps around the electrodes (cf. Fig. 2.3). Occasionally, however, other air gaps may be

observed along the insulator and on the further side of the electrodes, but the mechanism of their creation is the same as in the preceding ones [138].

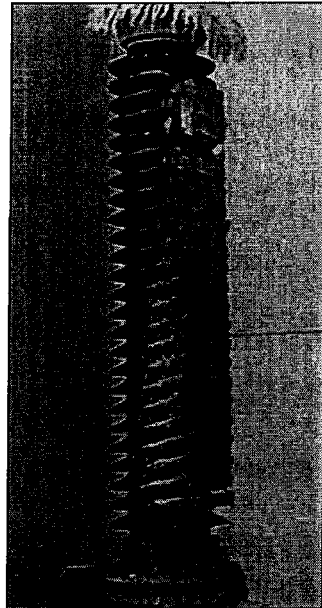


Figure 2.3 Air gaps formed during accumulation of ice [31].

When the voltage drop along the air gap is greater than the breakdown voltage, a partial arc appears along these air gaps. If the critical conditions are reached, these small arcs may lead to an insulator flashover, otherwise, the ice breaks away from some part of the insulator where the ice is not adhesive enough [48].

It is possible to determine the AC breakdown voltage of an air gap, in the absence of ice or water droplets, when one side of the electrode is an ice deposit in cylindrical form [48 and 51]. A study was carried out during the melting period and resulted in establishing a linear relationship between the breakdown voltage, V_b , and air gap distance, d , as follows [48].

$$V_b (\text{kV}_{\text{rms}}) = 4.10d (\text{cm}) + 3.8 \quad (2.1)$$

2.4.2 Effect of Various Parameters

2.4.2.1 Dry Arcing Distance

When the shedding distances are not obstructed by icicles, the flashover voltage becomes a function of several parameters, amongst which may be listed icicle length and insulator profile. Whenever the sheds are bridged with ice the creeping distance decreases radically. The flashover voltage is now a parameter of the dry arcing distance [40 and 45]. This relationship is mostly linear for short string insulators, according to several investigators [45, 83 and 116], whereas it seems to be non-linear for long insulators [128].

Where long insulators are concerned, the non-linearity of the relationship is a result of the change in the physical aspects of melting ice including changes in surface water conductivity, non-uniform distribution of ice along the insulator, and physical discharge phenomena [128].

2.4.2.2 Applied Water Conductivity

Applied water conductivity, σ_w , is a major parameter which causes variation in the flashover values of insulators [30, 45 and 116]. Technically speaking, natural rain is not pure water and the conductivity of applied water may vary as a function of air pollution to different values. Rahal showed that not only the solute, but also the solvent can influence discharge phenomena [118]. Since the conductivity of a solution is a

parameter of the temperature, its value is generally calculated and expressed at 20°C [30, 40 and 44].

In general, the lower the applied water conductivity the higher the flashover voltage is [30, 45 and 116]. This continues up to a certain value of the applied water conductivity and then the increase in this parameter seems to have no further significant influence on the maximum withstand stress, E_{WS} [30].

Pre-contamination of the insulator, which appears to occur more frequently in nature than in other situations, may also be considered an important parameter [29]. The least possible effect of such pre-contamination is a greater voltage drop along the air gaps. Thus, the creation of a partial arc may occur under lower applied stresses as a forerunner of the flashover phenomenon on ice-covered insulators. In the case of extensive pre-contamination, flashover may even occur during the accumulation period [29].

2.4.2.3 The Type of Voltage Applied

In the presence of ice, insulator performance is also a parameter of the type and polarity of the applied voltage [32], although the type and amount of ice may vary under different applied voltages, and the arc parameters may also change. A significant amount of investigation has concerned itself with identifying these influences.

Under lightning impulse, ice-covered insulators seem to perform in the same way as clean, dry insulators, although the experiments occasionally show that there may be as much as a 50% decrease in minimum flashover voltage, V_{MF} , under switching impulse with and without ice [40].

Under DC voltage, the polarity of applied voltage also becomes a significant parameter [32]. Where the insulator sheds are bridged by icicles, under the same conditions, the maximum withstand voltage of a short suspension insulator string covered with under DC+ is about 17% more than the same insulator under DC-, and it is approximately equal to the effective AC value as shown in Table 2.3 [40].

Table 2.3 Maximum withstand stress of a short string of IEEE standard insulators under wet- grown ice.

Type of voltage	E_{WS} (kV/m)
DC+	86
DC-	71
AC	85

2.4.2.4 Ice Type and Wind

The whole process is also dependent on ice type [30, 40 and 45]. A number of investigators have confirmed that there is less risk of flashover where the ice is compact and transparent (glaze), than in the presence of other ice types [45], and also that whenever the ice density is high, the maximum withstand voltage decreases [43 and 45]. A study of four types of insulators has shown that the ice grown in a wet regime is more susceptible to flashover than ice accumulated in a dry regime. The results of the experiments are shown Table 2.4 [30 and 41].

Table 2.4 E_{WS} of insulators covered with ice grown in wet and dry regimes.

Type of Ice	E_{WS} (kV/m)			
	IEEE	Anti-Fog	EPDM	Post-Type
Wet-Grown	70	84	96	90
Dry-Grown	> 148	> 146	> 168	> 197

As may be observed, the withstand voltage of wet-grown ice is about two times less than it is for the others. Any and all parameters which change the ice type may be considered as influencing factors for modification in the test results. These parameters include wind velocity and water-droplet size, as well as ambient temperature.

Wind velocity has several further effects on the flashover mechanism of ice-covered insulators. High velocity winds of more than ~ 5 m/s, cause icicles to deviate from the perpendicular [30], which means that the arcing distance increases even if the sheds are completely bridged. This results in higher withstand voltages for the same insulator length. Wind can also cause the disappearance of the electric ions, produced by previous discharges. Also, by increasing the heat exchange, winds can cause a drop in temperature of the arc channel and dry ice surface as well. Such factors can lead to higher minimum flashover voltages.

During de-icing periods, wind-created ice formed by an updraft is more susceptible to flashover than ice formed by a downdraft [71]. A significant decrease in the flashover threshold thickness of ice has been observed with a 45° updraft wind on porcelain insulators [71].

2.4.2.5 Ice Thickness

As was mentioned earlier, the presence of a greater quantity of wet-grown ice, after a white arc is established, will tend to increase the risk of flashover. In order to evaluate different quantity of accumulated ice deposit on the insulator surface during the experiments, several methods were applied. These methods may include the weighting of the ice, measuring the length of the icicles, timing the duration of the ice

accumulation process, and finally, monitoring the ice thickness on either a fixed or rotating cylinder [40].

It was observed that the maximum withstand stress, E_{WS} , decreases with the increase of ice thickness and then becomes independent of it [32]. This critical value varies for different types of insulators and ice thicknesses. The numerical value of the critical thickness is a function of a number of correlative parameters in individual test sets such as the velocity of rotation, or the distance of the cylinder from the nozzles, and may vary from one laboratory to another.

2.4.2.6 Air Pressure

As is the case with other atmospheric conditions, air pressure has a certain amount of influence on arc characteristics and thereby on the performance of the insulator itself [93]. The effects of air pressure have, to date, been introduced as an influencing factor on the arc voltage, and is known as the air density reduction factor, K_d , as follows [92]:

$$V_c = K_d V_0 \quad (2.2)$$

where V_c represents the critical flashover voltage, at any pressure and V_0 is the corresponding value at standard sea level pressure.

The value of this factor depends on a number of factors such as insulator profile, pollution severity, and type of voltage [92]. Several test results show a decrease in the flashover voltage of up to 40%, when the air pressure drops to 30 kPa from its sea level value of 101.3 kPa [93].

2.4.2.7 Supplementary Parameters

In regard to the explanation of the flashover mechanism, any parameter may be termed an influencing parameter if there is a possibility that it might have an influence on the presence of a water film. Such parameters include the maintenance of a partial arc, or the amount of ice reserve for creating a water surface, or any factor which might inhibit ice shedding. Among these parameters may also be listed the diameter, profile, and configuration of the insulator [40]. An insulator of a greater radius will tend to maintain more ice accumulated on the surface, which implies a decrease in leakage resistance [13]. Short-distance shedding will occur closer together than farther apart during the same period of accumulation, and thus it may be observed that the profile of insulators has an obvious effect on the incidence of flashover voltage.

2.5 Recapitulation of Main Points

A number of different conclusions may be obtained with regard to much of the research and resulting observations which pertain to the flashover of ice-covered insulators:

- High voltage equipment in cold climate regions is subjected to atmospheric ice precipitations seasonally. This type of precipitation generally decreases the electrical performance of the equipment and may cause a flashover with subsequent system failure;
- Wet-grown ice or glaze which has a relatively high density, is the most dangerous type of ice from an electrical point of view;

- Certain climate conditions result in wet-grown ice accretion on insulator surfaces and this type of ice may be produced at a rapid in the laboratory by imposing controlled climate conditions;
- Several main parameters have a certain amount of influence on the insulating performance of high voltage insulators. Among them may be counted insulator geometry (length, radius and material), applied water conductivity, ice type and amount, as well as climate conditions. In general, shorter insulator length, longer insulator diameter and higher applied water conductivity may each result in lower flashover voltage;
- The creeping distance of the arc in the presence of ice formed at a low air velocity, may decrease to as low as the dry arcing distance of the insulator;
- Ice formation under applied voltage is accompanied by the formation of air gaps;
- The flashover process is triggered by the presence of a highly conductive water film on the surface of the ice, which results in intense electric stress along the air gaps. This high stress breaks down these air gaps and leads to the creation of the corona discharges. The small violet corona discharges lead to the formation of a high-current white arc. The latter may lead to a sudden flashover under sufficiently high applied voltages.

CHAPTER 3

REVIEW OF LITERATURE ON SURFACE FLASHOVER MODELING

CHAPTER 3

REVIEW OF LITERATURE ON SURFACE FLASHOVER MODELING

Numerous experimental and theoretical studies have been carried out over the years to investigate the flashover phenomenon of insulator surfaces covered by a conductive layer [1, 3, 22, 40, 64, 70, 118, and 122]. It should be mentioned here that problems associated with the contamination of insulators have been officially recorded by utilities for almost a century [112].

Outdoor insulators may be covered with dust (which is slightly conductive but hygroscopic) and/or atmospheric ice [40 and 142]. This surface pollution accumulates as a result of natural sources or industrial emissions [142]. These two types of pollution occurring in combination produce more diverse effects than each one of them would separately. Electric arcs tend to occur under certain conditions and to develop up to the point of causing the total flashover of a given insulator. With the aim of improving insulator design, considerable work has already been accomplished, or is still under way, towards defining insulator behavior and the flashover process under contaminated conditions [21]. The model for flashover on polluted insulators, however, is still a challenge in the study of outdoor insulation, considering that the development of polluted insulator flashover models must take into account all of the surrounding physical conditions. This causes the modeling to be somewhat difficult due to the

complexity of pollution distribution which normally results from the non-uniformity of the deposits. In spite of problems, many partially successful attempts have been made to build models in order to predict the insulating performance of polluted insulators.

In this chapter, an overview of the different existing mathematical models for flashover on an insulator surface is provided. Most of these models are the static models describing DC flashover phenomena. DC voltage is the type of voltage most susceptible to insulator flashover, since DC insulators are liable to accumulate contaminants to a greater degree than AC insulators [17], and also flashover tends to occur more readily than on AC units under otherwise identical conditions [17]. Most of the electrical energy transfer in high voltage networks takes place under AC applied voltage. AC static modeling is also being carried out under the same assumptions as DC modeling with the addition of re-ignition conditions [22]. While certain static models display satisfactory performance in the calculation and predictability of critical flashover voltage on insulators [22, 107 and 150], they are designed to provide the temporal evolution of such main physical arc parameters as current and velocity. A few dynamic models have occasionally been proposed in the literature for overcoming this problem [4, 24, 82, 123 and 131]. An appropriate propagation criterion, as well as a velocity relation are necessary in order to create adequate dynamic models. The majority of the models, to be listed later, use an equivalent electrical network for arc modeling [1, 3, 22, 40, 64, 70, 118 and 122].

3.1 Basic Model

Obenaus was a pioneer in the field who carried out quantitative analyses of the arc phenomenon on the surface of insulators covered with a conductive layer [110 and

111]. He proceeded by considering an equivalent electrical circuit, constituted of an arc of axial length x in series with a resistance, R_p , and he then obtained the arc current using the Kirchhoff's voltage law, KVL. In Figure 3.1, L represents the total length of the insulator. It was assumed that the same current which passes through the arc also passes through the resistive layer. It is necessary to obtain the appropriate equations calculating the arc potential and resistance of the unbridged part of the conductive layer in order to solve the circuit. The circuit relationship needs to be accompanied by a physical theory so as to complete the model. This simple model became the basis of nearly all later works.

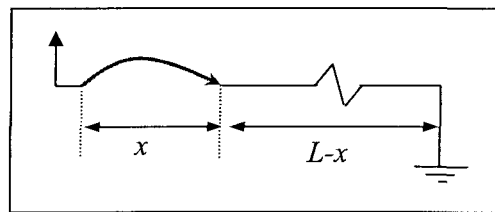


Figure 3.1 The Obenaus model.

3.1.1 Arc Models

3.1.1.1 Ayrton's Equation

Many investigators used Ayrton's arc gradient equation to model the arc [15 and 122]:

$$E_{arc} = AI_{arc}^{-n} \quad (3.1)$$

where I_{arc} is the leakage current, and A and n are arc constants. These constants may vary in accordance with the arc medium material and ambient conditions.

A survey of the literature shows that the values of A and n , as measured or utilized by different investigators, vary over a wide range for different types of arc (see Table 3.1) [3, 15, 21, 27, 40, 67, 70, 74, 82, 110, 111, 122, 127, 131, 133, 135, 137 and 149]. These values depend not only on the arc medium but also on the electrolyte used to form the resistive layer [70 and 118].

Table 3.1 Constants and exponents used by different investigators.

	Investigator	Current (A)	A	n	Excitation	Medium
1	Suits and Hocker (1939)	1-10	65 220 81	0.6 0.6 0.6	NS NS NS	air stem nitrogen
2	Obenaus <i>et al.</i> (1958)	0.1-2	100	0.7	ac	air
3	L. Alston <i>et al.</i> (1963)	0.1-15	63	0.76	ac	air
4	E. Nasser <i>et al.</i> (1963)	0.1-1.0	63	0.76	dc	air
5	Hampton (1964)	0.1-0.5	65 52	0.8 0.1	NS NS	air steam
6	E. Los <i>et al.</i> (1971)	1-3	52	0.43	dc	air
7	Nottingham (1973)	NS	44 310 39.2 203	0.67 0.985 0.67 1.38	dc	air
8	Claverie <i>et al.</i> (1973)	1-2	113 98.99	0.5 0.5	ac	air
9	Jolly <i>et al.</i> (1974)	1-3	296	0.397	ac	air
10	El-Arbaty <i>et al.</i> (1979)	NS	40	0.8	ac	air
11	F. A. M. Rizk (1981)	0.05-2.0	130 210.6	0.45 to 1.3	dc	air
12	Gers <i>et al.</i> (1981)	0.1-5	46.05 44.77 43.80 59.64	0.91 0.822 0.822 0.773	dc impulse dc dc	air
13	M. P. Verma (1983)	NS	53.45	0.5	ac	air
14	Mayr <i>et al.</i> (1986)	NS	40.6 50.20 114	0.724 0.708 0.714	dc	air helium nitrogen
15	D. A. Swift (1989)	1-3	80 60	0.5	dc	air
16	G. Zhicheng <i>et al.</i> (1990)	0.1-1.0	138 140	0.69 0.67	dc ac	air
17	F. L. Topalis (1992)	NS	131.5	0.374	NS	air
18	R. Sundararajan <i>et al.</i> (1993)	NS	60 63	0.8 0.5	dc	air
19	R. P. Singh <i>et al.</i> (1994)	NS	31 to 100	0.43 to 0.98	ac	air
20	N. Chatterjee <i>et al.</i> (1995)	NS	NS	0.7	ac	air
21	H. G. Gopal <i>et al.</i> (1995)	NS	60 100	0.25 1.20	NS	air
22	D. C. Chaurasia <i>et al.</i> (1996)	0.01-1.2	50 100	0.25 to 1.1	ac	air
23	A. S. Farag <i>et al.</i> (1997)	NS	530	0.24	ac	air
25	M. Farzaneh <i>et al.</i> (2000)	NS	84 209 205	0.77 0.45 0.56	dc- dc+ ac	air, on the ice
24	J. P. Holtzhausen (2001)	NS	59	0.53	ac	air

For comparison purposes, the typical values for A and n are examined here. A is considered to vary between 20 and 300, and n between 0.1 and 0.9. Figures 3.2 and 3.3 show the simulation results.

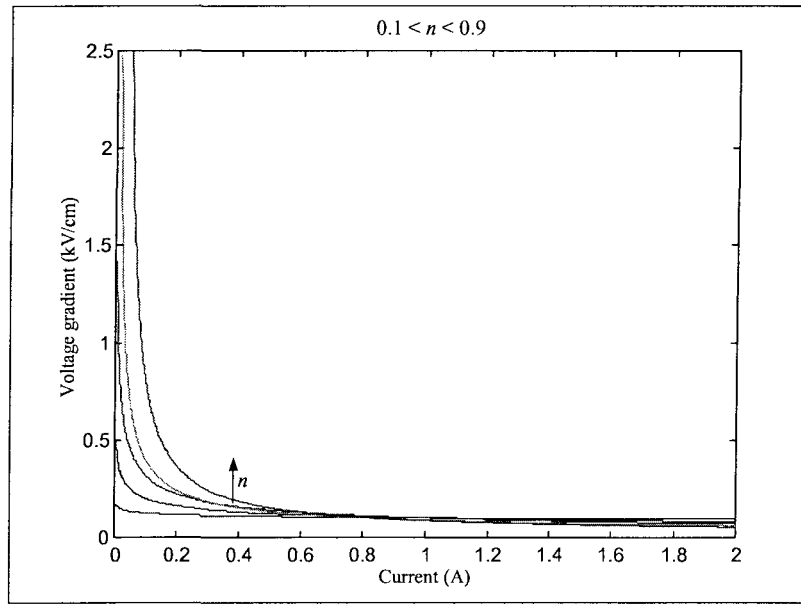


Figure 3.2 Effect of the variation in n .

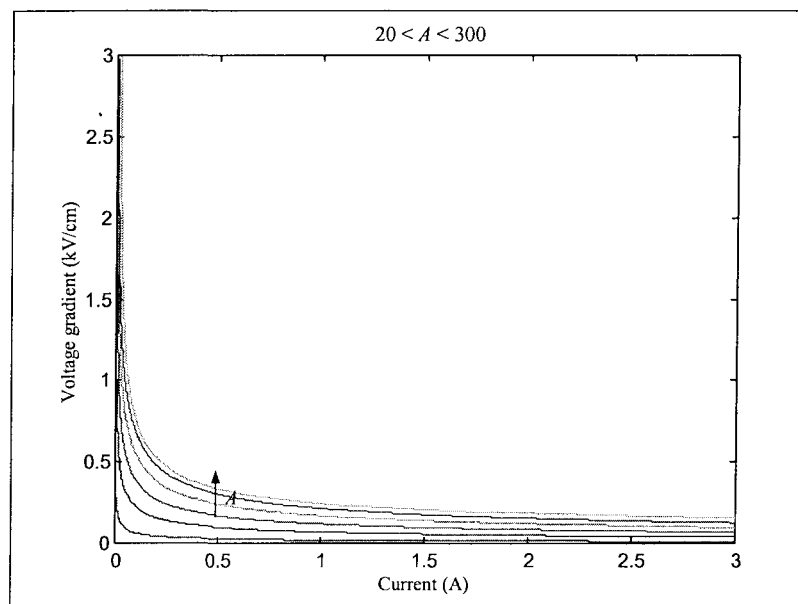


Figure 3.3 Effect of the variation in A .

It is clear that the voltage gradient is highly sensitive to changes in A and n , particularly for currents below 500 mA where the arc resistance will change from an initial value of about 3000 M Ω to a few k Ω .

3.1.1.2 The Gopal and Rao Model

Although most of the researchers made use of the same Ayrton equation for the arc, it was not the only model used. By introducing a new equation for electrical field calculation inside the arc channel, Gopal and Rao presented a further relation for arc voltage [68]. This relation is acceptable for free burning arcs in air. In the relation:

$$V_{arc} = \alpha + (\beta + x) \left(\ln \frac{I_{arc}}{\delta} \right)^{-3} \quad (3.2)$$

α , β and δ are constants, and their values depend on the nature of the electrodes.

3.1.1.3 The Cassie-Francis and Mayr Equations

Earlier papers have already addressed the subject of the time dependence of arc resistance in terms of two alternative semi-empirical equations containing several undetermined constants. After evaluating these constants in terms of experimental results, the equation is applied together with the circuit equation and Ohm's law to predict voltage, current waveform, and arc extinction or re-ignition.

One of these equations is the Francis equation [62], which was used to interpret the voltage-current oscillogram of discharge lamps. The Francis equation, after some simplification, reads as follows [95]:

$$\frac{1}{G} \frac{dG}{dt} = \alpha E_{arc}^2 - \beta \quad (3.3)$$

where $G=I_{arc}/E_{arc}$ is the arc conductance per unit length of the arc, and α and β are the undetermined constants.

The Francis equation is identical to what is known as the Cassie equation [12] in theories of circuit interruption for gas-blast circuit breakers. This equation, as well as the Mayr equation, has been used to describe the effect of conduction losses in an arc whose radius is assumed to be determined by convective flow [99]. The Mayr equation is:

$$\frac{1}{G} \frac{dG}{dt} = \gamma E_{arc} I_{arc} - \beta \quad (3.4)$$

where γ and β are the undetermined constants.

In these equations, β is simply $1/\tau$ where τ is the time constant for free decays of an arc. Having obtained the required material functions of density, ρ ; specific heat, C_p ; thermal conductivity, λ ; and the radiation emission coefficient, u ; the value of β may be obtained using the following relation [95]:

$$\tau = \frac{1}{\kappa(5.8/R_w^2 + u/S)} \quad (3.5)$$

where thermal diffusivity $\kappa=\lambda/\rho C_p$ should be considered constant, R_w is the radius of the channel where the arc burns, and S is the heat flux potential calculated as:

$$S_{(r)} = \int_0^{r(r)} \lambda dT \quad (3.6)$$

where T is the temperature. Some authors have considered the value of the time constant to be $100 \mu s$ [123 and 131].

Swanson, in a complex analysis, showed that if thermal diffusivity, κ , is constant, the Cassie-Francis equation is a good approximation when electrical

conductivity, σ , is linear with S , while the Mayr equation is a good approximation if σ is exponential with S as $\sigma = \sigma_0 \exp(bS)$, where b is a constant [132].

The Mayr equation is recommended as valid for low current regions, while the Cassie equation is more representative of higher current regions [136].

3.1.1.4 LTE and Saha's Equation

An enclosure containing a gas or a mixture of gases is considered here. This enclosure should include ions, neutral particles (atoms, molecules), and electrons either excited or not [75]. One whole system would be set at a given temperature, T , and each different particle would have the same mean kinetic energy. At each instant in time, ionization, recombination, excitation or de-excitation, photon emission or absorption, and similar events take place [75]. Equilibrium is attained for a certain value of temperature when all the particles are at the same temperature. The medium is then deemed to be in *Thermodynamic Equilibrium* [75].

In arc plasmas, the energy is transferred to the column by an applied electric field [75, 117 and 119]. Due to their relatively low mobility and high mass, ions are generally little influenced by the presence of the electric field. Electrons are accelerated and transfer their kinetic energy to heavy particles through elastic collisions [75]. From any point of view, heavy particles will never have the same temperature as electrons, and although they may be able to approach electron temperature, they can never reach it [75 and 100]. Considering that the temperature of heavy particles is close to that of electrons, the frequency of elastic collisions between electrons and heavy particles must be as high as possible. This implies a high electronic density. For all these reasons, thermodynamic equilibrium is never achieved in laboratory plasmas [8 and 75]; it is,

however, possible to define conditions for the partial application of certain laws which govern this equilibrium, known as *Local Thermodynamic Equilibrium* (LTE) [75]. The problem of defining the criterion for LTE was the main task of a number of research studies because of the importance of this factor in discharge physics [26, 75 and 108].

In the case of weakly ionized mono-atomic gases (noble gases, mercury vapor, most of the metallic vapors), a further simplification occurs because the phenomenon of ionization takes place without the complications inherent in chemical decomposition. By making certain simplifying hypotheses (such as assuming uniform temperatures within a section of a channel at a constant pressure, in one case), Saha obtained the electronic density, N_e , inside the channel [75]:

$$\frac{N_e N^+}{N_a} = 2 \frac{(2\pi m K_B)^{3/2}}{h_p^3} T^{3/2} \frac{U'(T)}{U(T)} \exp(-eV_i / KT) \quad (3.7)$$

where V_i is the ionization potential of the relevant atom, h_p is Planck's constant, K_B is the Boltzmann constant, N^+ is the density of the ions, and N_a is the density of the atoms. Functions U for the atom and ion are known as "partition functions". The first sum covers all the excited states of the atom while the second one covers all the excited ions. Higher ionized states are disregarded [75].

In a weakly ionized mono-atomic gas, the electron density N_e , and the atom ion density N^+ , are statistically equal to each other [75]. Therefore:

$$N_e \approx \text{Const.} N_a^{1/2} T^{3/4} \exp(-eV_i / KT) \quad (3.8)$$

From this expression, it is relatively easy to deduce an expression for the current:

$$I = N_e e b E \pi a^2 \quad (3.9)$$

where $b \approx \text{Const.} N_a^{-1} T^{-1/2}$ is the electron mobility under the field, E [75].

Using this method to calculate arc conductivity requires an estimation of arc channel temperature.

3.1.1.5 The Elenbaas-Heller Equation

Another way of estimating the arc resistance is to calculate its temperature and then apply the known dependence $\sigma_{(T)}$, thus making it possible to obtain arc conductivity.

The arc is considered to be a cylindrically symmetrical continuous current-conducting rod with a conductivity σ , from which the entire electrical energy supplied per unit volume, σE_{arc}^2 , has been removed because of the heat conduction to the cooled walls of the plasma room. The equation of the energy balance is as follows [5]:

$$\sigma_{(r)} E_{arc}^2 = -\frac{1}{r} \frac{d}{dr} (r\lambda \frac{dT}{dr}) \quad (3.10)$$

where λ is the thermal conductivity and r is the radial distance from the arc center. The boundary conditions for this equation are $T = T_w$ at $r = R_w$, where T_w is the wall temperature and R_w is the radial distance of the wall, for reasons of symmetry, and $dT/dr = 0$ at $r = 0$. By using the heat flux potential concept, S , (cf. Eq. 3.6), it is sufficient to work with a single material function, $\sigma_{(S)}$, instead of two.

This equation is known as the Elenbaas-Heller equation [75 and 119], obtained in 1934 [119], which is a simpler version of the general cylindrical heat transfer equation. In the latter, the net energy loss per unit volume due to radiation and radial convection, as well as the storage energy in the channel, was disregarded.

The combination of this equation and Ohm's law with the known dependences $\sigma_{(T)}$ and $\lambda_{(T)}$ (Figs. 3.4 and 3.5 [119]) make it possible to determine the temperature

distribution over a channel section for an electric field, E , applied to the arc. Because of the known distribution of $\sigma(T)$, once the temperature distribution is found, it becomes possible to calculate the total current of the arc, $I_{arc} = 2\pi E_{arc} \int_r \sigma(r) r dr$, the electrical power $P_{arc} = E_{arc} I_{arc}$ consumed by the arc, the average conductivity of the cross-section, the heat transfer rate to the wall of the plasmatron, and most other applicable data.

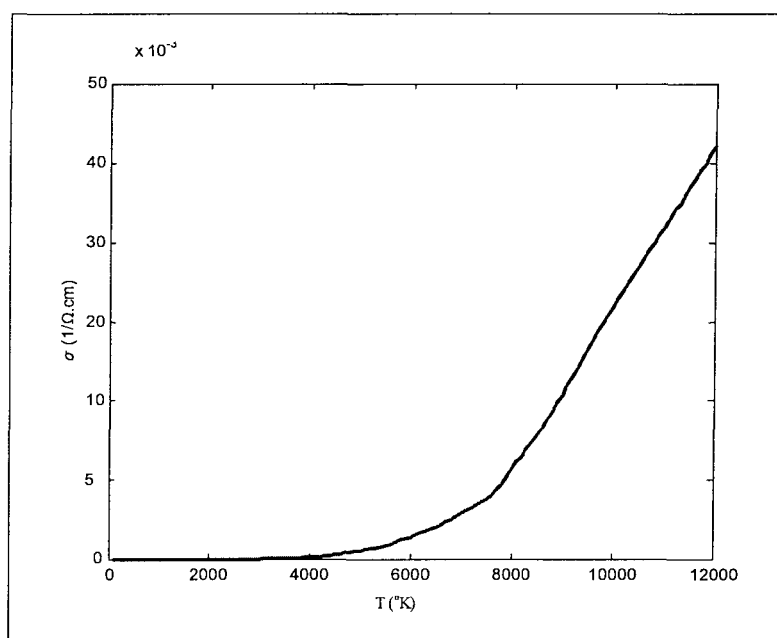


Figure 3.4 Temperature dependence of the electrical conductivity of nitrogen plasma at atmospheric pressure [119].

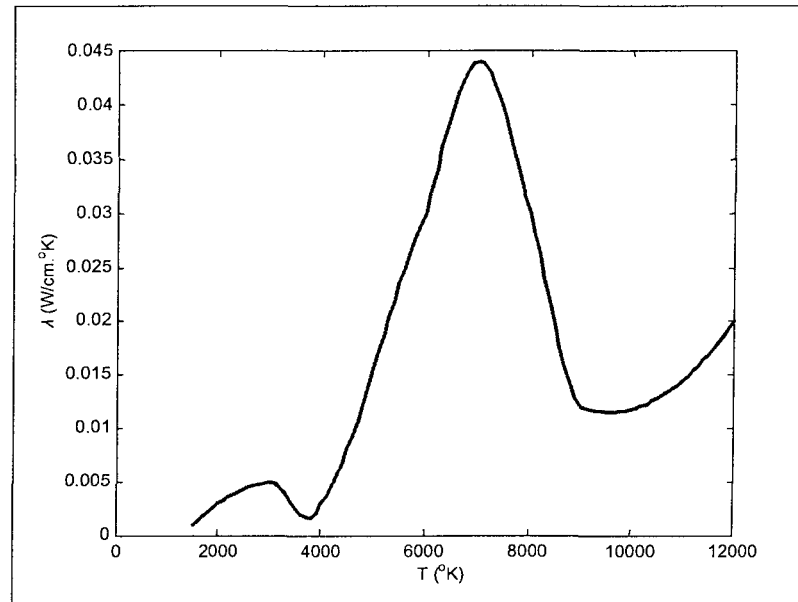


Figure 3.5 The dependence λ_{T} as a function of temperature [119].

Several analytical methods for solving this equation have already been presented. Parabolic [75], Logarithmic [75] and Channel models [55], Maecker's linearization method [96], the Zone-wise linear approximation [66], and a two-layered quasi-channel model [145] are among these.

These various formal methods are based on linearizing and/or splitting the integration domain into sub-domains. Certain further assumptions (such as the *Steenbeck's minimum principle*) are also necessary for solving the equations [55].

If the steep slope of the function $\sigma_{(T)}$ is taken into account, heat convection corresponds to a not too large temperature drop along the channel. For example, assuming that the arc current is weak, that the temperature and degree of ionization of plasma is low, and that electron-atom collisions affect the resistance more than electron-ion collisions, then the channel conductivity is proportional to electron density; and if ionization is thermodynamically in equilibrium, then electrical conductivity can be

approximated by an exponential relationship. For air, at $p = 1$ atm., in a temperature range of 8000 – 14000 °K, this relationship is considered as [119]:

$$\sigma_{(T)} = 0.83 \times 10^2 \exp(36000/T[K]) \quad 1/\Omega \cdot \text{cm} \quad (3.11)$$

Using the above-mentioned relationship and several further assumptions, Raizer obtained an arc characteristic equation as follows [119]:

$$E_{arc} = \frac{K_1}{I_{arc} [K_2 - \ln(I_{arc} / R_t)]^2} \quad (3.12)$$

where K_1 and K_2 are constants, I_{arc} is the arc current, and R_t is the tube radius. The arc channel radius relationship is then [119]:

$$r = K_r (I_{arc} / R_t)^{1/2} \quad (3.13)$$

where K_r may be considered constant.

It should be noted that the Elenbaas-Heller equation may be applied to confined plasmas, where a steady regime of heat transfer is established. In this type of arc, the current range is much higher than 1 A and the temperature is far removed from 5000 °K (maximum), as is typical of characteristic flashover arcs [2, 80 and 115]. The applicability of this equation to open propagating arcs, however, is doubtful. In a propagating arc, the heat transfer is still transient and cannot yet be deemed steady.

3.1.1.6 Numerical Solution

The general energy balance equation which applies to all volume elements of the arc is [95]:

$$\rho C_p \frac{\partial T}{\partial t} = \sigma E_{arc}^2 - U + \frac{1}{r} \frac{\partial}{\partial r} (r \lambda \frac{\partial T}{\partial r}) - \rho C_p v_z \frac{\partial T}{\partial r} \quad (3.14)$$

The terms on the right hand side are, successively, the input energy due to the electric field E_{arc} , and the net energy loss per unit volume due to radiation, thermal conduction, and radial convection where v is the radial velocity. This equation may be solved using different numerical methods such as the finite element. The boundary conditions are the same as the Elenbaas-Heller boundary conditions.

A numerical solution of this equation has shown that even under stationary confined plasmas, the central temperature of the arc may not exceed 6000 °K (cf. Fig. 3.6). In this model, for the sake of simplicity, the current instead of voltage was considered to be the independent parameter [95].

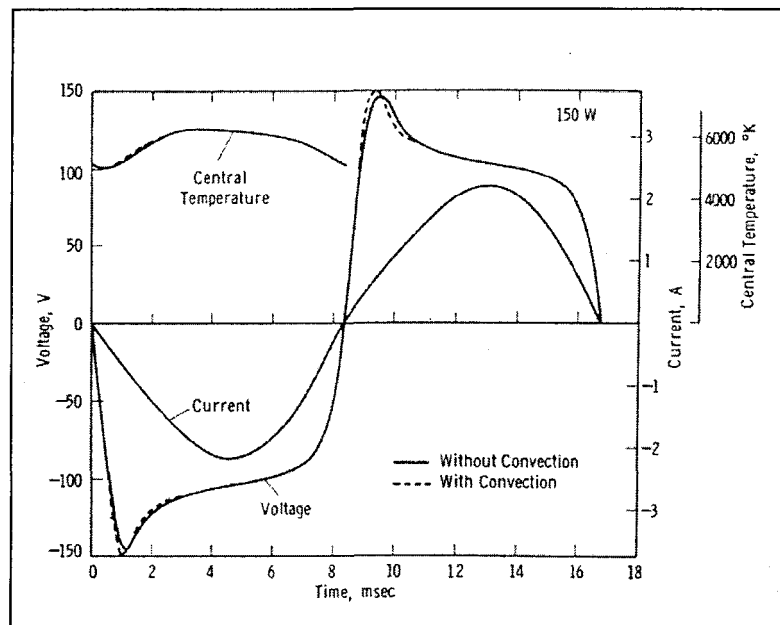


Figure 3.6 Variations of central temperature and voltage of arc versus time for a 1.5 A mercury arc [95].

3.1.2 Resistance of the Conductive Surface

3.1.2.1 Form Factor Concept

The total resistance of a polluted surface, covered with a uniform conductive layer of a surface conductivity γ_s , may be written:

$$R_p = \frac{1}{\gamma_s} \int_0^{L-x} \frac{dl}{\pi D(l)} \quad (3.15)$$

where dl is the element of the leakage path, $(L-x)$ is the total length of the unbridged leakage path, and $D(l)$ is the insulator diameter at dl increment.

The integral term of the above-mentioned equation is known as the Form Factor, $F(x)$, of the insulator. This factor is a characteristic of the insulator where its value is a parameter of insulator geometry, and the type and value of the conductive layer have no influence on it (cf. Fig. 3.7). This concept was used by Obenaus and Boehme in their composite layer model to calculate the resistance of polluted surfaces [6]. A number of other authors made use of this concept [1, 3, 22, 81, 118, 123, 131 and 142].

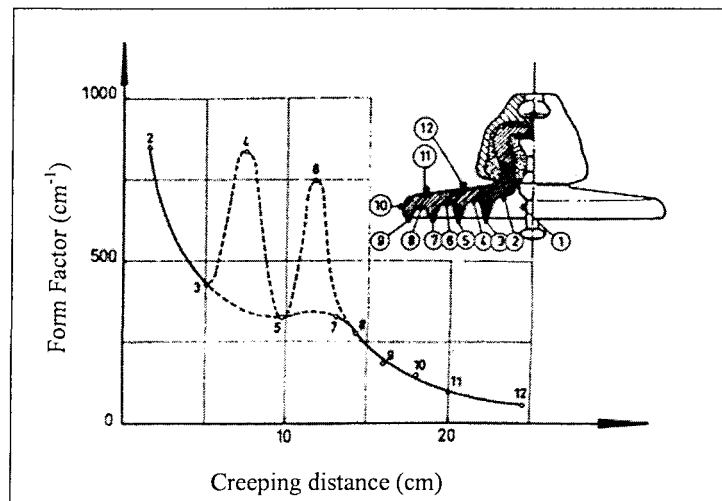


Figure 3.7 Form Factor plotted against creeping distance for a cap and pin insulator [22].

3.1.2.2 Circular Disc Model

Woodson and McElroy used the geometry of Figure 3.8 to express the resistance of a wet polluted surface of a disc insulator [143]. By disregarding the arc radius effects, the result may be written as:

$$R_p = \frac{\text{const.}}{\gamma_s} (r_o - r_a)^m \quad (3.16)$$

where *const.* and *m* were experimentally determined subsequently as 1.6×10^{-2} and 1.4, respectively.

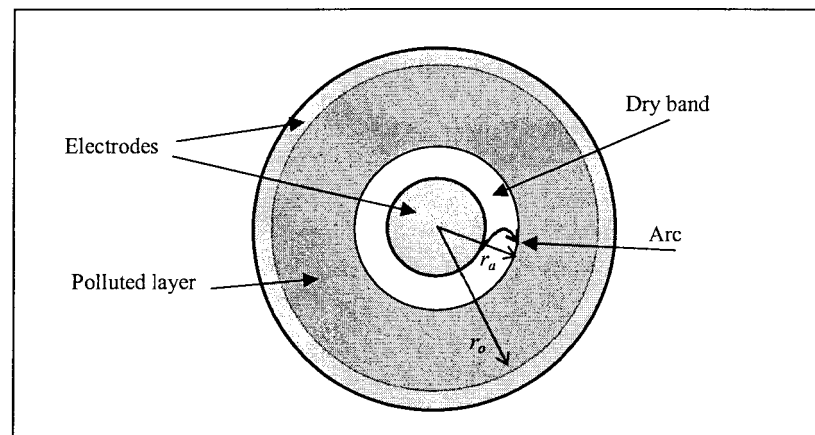


Figure 3.8 Disc insulator model as studied by McElroy [143].

3.1.2.3 The Wilkins Equations

Näcke was the first to investigate the effects of current concentration at the arc root on the resistance of a conductive wet layer [106]. Assuming the discharge root to be circular, as shown in Figure 3.9, the calculation of the polluted surface resistance between each discharge root and its corresponding electrode, R , becomes a 2-

dimensional Laplacian field problem which may be solved using the theory of conjugate functions. His relationships for pollution resistance were composed of two parts, one internal due to the two semicircles, and an external resistance between the two semicircles representing the outer boundaries of the arc foot points.

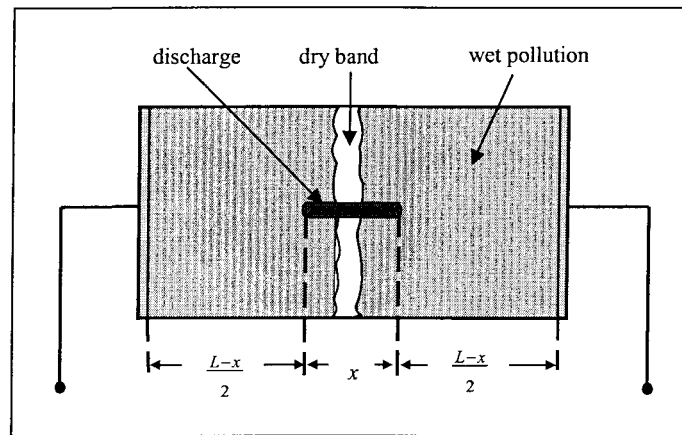


Figure 3.9 The Wilkins model for flashover of a polluted strip [142].

These solutions were developed by Wilkins who obtained two cases of interest [142]:

- (a) The narrow strip, where the width of the series resistive layer is less than its length. For this case, the series resistance is given by

$$R_p = \frac{1}{\pi\gamma_s} \left\{ \frac{\pi(L-x)}{w} + \log \frac{w}{2\pi r} \right\} \quad (3.17)$$

where r is the radius of the discharge root, and w is the width of the pollution band assumed to be constant.

- (b) The wide strip, where the width of the series layer is greater than three times its length. For this case,

$$R_p = \frac{1}{\pi\gamma_s} \left\{ \log \frac{2L}{\pi r} - \log \left(\tan \frac{\pi x}{2L} \right) \right\} \quad (3.18)$$

In order to calculate r , Wilkins established the relationship between the arc root current and its radius as:

$$\frac{I_{arc}}{\pi r^2} = k \quad (3.19)$$

where k is a constant [142].

3.1.2.4 Plane Model

In an attempt to represent the pollution surface resistance of a cap-and-pin insulator, Zhicheng and Renyu replaced the cap-and-pin insulator with a plane model as shown in Figure 3.10 [150].

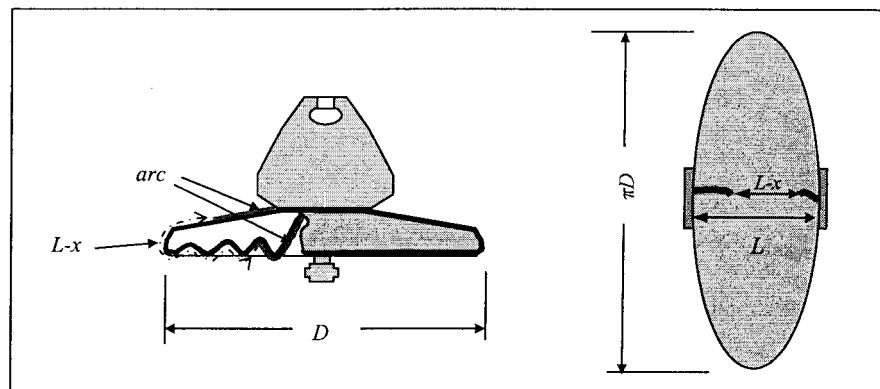


Figure 3.10 Cap-and-pin insulator and its plane model [150].

If the plane model of an insulator is wide enough, the resistance of the remaining polluted layer between the two arc roots may be expressed as the resistance between

two small circular electrodes. Through further simplification, the following simple expression for the resistance of the polluted layer was obtained:

$$R_p = \frac{1}{\pi\gamma_s} \ln \frac{L-x}{r} \quad (3.20)$$

3.1.2.5 Dry and Polluted Band Impedance

The geometry shown in Figure 3.11 was used by Mekhaldi *et al.* to establish a semi-empirical model [102].

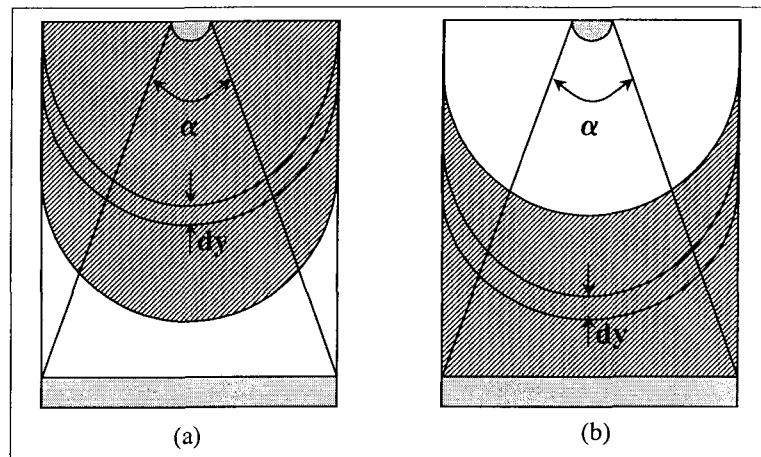


Figure 3.11 Plate model and pollution band, (a) near HV, and (b) near ground electrodes [102].

It was assumed that the surface of the insulator is covered by a dry band in series with a polluted band. The polluted band is situated either near the HV electrode or near the ground electrode. The impedance of the dry band was expressed by the following empirical relationship:

$$Z_d(y) = Z_{0d} \left[\frac{L-y}{L} \right]^{0.42} \quad (3.21)$$

where y is the length of the polluted band, L is the total length of the plate, and Z_{0d} is the measured impedance of the clean plate.

In order to simplify the model, the impedance of the polluted band was assumed to be resistive, and thus the following relationship for the polluted band resistance was obtained:

$$R_p(y) = \frac{K_t}{\gamma_s} \log \left[\frac{R+y}{R} \right] \quad (3.22)$$

where R is the HV electrode radius, γ_s is the surface conductivity, and K_t is a constant.

The equivalent impedance, Z_t , between the electrodes may then be expressed as:

$$Z_t(y) = Z_d(y) + R_p(y) \quad (3.23)$$

For $L = 40$ cm and $R = 2.5$ mm, K_t was experimentally found to be 8.26×10^8 [102].

3.2 Static Modeling

3.2.1 DC Static Models

Based on the model of the simple circuit shown in Figure 3.1, as proposed by Obenaus, the governing equation of this circuit leads to:

$$V = V_{ap} - V_e = V_{arc} + R_p I_{arc} \quad (3.24)$$

where V_{ap} is the voltage applied to the circuit, and V_e is the total electrode voltage drop. Glow-to-arc transitions were observed for currents of the order of 100 A only, therefore V_e may be considered as a constant [118]. In this equation, I_{arc} represents the arc current, while the circuit implies that the same current which passes through the arc will also pass through the conductive layer. Thus, the DC flashover voltage of an insulator may be obtained when both of the following equations are satisfied:

$$\frac{\partial V}{\partial I_{arc}} = 0 \quad (3.25)$$

$$\frac{\partial V_m}{\partial x} = 0 \quad (3.26)$$

where V_m is the solution to the first equation as a function of length. The solution to the second equation provides the critical voltage, V_c , and the length, x_c , corresponding to this critical voltage. At this point, the value of the critical current, I_c , may be obtained using the circuit equations. In order to solve the above-mentioned equations, appropriate relationships for the calculation of arc voltage and the resistance of the conductive layer are required.

Obenaus developed these equations using Ayrton's equation for the arc, and a fixed resistance for a polluted surface, R_p , so as to obtain the appropriate relationship for critical arc length [111]. His research was later developed further by Boehme who found an expression for the minimum direct voltage, V_{cx} , which is able to sustain an arc over a certain length, x [7].

The equations were subsequently developed even further by Neumärker [109], and Alston [3] using the same concept and applying a uniform pollution resistance per unit of length, r_p , thereby obtaining the closed form of a set of equations with which to calculate critical values of voltage, length and current. A visual illustration of the above-mentioned solution may be seen in Figures 3.12 to 3.14.

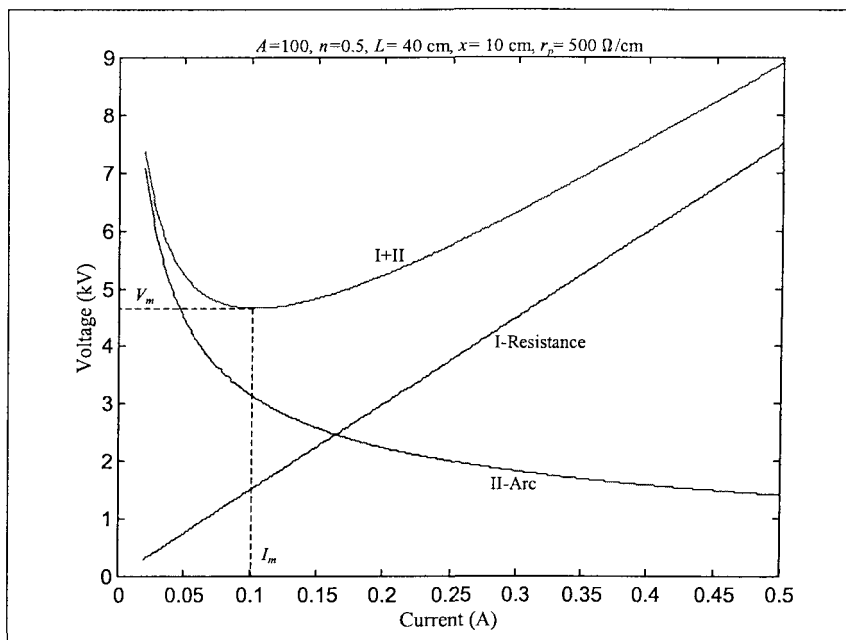


Figure 3.12 Typical arc and uniform conductive layer resistances in a given arc length.

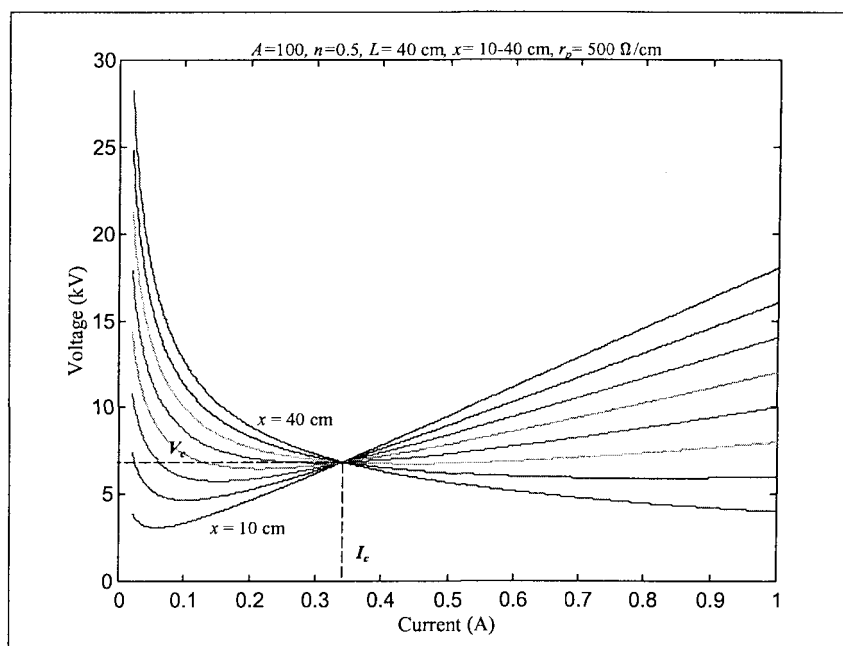


Figure 3.13 Typical arc and uniform conductive layer resistances for a variety of arc lengths.

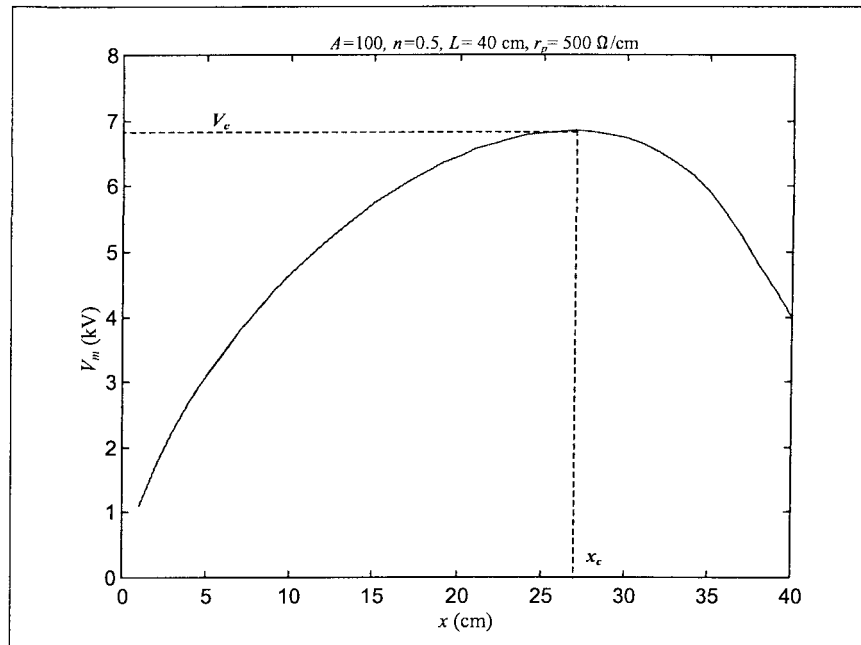


Figure 3.14 Critical arc voltage and length.

Figure 3.12 shows the arc and pollution voltages for a certain length of arc, x , followed by the sum of these two resistances. In this figure, V_m is the minimum voltage which is necessary to sustain an arc along x . Similar curves for different lengths of the arc are illustrated in Figure 3.13 while Figure 3.14 shows the V_m curve for the different values of x , as obtained from Figure 3.13. It will be observed that, for a certain arc length, x_c , the necessary applied voltage able to sustain the arc length along this length, V_c , is the maximum when compared to the other values of V_m , even for greater x lengths. The values of V_c and x_c are called the critical flashover voltage and the critical arc length, respectively. Thus, it may be concluded that: *if* the relationships that govern the arc phenomenon are such as shown in Figure 3.12, then a critical arc length exists, and *if* the applied voltage is high enough to sustain the arc along this length, then no

further voltage is required to reach the flashover point, and therefore flashover will inevitably occur under this voltage.

Using Wilkins' equations to calculate the critical flashover voltage of wide and narrow polluted strips provides results of different values. Given the same test-object characteristics as were used to obtain Figures 3.12 to 3.14, with a narrow polluted strip of different bandwidths, the simulation produced flashover results as shown in Figure 3.15. In order to obtain the arc radius, Wilkins' concept was once again applied, where the current density is a given constant $k = 1.45 \text{ A/cm}^2$ [142]; the pollution layer resistance was obtained using Eq. 3.17; and w is the bandwidth of a polluted surface. In order to compare the results, the same curve as Figure 3.14 is inserted in the figure, having been obtained using the form factor concept.

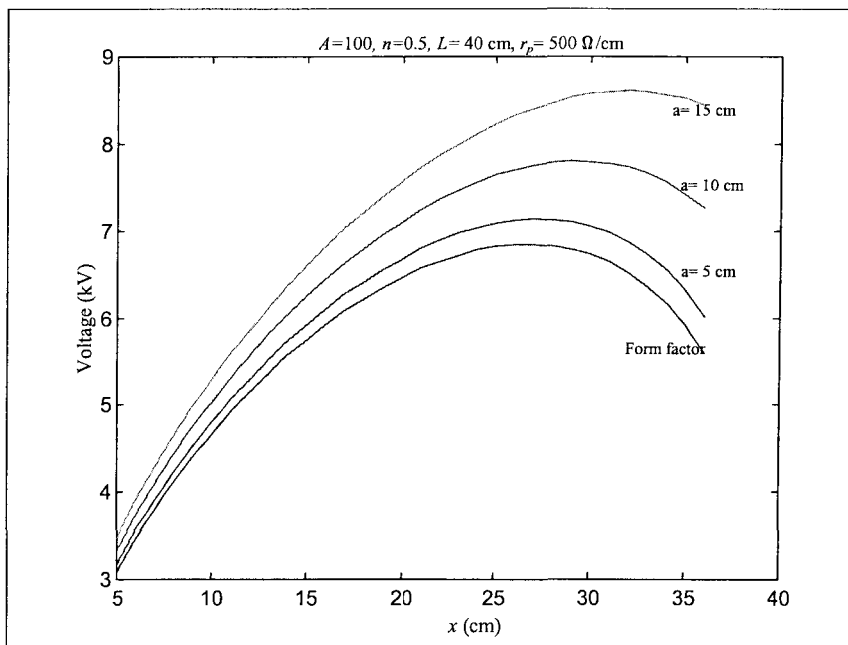


Figure 3.15 Arc characteristics for a narrow-strip polluted band using Wilkins' equation.

Figure 3.16 shows the same simulation made for calculating a wide pollution band where the pollution resistance was obtained using Eq. 3.18.

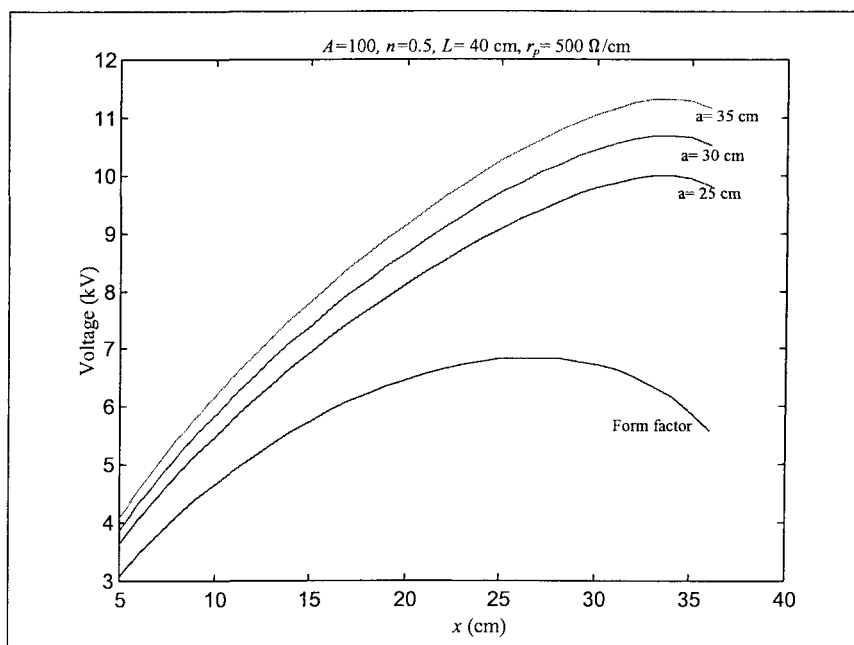


Figure 3.16 Arc characteristics for a wide-strip polluted band using Wilkins' equation.

From Figures 3.15 and 3.16 it will be observed that, by taking into account the effects of arc current concentration in the root for both narrow and wide strips, not only does the critical length change drastically, but so do the critical voltage values; whereas for the wide strip, the deviation of the results from those obtained with the form factor method is noticeably greater where the critical length concept is no longer applicable, and this length then increases to reach almost the total length of the insulator.

Static modeling does not take into consideration the physical mechanism involved in arc phenomena. It will be observed, from Figure 3.13, that at any arc length, when the voltage applied to the insulator is higher than V_m , the arc *may* or *may not* be sustained along this length, and thus the arc elongation from each length to a new

greater length is not certain for lengths less or greater than critical length. Theoretically speaking, even applying voltages which are higher than the critical voltage, does not ensure that the arc will propagate to the next electrode and thus lead to flashover; therefore the arc may be considered stationary at any given length for any undefined time period.

3.2.2 AC Static Models

Since, under AC applied voltages, flashover occurs around the peak value of the applied voltage [3], the same analysis of DC applied voltage is used to calculate the AC critical flashover voltage [3 and 122]. On the other hand, during the voltage cycles before the last propagating cycle is reached, the arc current drops to zero, and the arc voltage required to re-ignite the arc depends on the initial arc characteristics and the remaining polluted conditions.

In order to take into account the effects of arc re-ignition, an experimentally based relationship was proposed and used by Claverie to calculate the minimum voltage, V_{peak} , able to re-ignite the arc which carries the current, I_{peak} , along the length x , as follows [22]:

$$V_{peak} = \frac{Kx}{I_{peak}^b} \quad (3.27)$$

where K and b are constants. Different authors based their calculations on different values for K and b , but these were generally set at 800 and 0.5, respectively, for polluted insulators [122], and 1118 and 0.53, respectively, in ice models [40]. Thus it was considered that, when an arc occurs under AC voltage, the current and the voltage are calculated using DC relationships (Eqs. 3.25 and 3.26). If the above-mentioned

condition (Eq. 3.27) is not satisfied, however, the arc will not be able to stabilize or to extend.

This type of model is considered to be experimental, since it does not refer to any specific physical mechanism by which the AC arc is maintained, and it is based solely on experimental results. Based on Mayr's equation, Maikopar established an analytical formula in order to calculate the minimum voltage, U_c , necessary to sustain an arc at any position along an insulator of length, L , covered with a pollution layer of a resistance per unit, r_p [97]. By using a heat transfer equation in the arc channel, Rizk obtained an equation for calculating the same parameter as follows [122]:

$$\frac{U_c}{L} = 23r_p^{0.4} \quad (3.28)$$

It should be noted that this relationship was obtained using a combination of experimental results and analytical evaluation.

3.3 Dynamic Modeling

In order to develop a realistic arc model, it is necessary to adopt a dynamic approach where a model is based on the physical processes constituting the phenomena. The model should consist of mathematical equations formulated from considerations of these processes, so that the model performance is likely to be accurate over a wider range of operating conditions.

The study of arc processes has so far been implemented using static models, for the greater part, yet most of the parameters involved in the phenomenon tend to change over time. Dynamic models may be used in order to better understand the evolution of arc parameters, and mainly arc current itself, as a function of time. In this type of

modeling, physical laws are used to establish the propagation criterion of the arc, and to study the dynamics of the discharge, mainly arc velocity. A typical flowchart of dynamic models may be seen in Figure 3.17.

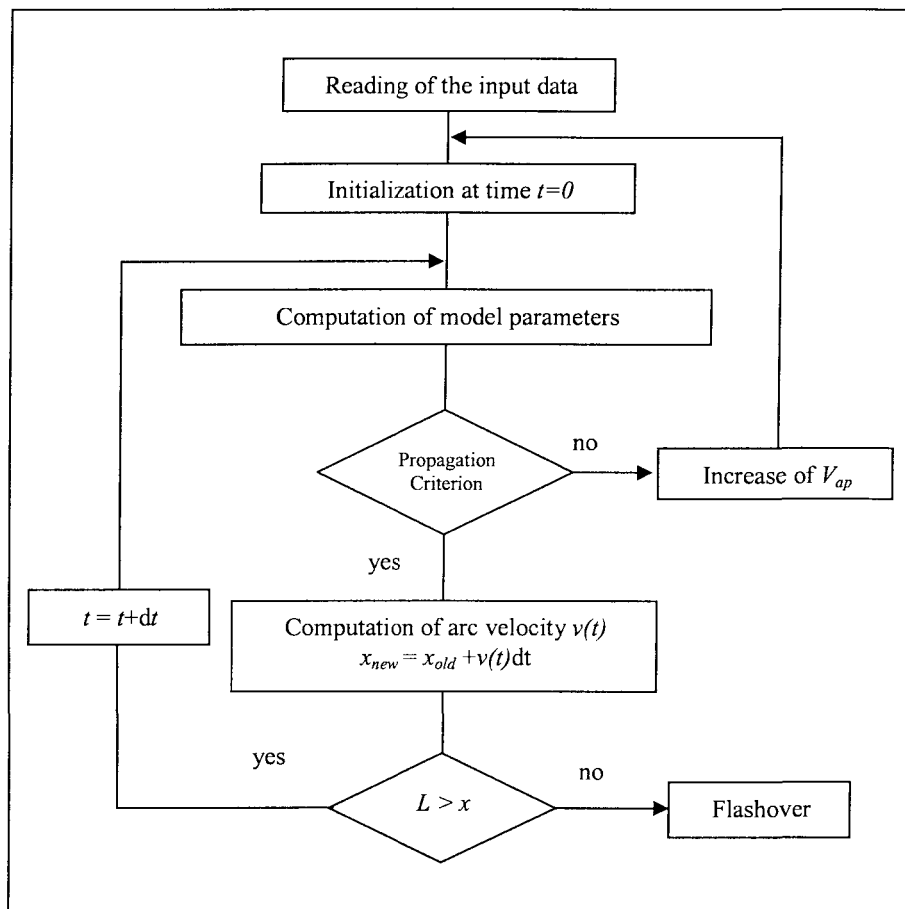


Figure 3.17 General flowchart of a dynamic model.

Input data include the conductive layer characteristics and insulator geometry. A physical hypothesis and a principal model may be used in order to initialize the model equations and to compute different parameters such as current. The *Propagation*

Criterion and *Velocity Relationship* are two essential parameters of dynamic models, as may be seen from the flowchart.

3.3.1 Arc Elongation Mechanism

A number of suggestions have already been presented to explain the mechanism responsible for arc elongation [1, 70, 73, 81, 94, 105, 111, 112, 118 and 141]. These include such aspects as the electrostatic, thermal or magnetic forces which pull the arc along the surface, the drying of the wet film known as dry band mechanism, and the ionization processes occurring ahead of the arc tip. A mechanism proposed by Wilkins [141] for arc propagation on the electrolyte surface may be described as *elongation by ionization and successive root formation*, and will be explained by referring to Figure 3.18. The theory states that elongation is produced by new ionization pathways created at the partial arc root. There is a greater probability of ionization occurring immediately ahead of the partial arc root, owing to the high temperature and high electric field strength in this region.

If the ionization rate is high enough, some current may flow through the ionized pathway ahead of the partial arc root as shown in Figure 3.18 (b). A new current pathway carrying a current, i_d , is then established, in parallel with the conductive film layer current, i_w .

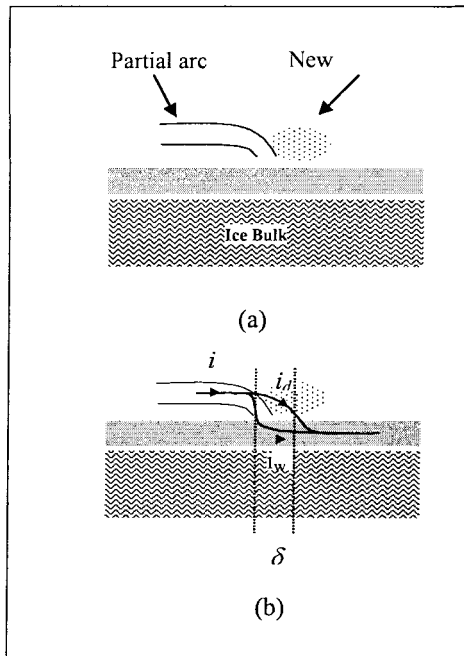


Figure 3.18: Wilkins' proposed mechanism of elongation [141].
 (a): Ionization ahead of the partial arc tip
 (b): Possible current pathways

The conductivity of the new pathway increases with an increase in current, while the conductivity of the water film pathway remains roughly constant, and thus the total current will gradually divert to the new path, producing an elongation of the discharge, δ . This theory seems to be in agreement with previous studies performed by Gallimberti *et al.* [63]. The latter suggest that discharge propagation over insulating surfaces is mainly controlled by increased ionization and attachment coefficients. Due to similarities, Wilkins' model can be applied to the arc propagation phenomenon on ice surfaces, where the conductive surface is considered to be the electrolyte, or water film.

3.3.2 Arc Velocity Models

The following sections recapitulate the main mathematical models established over the years to account for discharge propagation velocity on insulating surfaces.

3.3.2.1 The Al-Baghdadi Model

From high-speed camera studies of an arc propagating over a polluted surface, Al-Baghdadi *et al.* derived the following empirical formula [1]:

$$v(t) = 1.5 \times 10^{-4} r_p^{2.5} (I_{arc}^4 - I_c^4) \quad (3.29)$$

where r_p is the pollution resistance per unit length, I_{arc} is the leakage current, and I_c is the critical current. This relationship, in its original unmodified form, seems to be valid only for the insulator profiles used by the authors.

3.3.2.2 The Tominaga Model

In a theoretical and experimental investigation of the contamination flashover of model plates, Tominaga assumed that arc propagation takes place as a result of the successive drying and breakdown of the electrolytic pollution layer, and that a minimum power density, P_o , is required for arc growth as follows [134]:

$$v(t) = K_s (\zeta E_{pr}^2 - P_o) \quad (3.30)$$

where K_s represents a parameter proportional to the arc radius, ζ is the volume conductivity of the pollution layer and is a function of temperature, E_{pr} is the electric field in the vicinity of the arc foot point, and P_o is the energy required for arc growth.

According to Rizk, this mechanism cannot have general applicability, since it does not even explain arc growth along a water column.

3.3.2.3 The Jolly *et al.* Model

Based on investigations performed on electrolytic surfaces, Jolly *et al.* assumed that the energy required for the creation of a new arc length comes from the electrode voltage drop at the water surface, as follows [82]:

$$v(t) = \frac{V_e I_{arc}(t)}{Q} \quad (3.31)$$

where V_e stands for the electrode voltage drop, $I_{arc}(t)$ is the arc current, and Q is the arc energy content per unit length.

Even though satisfactory agreement may be found between theoretical and experimental data, one drawback prevents it from global applicability since, according to the model, a stationary arc ($v = 0$) would have no electrode voltage drop [122].

3.3.2.4 Arc Mobility Model

This model which determines arc velocity as a proportional function of the electric field within the arc reads as follows [131]:

$$v(t) = \mu E_{arc} \quad (3.32)$$

where μ is arc mobility (5 to 50 cm²/Vs), and E_{arc} represents the arc voltage gradient. This model seems to be the simplest and has been used in certain dynamic models [131].

3.3.2.5 The Gallimberti Model

From experimental data records, Gallimberti predicted a relationship between I_{arc} and v [119]:

$$v(t) = \frac{I_{arc}(t)}{q} \quad (3.33)$$

where q is the electric charge per unit length of the arc.

This model was originally established for discharge on long air gaps and it has been used recently to simulate arc speed over a polluted insulator surface [60]. The fundamental shortcoming here, however, is the quantification of the parameter q which, in practice, is not constant throughout the duration of the discharge propagation.

3.3.2.6 Rahal's Model

Rahal supposed that arc displacement is governed by ions which are subsequently accelerated by the total field, $(E_{pr} - E_{arc})$. The mean velocity is therefore proportional to this total field represented by [118]:

$$v(t) = \mu(E_{pr} - E_{arc}) \quad (3.34)$$

where μ represents electron mobility in the arc channel, and E_{pr} is the electric field at the arc root calculated as follows [118]:

$$E_{pr} = \frac{I_{arc} r_p}{2hw} \left[\frac{sh\left(\frac{2\pi r}{w}\right)}{ch\left(\frac{2\pi r}{w}\right)} + 1 \right] \quad (3.35)$$

where h , w , r_p represent the conductive layer thickness, width and resistance per unit, respectively, and I_{arc} and r are the leakage current and arc radius. Experimental evidence has shown that discharge lengthens by photo-ionization. Its velocity, however, was mainly found to be higher than those of charge carriers [120].

3.3.2.7 The Alston *et al.* Model

Alston *et al.* established this model based on the hypothesis that arc lengthening is related to the power available at the arc inception, and also to the energy necessary to create it [3]. Thus:

$$v(t) = \frac{V_{ap}^2(t)}{\sigma r_p^2 (L - x) Q} \quad (3.36)$$

where σ represents the discharge conductance, Q is the arc linear energy density, x is the arc length, and r_p is the pollution resistance per unit length.

Besides the difficulty of quantifying the parameters involved, the general applicability of this mechanism is also questionable, since arc growth should be related to residual pollution resistance instead of to r_p .

3.3.2.8 The Fofana *et al.* Model

Based on energy considerations, Fofana *et al.* derived the following model [56]:

$$v(t) = \left(\frac{\beta}{\varepsilon \rho} \right)^{1/2} \left(\frac{\int I_{arc}(t) dt}{\pi r^2(t)} \right) \quad (3.37)$$

where ρ represents arc channel density, β is the fractional part of the available energy used for arc propagation, ϵ is the permittivity of the medium in which discharge is propagated, and r is arc radius.

To the best of our knowledge, this model is the only one which has been used and validated for discharge propagation in various mediums such as air [56], liquid [58], and polluted [23] and iced [39] surfaces. The parameter β with should be determined with greater accuracy, however, considering that this parameter was not justified in sufficient detail.

3.3.3 Propagation Criterion

A number of models have already been presented elsewhere to establish a criterion for the propagation of an arc on conductive surfaces [122]. According to these models, the condition of propagation relies mainly on the electrical field, arc current or the energy injected from the source.

3.3.3.1 The Hampton Model

In order to obtain an arc propagation condition, Hampton carried out several experiments on a simple model where pollution resistance was replaced by a column of flowing water of constant conductivity. Based on his experimental results, he established that the arc cannot propagate unless the voltage gradient in the water column, E_p , exceeds the voltage gradient in the arc column E_{arc} [70]. Therefore the propagation condition is:

$$E_{arc} < E_p \quad (3.38)$$

If the equations which govern the arc and pollution layer are of the pure resistive form, then under positive applied voltage, this criterion decreases to:

$$r_{arc} < r_p \quad (3.39)$$

where r_{arc} and r_p are the arc and the pollution resistances per unit length, respectively.

3.3.3.2 The Hesketh Criterion

Based on the concept that an arc in series with a wet polluted surface tends to draw maximum current from the source, Hesketh deduced a criterion for arc propagation as follows [73]:

$$dI_{arc}/dx > 0 \quad (3.40)$$

This criterion was firstly presented by Shkuropat [142]. Under certain assumptions, this equation reduces to Eq. 3.39.

3.3.3.3 The Wilkins Criterion

Based on the theory that a system tries to draw the maximum energy from its source, Wilkins proposed a propagation criterion, as follows [142]:

$$dP_s/dx > 0 \quad (3.41)$$

where P_s is the power taken from the source, implying that the arc propagates when the power, P_s , increases with an increase in the length, x . Under constant applied voltage, this criterion reduces to the Hesketh criterion [142].

3.3.3.4 The Anjana *et al.* Criterion

By considering the arc as a gas in LTE, Anjana *et al.* presented a condition necessary for arc propagation [4]. Based on their model, if the total energy taken from the source, E_{total} , is equal to or greater than the energy which is necessary to maintain the LTE in the gas, E_{th} , then the arc will propagate. The condition may then be written as follows:

$$E_{total} > E_{th} \quad (3.42)$$

3.3.3.5 The Ghosh *et al.* Model

By considering a series of parallel multiple arcs, Ghosh *et al.* established a propagation criterion as follows [64]:

$$dR(x)/dx < 0 \quad (3.43)$$

where $R(x)$ is the total arc resistance and x represents the arc length. This basic idea was used later by Dhahbi in order to establish an analytical propagation criterion [23].

3.3.4 Dynamic Models

3.3.4.1 The Jolly *et al.* Model

The first dynamic model able to calculate the temporal evolution of such arc phenomenon parameters as current and velocity was submitted by D. C. Jolly *et al.* [82]. Firstly, based on the Townsend ionization theory, an arc growth mechanism was proposed where the arc propagation was considered to be a result of electrical breakdown in the arc tip region. In order to calculate the electrical field in this region, a combination of Townsend equations was used. Then, by using the basic model shown in Figure 3.19, two governing equations for the circuit may be obtained, since not only the

resistance in series with the arc was considered, but also one other resistance path in parallel with the arc channel was taken into account.

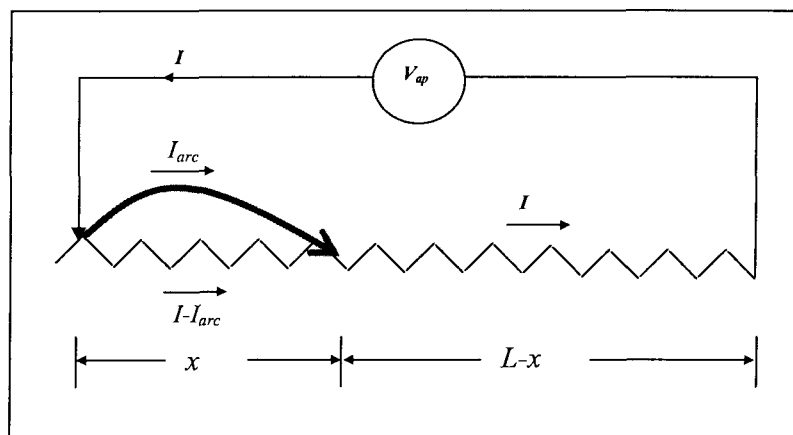


Figure 3.19 Equivalent circuit used by D. C. Jolly *et al.*, for arc propagation modeling [82].

In order to calculate the arc resistance, Mayr's equation (Eq. 3.4) was used, and the pollution resistance was determined using the form factor concept (Eq. 3.15). The arc velocity was calculated using a relationship previously established by the authors (cf. Eq. 3.31). The model was applied to DC voltage sources.

3.3.4.2 The Rizk Model

In order to model the discharge phenomenon on polluted surfaces under DC applied voltage, Rizk *et al.* used a further form of Mayr's equation (Eq. 3.4) to model arc behavior [123]. In their model, the temperature of the electrolyte surface was calculated by considering different terms of energy loss such as evaporation, condensation and convection. This temperature value is necessary to calculate the

electrolyte thickness in order to obtain the surface resistance. This idea was used previously by Wilkins in his static model in order to increase the value of the surface conductivity, since Wilkins' resistance equations (Eqs. 3.17 and 3.18) result in relatively higher values compared to the values obtained using form factor concept. The velocity was calculated using a modified version of Al-Baghdadi's equation (Eq. 3.29). The simulation results reveal the highly satisfactory performance of the model in predicting the influence of protection resistance in series with high voltage electrodes.

3.3.4.3 The Anjana et al. Model

In this model [4], where the basic circuit is the same as Figure 3.1, the arc resistance was calculated using Mayr's equation (Eq. 3.4). The arc propagation criterion was a condition already established by the authors (Eq. 3.42). In order to calculate the arc maintenance energy, the following equation was used:

$$E_{th} = \frac{3}{2} K_B T n \quad (3.44)$$

where K_B is the Boltzmann constant, T is the arc temperature, and n is the number of charged particles in the arc. In order to perform the simulation, the arc temperature, T , was considered constant at 3000 °K, and different values between 1-10 cm²/s/volt were considered for n . Arc velocity was then calculated using the arc mobility model. The method of simulation was based on the dry band mechanism, while the resistance of the polluted layer was calculated using the form factor concept (Eq. 3.15). Simulation results were presented for DC applied voltages [4].

3.3.4.4 The Sundararajan *et al.* Model

The model presented by Sundararajan *et al.* [131] also made use of the Obenaus model (see Fig. 3.1). The arc voltage was calculated using the same form of Mayr's equation (Eq. 3.4) used by Rizk (cf. Section 3.3.4.2) while the resistance of the conductive layer was obtained using the form factor concept (Eq. 3.15). The propagation criterion for arc growth was Hampton's criterion (Eq. 3.38). In order to use this criterion, the electrical field on the polluted surface was calculated using the following equation:

$$E_p = A^{\frac{1}{n+1}} r_p^{\frac{n}{n+1}} \quad (3.45)$$

where r_p is the uniform pollution resistance, and A and n are arc constants. The use of this equation, for critical stress calculation may be viewed as distinctly debatable.

The arc velocity was obtained using the arc mobility model (Eq. 3.32). The only modeling results shown in the work are the critical flashover values of different insulator profiles for DC applied voltages. These results are in satisfactory conformity with experimental results, whereas a simulation of the model shows a diminishing form for arc velocity over time. The model was later developed for application to AC voltages [85].

3.4.4.5 The Dhahbi and Bérroual Model

Based on an already existing model for discharges in long air gaps presented in [56], the researchers used the circuit shown in Figure 3.20 to model the arc propagation phenomenon on insulator surfaces covered with a conductive layer [24].

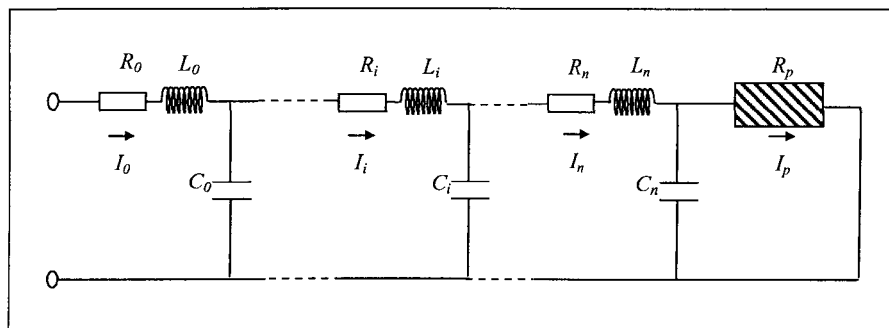


Figure 3.20 Equivalent circuit used for arc propagation modeling [24].

In Figure 3.19, each cell of the RLC elements represents a propagation stage of the arc. When the propagation criterion is met, the arc propagates and a new cell is added to the circuit. In order to evaluate the propagation condition, Eq. 3.39 was used, where, instead of the resistance of the total arc, the resistance of the last cell was considered to calculate r_{arc} . The resistance of each cell was obtained using Mayr's equation (Eq. 3.4). Appropriate relationships were used to calculate the inductance and capacitance of each cell. The resistance of the polluted surface was obtained using both of Wilkins' equations (Equations 3.17 and 3.18). Finally, the arc velocity was calculated using the Fofana *et al.* model (Eq. 3.37). This model was applied to AC, DC and Impulse connected voltages [23].

3.3.4.6 The Farzaneh *et al.* Model for Iced Insulators

Arc propagation on an iced surface involves a different mechanism compared to arc propagation occurring on polluted surfaces. Since an arc propagates on the surface

of an electrolyte, however, the same theory is applicable to modeling arc propagation on ice-covered insulator surfaces. Farzaneh *et al.* presented a simplified self-consistent dynamic model applicable to DC arc development on an ice-covered insulator [39]. The input data of the model were the insulator geometry, ice layer parameters, and certain initial values. The model makes it possible to predict (i) leakage current and corresponding charges, (ii) arc channel radius, trajectory and electric stress, (iii) propagation velocity and energy injected into the air gaps, and, (v) the DC critical flashover voltage of an ice-covered surface. In order to carry out the modeling, the circuit model shown in Figure 3.21 was used.

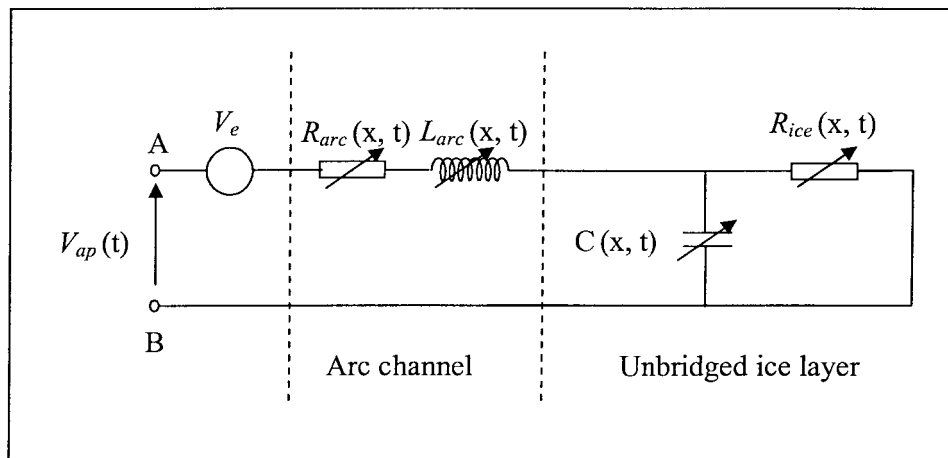


Figure 3.21 Equivalent circuit used for modeling arc propagation on iced surfaces [39].

In this figure, the arc channel is characterized by the impedance consisting of resistance, R_{arc} , in series with inductance, L_{arc} , and capacitance, C , between the arc tip and the opposite electrode. These parameters vary over time in accordance with channel characteristics and the discharge geometry. The residual ice is represented by the

resistance R_{ice} . The value of the electrode voltage drop used in this model for negative and positive arcs on the iced surface was calculated experimentally at 526 V and 799 V, respectively.

In order to calculate the arc resistance, R_{arc} , the classical model of a cylinder with a radius, r , was used:

$$R_{arc} = \frac{x}{\sigma \pi r^2} \quad (3.46)$$

where r may be obtained using the Wilkins model (cf. Eq. 3.19). The arc current density, k , in Eq. 3.19, was determined elsewhere by Farzaneh *et al.* as 1.75 for DC+ and 1.67 for DC- for an arc propagating on the surface of the ice [52]. In order to estimate the channel conductivity, the arc temperature during propagation was considered to be constant. In the absence of a well-developed theory, and also for the sake of simplicity, it was assumed from the outset that a relationship exists between the supplied voltage, V_{ap} (in kV), and the temperature T (in Kelvin), inside the arc core. A series of simulations related to leakage distances of less than 1 m was carried out by the authors. The simulation results showed that the arc temperature may be determined as follows:

$$T = 3.30V_{ap} + 4140 \quad \text{DC-} \quad (3.47)$$

$$T = 4.90V_{ap} + 4100 \quad \text{DC+} \quad (3.48)$$

These equations (3.47 and 3.48) revealed that less voltage is required to reach a given temperature under DC- than under DC+. The model would therefore predict a lower flashover voltage under DC- than under DC+ since experimental observations have shown that DC+ arcs are hotter and thinner than DC- arcs. These experiments were performed by Ishii *et al.* [80] on a physical plane model simulating an insulator

contaminated with sodium chloride. The residual ice surface resistance, R_{ice} , was calculated on the basis of the same approach used for polluted insulators [142] by taking into account the insulator geometry and the constriction of current at the arc root. A number of other appropriate relationships were used to calculate the arc inductance and arc tip capacitance. The arc propagation velocity was calculated using the equation proposed in [56] (Eq. 3.37) and the arc propagation criterion used was the Hesketh criterion (Eq. 3.40) [72].

The simulated data were compared to those experimentally obtained using an ice-covered insulating cylinder covered with artificial ice. The results obtained indicated that this self-consistent model was suitable for describing the dynamic behavior of an arc on an iced surface. The simulation results for leakage current, propagation velocity and arc trajectory were in relatively accurate agreement with those obtained experimentally. Figures 3.22 to 3.25 show the simulation results.

There is also satisfactory agreement between the predicted maximum withstand voltage of a short string of five IEEE standard insulators covered with ice and the values computed from the model. Figures 3.26 and 3.29 show the maximum withstand voltages predicted by the model where the maximum calculated error is about 4% for both voltage polarities [39]. All the Figures were taken from the reference [39].

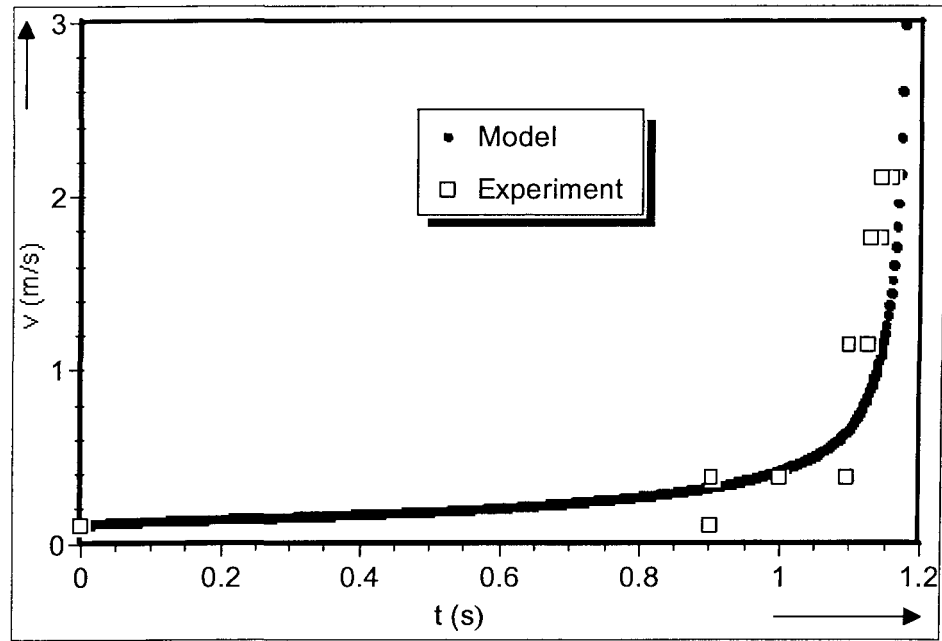


Figure 3.22 Comparison between the measured and computed positive arc velocity.

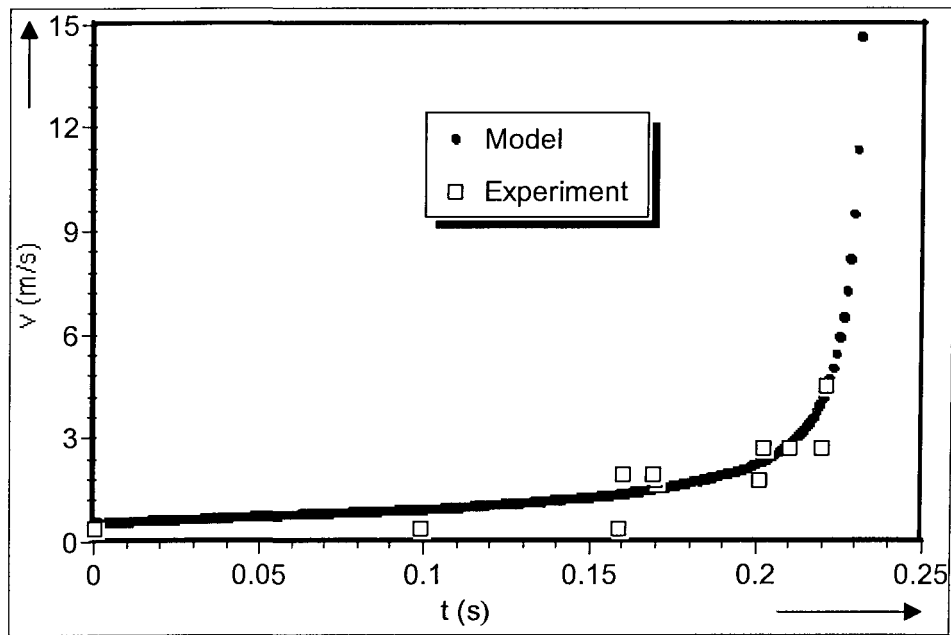


Figure 3.23 Comparison between the measured and computed negative arc velocity.

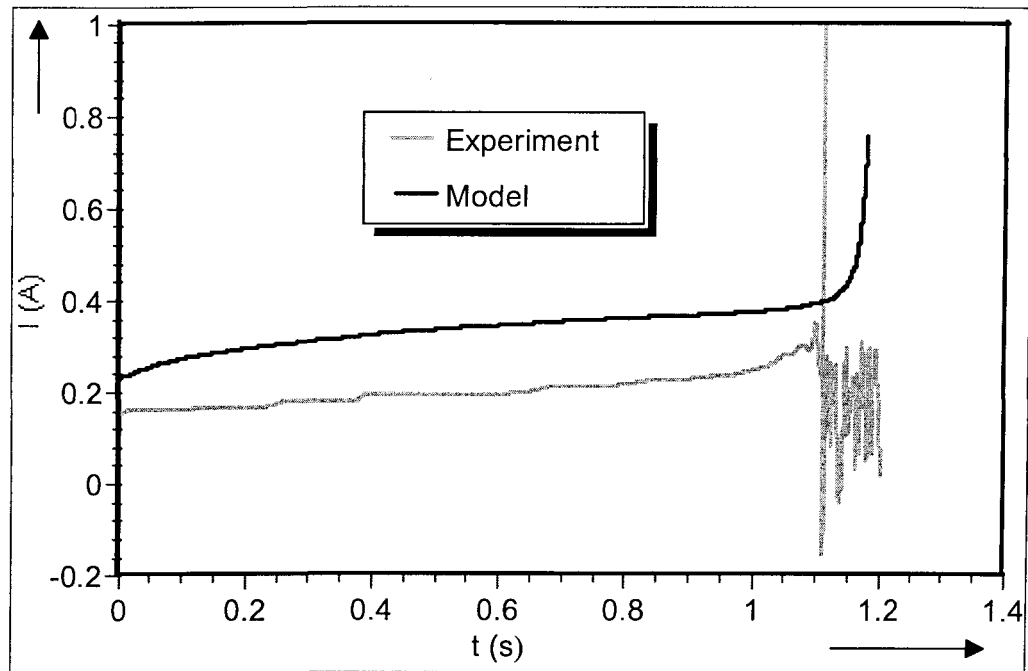


Figure 3.24 Comparison between the measured and computed leakage currents of the positive arc.

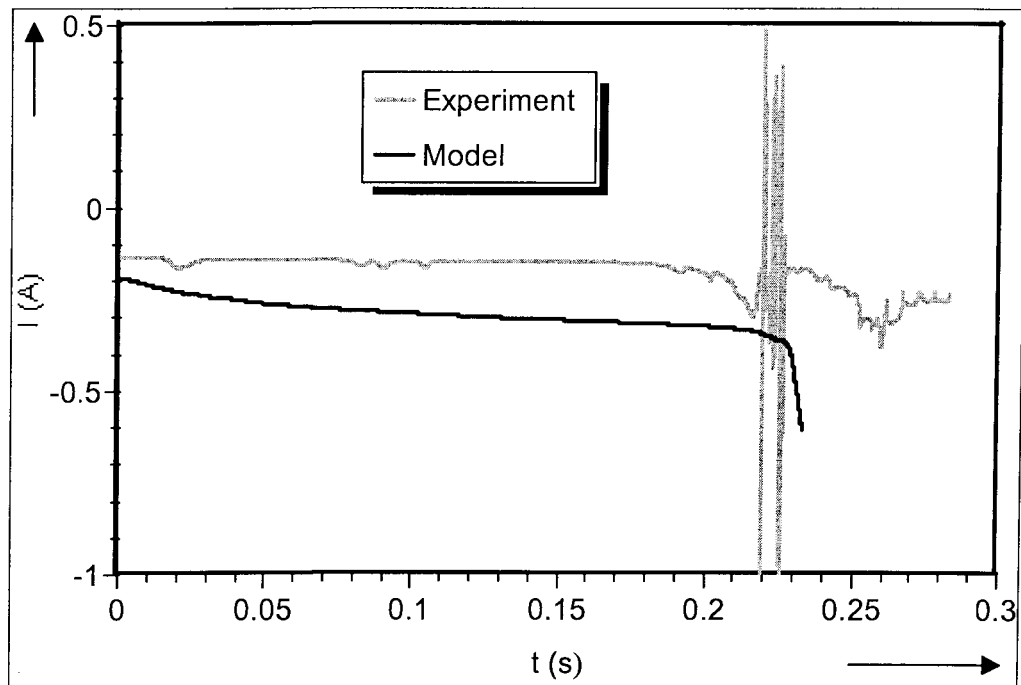


Figure 3.25 Comparison between the measured and computed leakage currents of the negative arc.

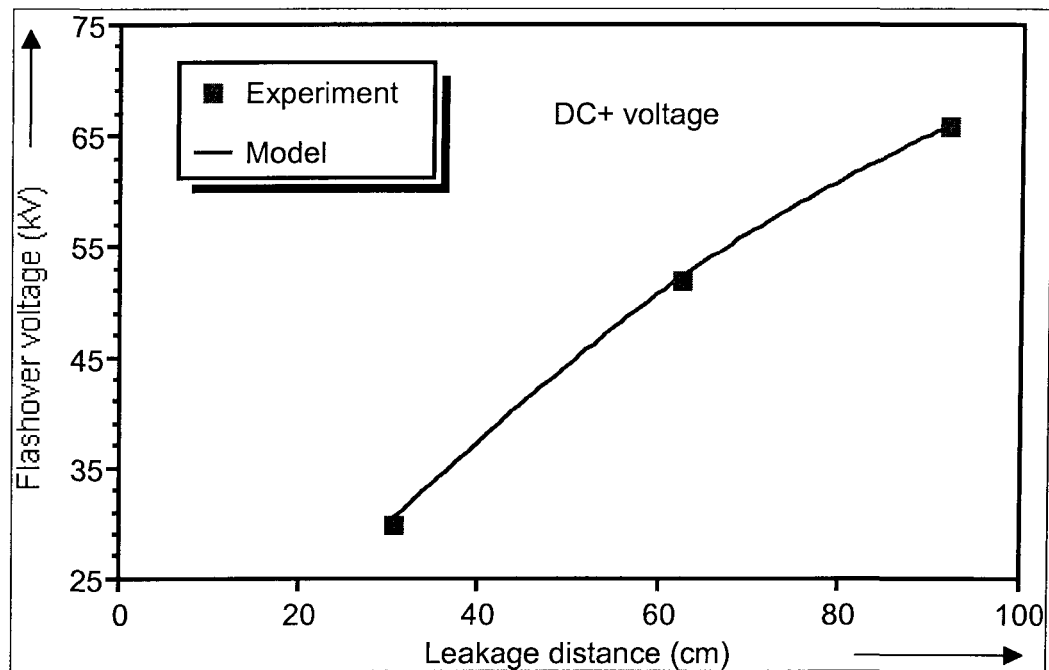


Figure 3.26 Comparison between the critical voltages measured under DC+ for various arcing distances and those computed from the model.

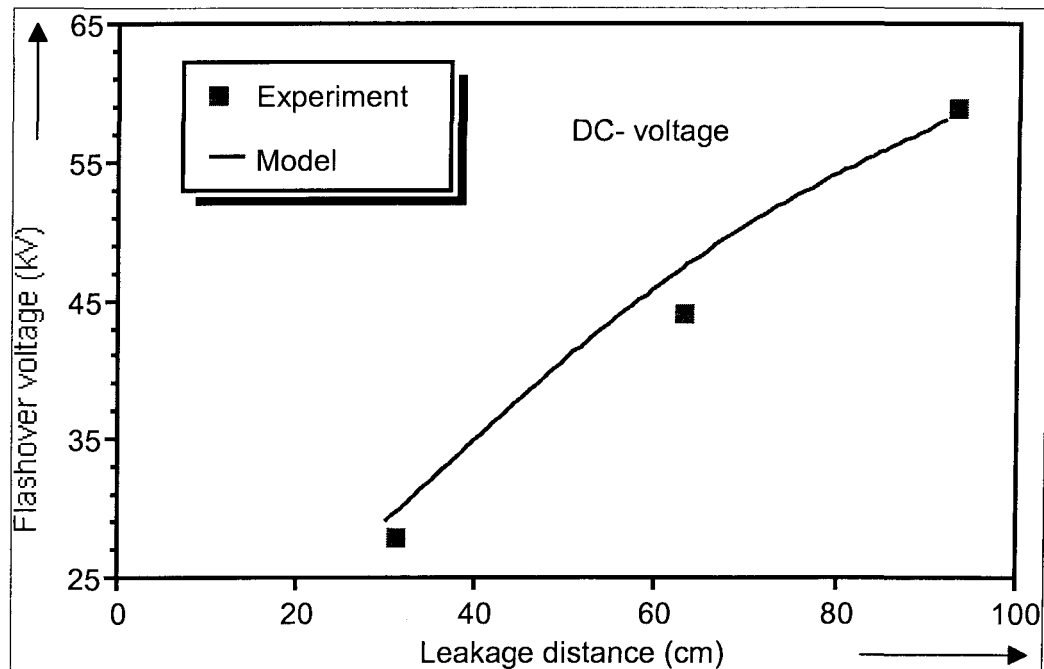


Figure 3.27 Comparison between the critical voltages measured under DC- for various arcing distances and those computed from the model.

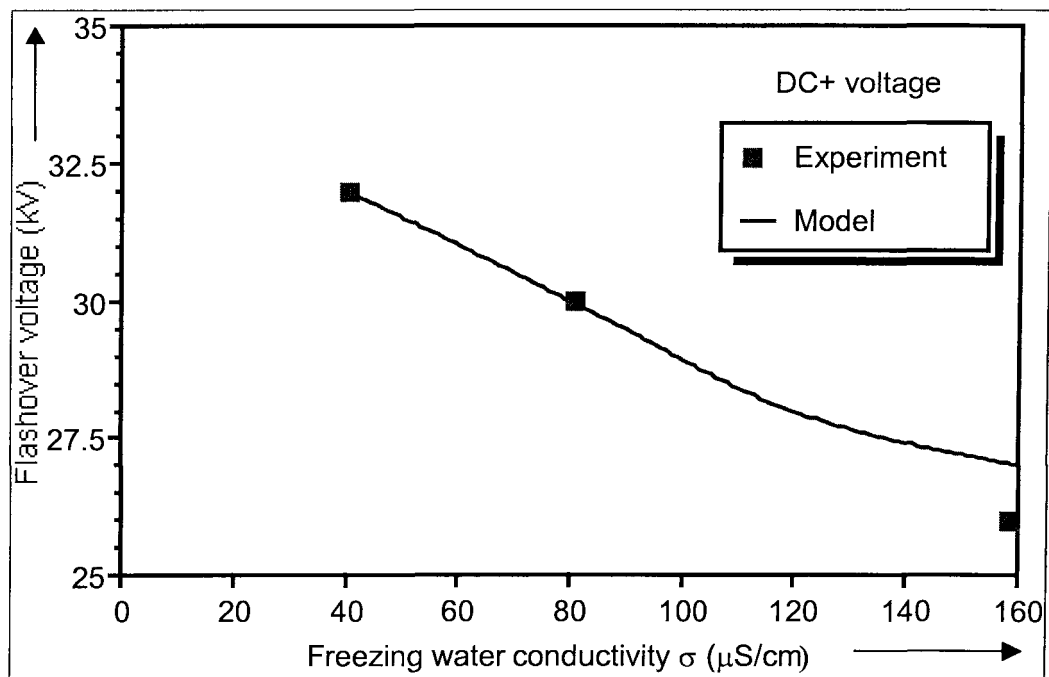


Figure 3.28 Comparison between the critical voltages measured under DC+ and those computed from the model.

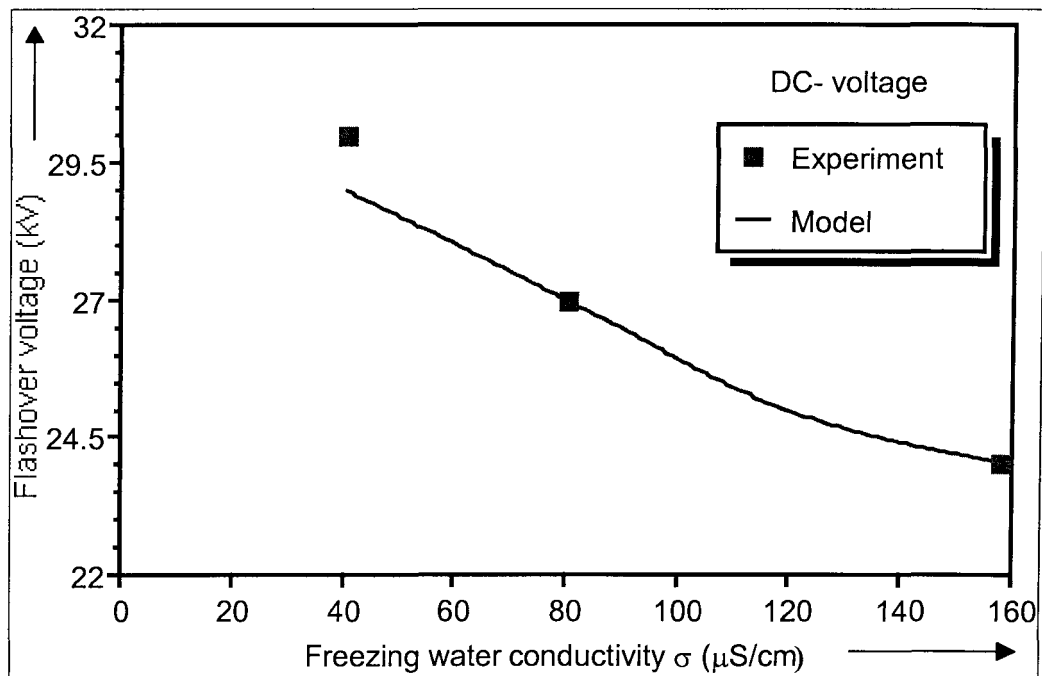


Figure 3.29 Comparison between the critical voltages measured under DC- with those computed from the model.

3.4 Recapitulation of Main Points

As regards the numerous valuable research attempts into modeling of the arc process on conductive surfaces, it may be concluded that:

- Several different models have been used in order to determine arc gradient and conductive layer resistance;
- Almost all of the static and dynamic models are based on the Obenaus concept;
- Static models, in the main, make use of Ayrton's equation, since this equation leads to a simple analytical form of the solution;
- Different investigators used a variety of values for the arc constant and the arc component, and the range of the values used is significant;
- The aim of static models is to calculate the critical flashover voltage although they are unable, as yet, to determine the temporal evolution of arc variables;
- The flashover phenomenon on polluted insulators, and under AC voltage, is considered to occur when the applied voltage is in the vicinity of its peak value;
- Most of the investigators make use of the re-ignition concept to determine the critical flashover voltage, where this condition is purely empirical;
- The *only* existing model that contributes to AC critical flashover voltage calculation of ice-covered insulators is a static model;
- Dynamic modeling is based on the velocity relationship and the propagation criterion where, for each of them, several limited models have been presented to date and used in the literature;
- Very few dynamic models were presented to investigate arc phenomena on polluted insulators. All of these models make use of the Mayr equation. Some of these models make use of an unrealistic and often unfounded sequence of

relationships and considerations. Only two of these models present the temporal evolution of the variables, while the others are barely able to calculate critical flashover voltage. The only model that compares the temporal evolution of the arc current against experimental results was presented for DC applied voltages;

- The only dynamic model presented for studying of the arc process on ice-covered insulators, displays satisfactory performance in simulating the arc variables.

Hence the necessity for designing a dynamic model capable of calculating the arc variable calculation over time, not only for ice-covered insulators, but also for polluted insulators is justified.

CHAPTER 4

AC ARC PROCESSES AND MODELING ON THE SURFACE OF ICE ACCUMULATED ON INSULATORS

CHAPTER 4

AC ARC PROCESS AND MODELING ON THE SURFACE OF ICE ACCUMULATED ON INSULATORS

4.1 The Flashover Process

A thorough understanding of all aspects of the flashover process on electrolyte surfaces is required in order to explore the subject further. Such a task would necessarily involve an examination of the main tenets of the physical, electrical, mechanical, thermal and thermodynamic aspects. To the best of our knowledge, there has been no exploratory research work carried out, to date, concerning the physical mechanisms leading to the flashover of ice-covered insulators. With this fact in mind, therefore, an all-inclusive study of the development of an electric arc should prove to be timely. This type of study would include a discussion of the fundamental mechanism leading to the inception and propagation of partial arcs and their transfer to a relatively high current arc which may lead to flashover as well as to dielectric breakdown conditions.

An ice layer forms in a non-uniform manner on an insulator and it is interrupted by air gaps formed by partial arcs on ice-covered insulator strings during the icing period [40]. These air gaps are usually created in close proximity to the electrodes where the electric field is relatively high [138]. Ice bulk is considered to be non-

conductive [17], whereas an increase in ambient temperature, or some other atmospheric event such as dew, will produce a water film on the surface of accumulated ice which tends to be conductive [40]. The temperature at the ice surface is also strongly influenced by heat exchanges between the ice layer itself and the surrounding air, as well as by known insulator characteristics. At standard atmospheric pressure, the temperature inside a local arc channel is capable of reaching values higher than 4000°K [121]. Under such conditions, the leakage current on the ice surface, at air temperatures even below 0 °C, tends to contribute greatly to raising the temperature on the ice surface.

The presence of a highly conductive water film on the ice surface then causes a voltage drop along the air gaps. A number of studies, to date, have revealed that in the presence of even a low conductive water film layer, the totality of the applied stress to the insulator appears along the air gaps [138]. If the level of stress is higher than the air breakdown threshold, the air gaps will break down and small luminous partial arcs will appear along them. The initiation of corona discharge leading to the development of partial arcs in these zones will then cause a substantial increase in leakage current [116]. Under sufficient electrical stress, arcs propagate along the ice surface forming a white arc. When the white arc reaches a certain length, the whole insulator suddenly undergoes complete flashover [40]. The study of the formation and maintenance of these partial discharges may be carried out by investigating the electromagnetic field surrounding the insulator. The above-described flashover process may be classified into three successive stages [17]:

- I- The first stage is measured from the appearance of the first water droplets on the surface of the ice until the white arc is established, at which point the

current peaks to a maximum of ~ 25 mA [71]. The duration of this stage depends mainly on the rate of the increase in air temperature.

- II-** The second stage starts from the instant a white arc is established and continues to the moment when the arc starts propagating. The arc length reaches to 45-60 % of total length of insulator [148]. The current increases to several hundred mA, although the exact duration of this stage still remains unclear.
- III-** The final stage starts when the arc begins to propagate toward the next electrode to cause a complete flashover when the process terminates [148]. This event happens in a fraction of a quarter of a cycle when the applied voltage is at approximately its maximum value.

These three stages are shown schematically in Figure 4.1. In the case of withstand result, the arc extinguishes after a maximum increase in the current during the second stage.

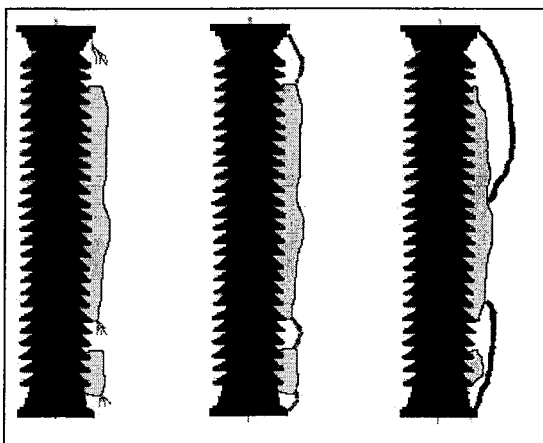


Figure 4.1 Different stages of arc development on an ice-covered insulator.

In the first stage, the ambient temperature is a significant contributing factor, while the rate of increase in the ambient temperature may modify subsequent events [148]. Also, the capacitive current is greater at this stage, due to the presence of air discharges and coronas. The heat delivered from the coronas participates in producing an additional volume of water film [148] which, in its turn, leads to increased surface water volume, where the current increases perceptibly. Therefore, the small violet arcs gather together to form an established white arc.

During the second stage, the arc burns freely in the air in a relatively fast-moving undulating pattern. The heat dissipated from the burning arc appears to be a more dominant factor in the ice-melting process, and the ambient temperature has less influence than in the earlier stage. The rate of water flow increases as a result of ice melting while the ice volume diminishes considerably due to the same melting, and the ice bulk thus becomes less adhesive. The loss of the ice creates a longer air gap causing the arc to extend to a new length. An increased surface water volume and conductivity, as well as gradual lengthens of arc, provides less surface resistance and the current increases as a result. Although the arc burns intensely, the duration of this stage is relatively long, in the region of a few minutes, in which the arc temperature increases with an increase in the arc current, which implies an increase in air conductivity which then results in a further current increase, and so on. This positive loop results in an intensely hot arc column and high currents, although experimental measurement of the variation in axial arc temperature of a 2 A AC-arc in air at atmospheric pressure showed that the arc temperature will not persist beyond 5000 °K [2] because of the heat

exchange between the arc column and the cold ambient air. Thus it appears that there is a form of thermal equilibrium in the arc state for relatively long periods of time.

Finally, when the surface conductivity reaches a certain value, the current increases gradually, and if the voltage is sufficient to provide a strong enough field at the arc tip, a sudden flashover occurs. Under AC applied voltage, this stage can take place in the space of only one quarter of a cycle [147].

Alternating and successive losses from the thawing of ice in the second stage may result in an ice length where the voltage source is no longer able to sustain the arc, and the arc is thus extinguished eventually. The test results here represent an adequate “Withstand” result.

The above-mentioned process was submitted here for the AC arc process, although the same principle is generally applicable to DC burning arcs, where the temperature should reach higher values as compared to the AC process.

4.2 Basic Model

An electric circuit analogue was applied in a number of distantly related research domains such as mechanical structures and chemical processes [25]. In this type of modeling, process elements are modeled using a corresponding electrical element. The electrical connections represent the intrinsic connections between the original parts of the main process variables. Ultimately, an equivalent circuit is obtained which may be considered to behave like the original element. Thus, in this circuit, the voltage and current of each node and branch are the exact representative of their real-life variables. The existence of several methods developed in the field of electrical engineering makes it possible to solve any circuit efficiently. Once the final circuit is solved by such known

mathematical methods, the output results will represent the real values of the modeled objects in a typical physical model.

Obenaus was the first to apply this form of modeling to simulate arc behavior on polluted surfaces [110 and 111]. Here, the same basic idea is used for modeling arc propagation on iced insulator surfaces. Referred to the Wilkins' model (c.f. Fig. 3.18), space charge is only situated around the arc tip. This is due to the conductive connection between the arc and the next electrode through the conductive layer of water film. This implies the transformation of discharge to arc state within any propagation in arc length. This process is shown in Figure 4.2, where by transformation of discharge to arc, the space charge around the discharge column is attracted into the arc column during return stroke.

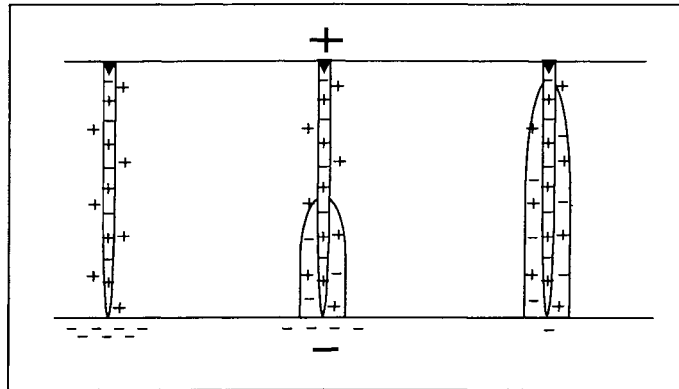


Figure 4.2 Transformation of discharge to arc during return stroke.

Thus, the arc is considered to be constituted of a resistance in series with an inductance and it is considered that arc current is constant through all cross sections of arc column and there is not any other leakage pathway along the arc length. The ice bulk and the water film on its surface are considered to behave as a single resistance as was

described elsewhere by other researchers [13, 17, 39, 50-52 and 148]. Thus for the purpose of this study, a resistive element is used to model the ice and surface water-film. To date, the area of the arc tip, composed of coronas and streamers, remains a not yet fully-known quantity. In order to describe the production of electrical charges, a capacitance is inserted in the model as shown in Figure 4.3, where the main output of the circuit, I_{arc} , is the arc current.

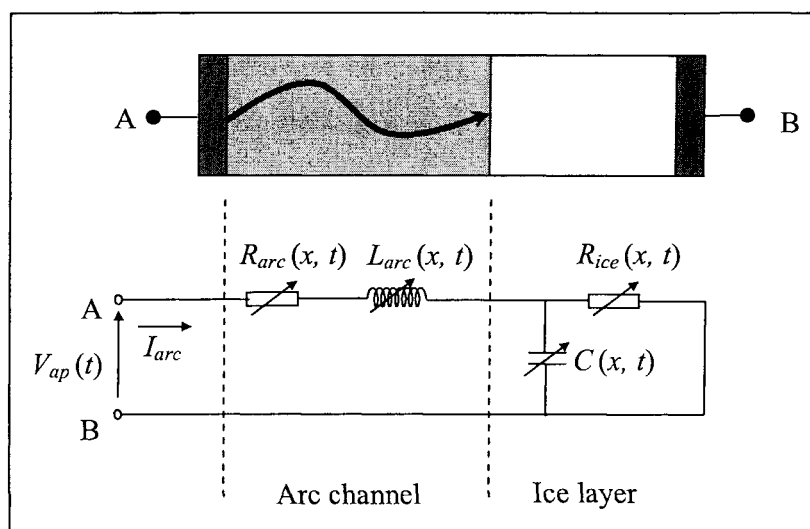


Figure 4.3 Principal model of arc propagation on an ice-covered insulator surface.

In Figure 4.2, V_{ap} is the voltage applied to the whole test set, R_{arc} and L_{arc} are the total arc resistance and inductance, respectively, C represents the capacitance, and R_{ice} is the total resistance of the unbridged iced layer.

It should be noted that the arc channel conductivity is a function of air temperature, and that air as a medium is endowed with complex properties such as conductivity, specific capacity, and density, which are all non-linear functions of temperature [119]. The total resistance of a conductive surface layer is a function of its

surface conductivity which changes dynamically during different stages of arc propagation [40]. Recent research has revealed that the capacitance of a test object in the form of a rod-plane is non-linear [57]. The above facts dictate the use of non-linear and time-variant circuit elements.

The model is considered to be applicable over the entire simulation process, lasts from the appearance of the white arc to the occurrence of total flashover, thus involving the last two described stages (cf. Section 4.1).

By obtaining the proper relationships for calculating the circuit elements, it is possible to solve the network equations for the entire time period covered by the target process. The simulation of the second and third stages of the process is based on a hypothesis which will be explained in the following sections.

4.3 Simulation Method

4.3.1 Simulation of the Second Stage

As mentioned above, the arc temperature varies during this stage, but the maximum temperature is limited to values of about 5000 °K [2]. Due to the alternating nature of the voltage during each period, however, the voltage varies greatly, but the variation of the temperature curve, during a period of voltage, is negligible in the established regime of the heat transfer between the arc column and the ambient air [95]. Since the air conductivity is a function of temperature (cf. Fig. 4.4 [99]), this confirms that the arc is sustained in a hot tube of air of a near-constant conductivity.

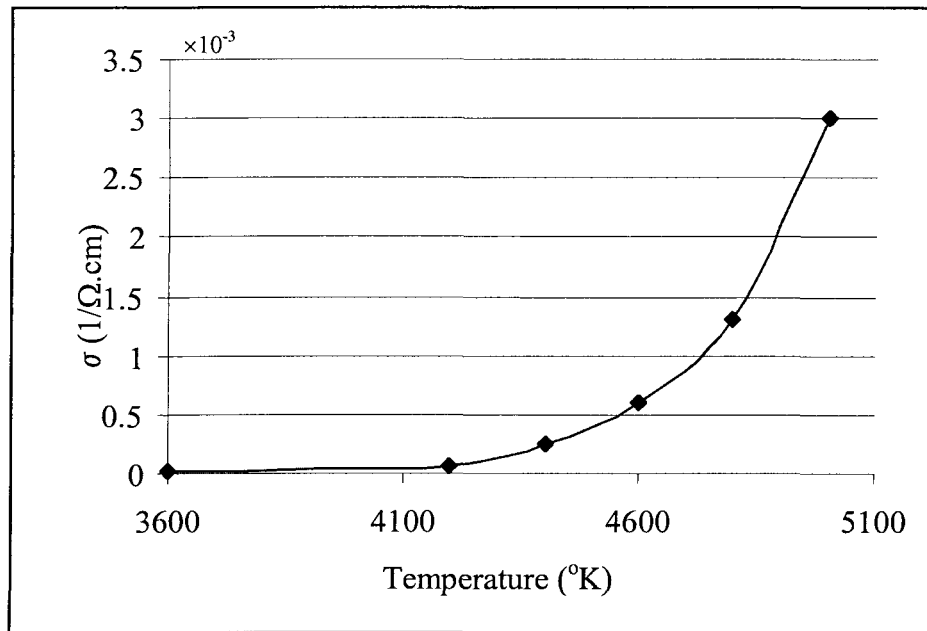


Figure 4.4 Air conductivity as a function of air temperature [99].

The total arc resistance is also dependent on the arc root radius and arc length. During this period of the test, the arc resistance is high compared to the ice and surface water resistance. As was mentioned earlier, the arc length throughout this stage is extended due to thawing or shedding of ice. This length may also diminish, since the arc current attempts to flow through the least resistive path in the direction of the next electrode.

The resistance of the ice layer is a result of the presence of a water film on the ice surface, and the conductivity of this surface layer determines the second resistance of the circuit. This conductivity is a function of a number of other parameters, among which are included ice and air temperature, the applied voltage and current injected into the channel, ice type, and applied water conductivity.

The complexities inherent in the heat-transfer equations and the melting-ice phenomenon made it impossible for us to establish a useful algorithm for obtaining the temporal evolution of surface water conductivity as well as arc length and temperature during this stage. This implies that time duration, as well as the current value, throughout this stage may be simulated, but cannot be predicted. Thus only by having the exact values of different variables such as arc length and temperature and surface conductivity, the arc current may be simulated, otherwise, the prediction of the arc current during this stage can not be carried out.

4.3.2 Simulation of the Third Stage

At the beginning of the third stage, it is necessary to determine different parameters. The time period covered by this stage is relatively short. Experiments have shown that, under AC applied voltage, a flashover event occurs within the last positive quarter cycle [147]. The arc starts to propagate toward the next metallic electrode when the minimum ice bulk resistance is obtained, if the applied voltage is high enough. In order to calculate the flashover voltage value, the same hypothesis assumed in static models is applied, where the whole process occurring within a cycle around the maximum value of the applied voltage is taken into account [3 and 142]. Thus, the applied voltage in the AC case may be regarded as constant and equal to peak alternative voltage [142]. This is because, in AC case, the applied voltage is within 5% of its peak value for almost 40% of the half cycle [142]. As a first approximation, the time duration of this stage, Δt , is assumed to be 1.1 ms around the voltage crest time, when the applied voltage is $\pm 98\%$ of its maximum value at 60 Hz. This value for Δt may be modified using experimental results.

In order to simulate this stage, the initial values of different circuit elements are required. If the initial arc temperature is taken as a relatively high value of 4550 °K maximum [2] ($\sigma = 0.0006 \text{ 1}/\Omega\cdot\text{cm}$), it will ensure attaining a minimum value for critical flashover voltage, since it results in a minimum initial arc per unit resistance. The initial arc length is assumed to be equal to its final value which resulted from the preceding stage. It should be noted that this length is not the same as the initial air gap length, and also that it may become modified during the melting period [17 and 147]. Compared to the much higher speed of the flashover mechanism and the heat transfer phenomenon on the ice surface, the change in surface conductivity during the arc propagation stage is negligible. Thus, its value is assumed to remain constant at latest values obtained in the preceding stage. The initial value of the voltage applied may be determined using the Claverie model which was proposed in order to calculate the minimum peak voltage, V_0 , able to re-ignite an arc which carries the peak current, I_0 , along the initial arc length, x_0 (cf. 3.2.2) [22]. Using the constants proposed for ice-covered insulators, the relationship reads as follows [40]:

$$V_0 = \frac{1118x_0}{I_0^{0.5277}} \quad (4.1)$$

After obtaining the peak value for the critical flashover voltage level, the real-time modeling of the last stage (including the last quarter cycle before the propagating period) may be repeated quasi-indefinitely. In each time step, dt ($= 10^{-6}$ s, the arc constant is assumed to be $100 \mu\text{s}$ [123 and 131]), the voltage is applied to the circuit, and then the current through the electric network is calculated by making use of the initial values of all components. If propagation is to occur, the arc must be extended to a new length. In order to evaluate whether the arc is capable of prolonging itself or not, an

appropriate criterion must be met. This new length should be calculated as a function of several other parameters. Thus, an adequate propagation criterion, together with the velocity relationship, is the most important aspect of the dynamic modeling of arc propagation. With the new length, the entire process will be repeated, and in all iterations the criterion should consistently be met. In the case that the arc is not able to extend further, the arc will be extinguished, which means that the applied voltage is no longer sufficient to create the flashover, and consequently the insulator will withstand this voltage level. In such a case, the applied voltage should be increased and all the steps repeated once more. Meanwhile, after each increment in length, the arc length is compared with the total arcing distance and if this length is greater, flashover takes place and the simulation comes to halt. Since the flashover voltage has already been calculated and will not be modified any further in this step of the simulation, the occurrence of flashover earlier than the desired time (the duration of this stage) reveals the high velocity of the arc. The velocity should therefore be decreased and the simulation should be repeated in order to achieve a flashover at the expected moment. In the case where the length is not equal to or greater than the total length, the simulation continues up to completing this stage. If the axial arc length is still less than the insulator length, the simulation should be repeated using a higher velocity factor. Starting from a low velocity factor ensures the flashover event after the desired moment is reached. The process is shown in the following flowchart (Fig. 4.5).

The input data in this flowchart are the surface conductivity of the ice and such insulator specifications as length and radius. These data will be used to calculate the ice layer resistance. In the flowchart, L represents the total arcing distance, and x is the axial length of the arc.

The output of this flowchart is the peak value of critical flashover voltage (rather than its effective value); arc current and velocity; and, total and per unit values of arc and ice resistances throughout the arc propagation period.

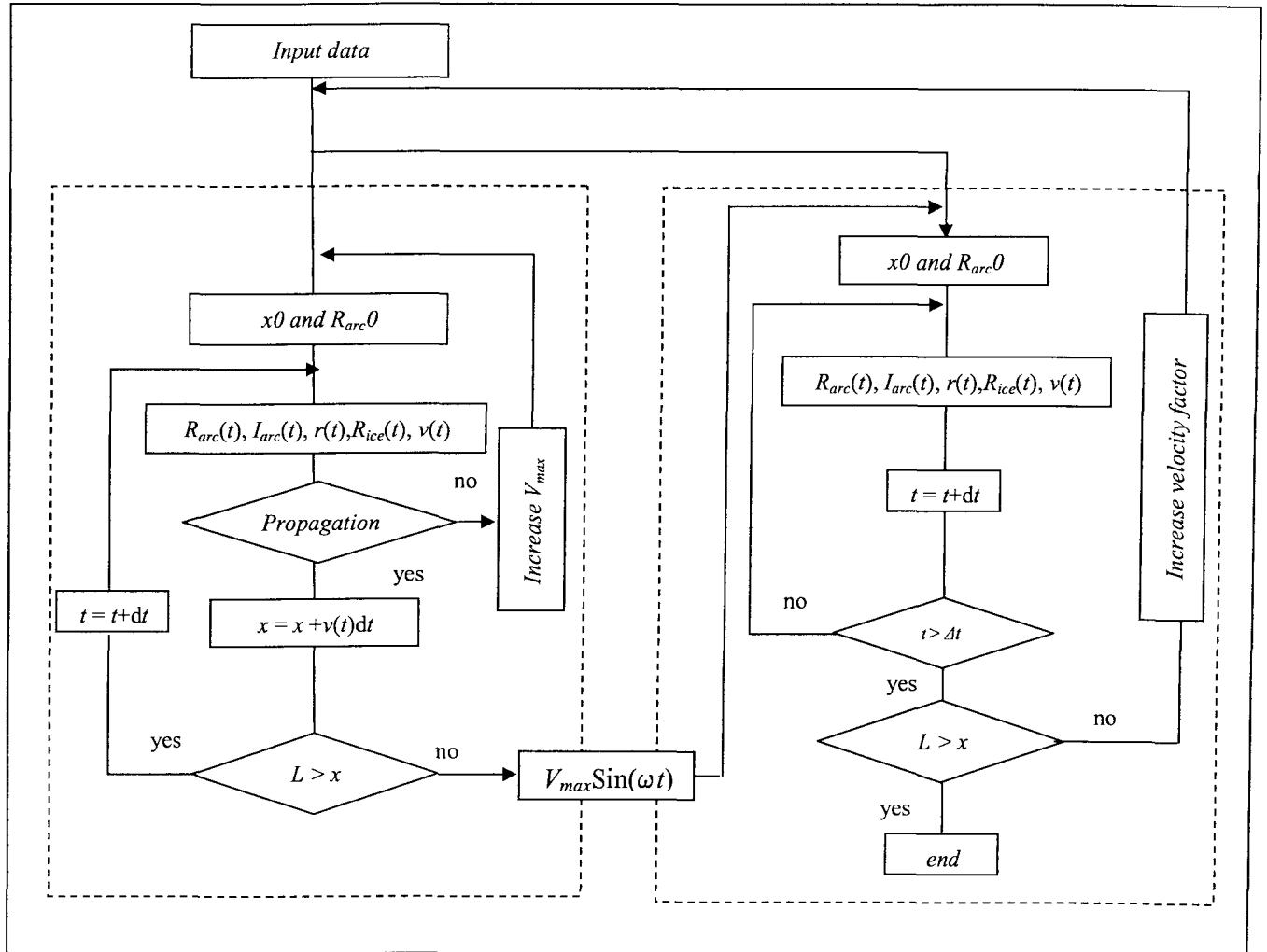


Figure 4.5 Flowchart of AC modeling.

x : Axial arc length	R_{arc} : Arc resistance
L : Arcing distance	r : Arc radius
v : Arc velocity	t : time
I_{arc} : Arc current	R_{ice} : Ice resistance
V_{max} : Peak value of applied voltage	Δt : Propagation duration

The remaining part of the modeling is for the purpose of deducing the precise functions for arc and ice resistances, and for channel inductance as well as circuit capacitance. By combining these equations with the propagation criterion and the velocity equation, it will become possible to proceed with a satisfactory simulation. It was mentioned earlier on, that several parameters such as initial arc length also need to be derived from experimental data. These experiments will be discussed in subsequent sections of this text.

4.4 Circuit Elements

The pertinent relationships for determining the circuit elements are essential to successful simulation and modeling. These relationships should reflect all known physical properties of intervening parameters. The impedance of the arc, constituted of a resistance in series with an inductance, must take the heat transfer energy equations into account as well as electromagnetic aspects of the channel through which the current flows. The need for the accurate reflection of the relationship also applies to the modeled ice layer.

An important point which should also be mentioned here is the direct connection in the electrical network between the arc head and ice layer resistance, that is to say, the fact that the arc head touches the ice layer. This direct connection was assumed for the sake of simplicity, since in reality, this type of contact is not yet well-defined, considering that this area seems to be constituted of such varied discharge phenomena as streamers and coronas. This implies the existence of a non-uniform resistance for the whole arc length, and a capacitive property for the arc tip. A model of a discharge head for the spark channel has already been published [56].

4.4.1 Ice Resistance

If an axially symmetrical insulator is covered with a thin uniform conductive film of a constant thickness, h , and constant specific conductivity, σ_v , then the surface conductivity at any point of the film is defined by:

$$\gamma_e = \sigma_v h \quad (4.2)$$

where γ_e is obtained in S ($= 1/\Omega$). In order to take into account the effect of current concentration at the arc root, Wilkins' investigations for the geometry shown in Figure 4.6, in which narrow strip ($w < L$) is concerned, lead to following equation [142]:

$$R_p = \frac{1}{2\pi\gamma_e} \left\{ \frac{2\pi(L-x)}{w} + \log \frac{w}{2\pi r} \right\} \quad (4.3)$$

where w , $(L-x)$, and γ_e are the width, arcing distance and conductivity of the conductive layer, respectively, and r is the arc root radius.

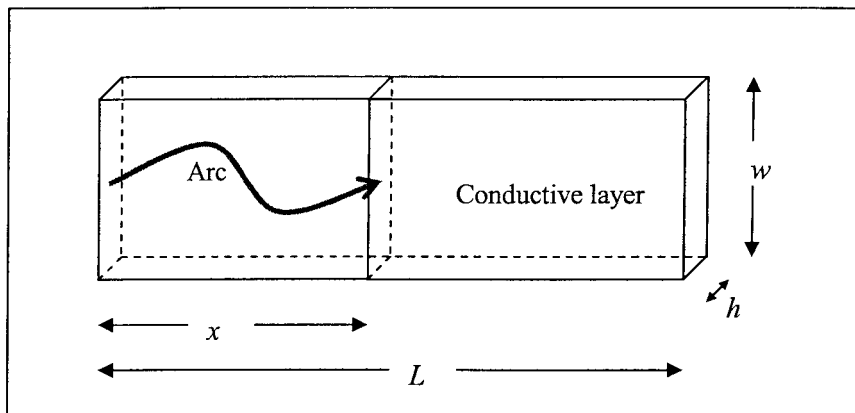


Figure 4.6 A rectangular conductive layer in the presence of an arc.

In the case of ice-covered cylindrical insulators, the ice width is assumed constant [13, 17, 51 and 146-148]. If the ice is thick enough, the shedding distances

between the insulator skirts are bridged. Small shedding distances, under sufficient ice thickness, result in an almost uniform ice surface. After this occurs, the insulator profile has no further influence on the calculation of the ice layer resistance. For the sake of simplicity, in almost all previous studies on ice modeling, the conductive water film on the ice surface was replaced by an equivalent cubic volume (similar to that of Fig. 4.6), with a constant surface conductivity, γ_e [13, 17, 51, 146-148]. At this point the resistance of this water film was calculated using Wilkins' equation (Eq. 4.3), where w is the ice layer width and $(L-x)$ is the total length of the unbridged ice surface [13, 17, 51, 146-148]. The total ice layer resistance would then be a function of a number of parameters, including arcing distance, ice width, water film conductivity, water film thickness and arc channel radius and length.

Based on previous investigations, a linear relationship was established between the applied water conductivity used and the surface conductivity at the time of flashover [51]. This equation for AC applied voltages reads as [51]:

$$\gamma_e = 0.0675\sigma_w + 2.45 \quad (4.4)$$

where surface conductivity, γ_e , is obtained in μS and the applied water conductivity, σ_w , is in $\mu\text{S/cm}$ at 20 °C.

As regards the test setting in question, this relation (4.4) was obtained by assuming equality between the surface resistance measured and its analytical relation [51]. Such a relation is based on the results from a test object of relatively small length [51]. This equation was then applied to different insulator geometries and satisfactory results were obtained [13, 51 and 147].

In static models arc parameters are considered constant (A and n) [147], also the arc re-ignition parameters, K and b [147]. Therefore, the use of this relationship in static

models, affirms that the value obtained using Eq. 4.4, should be the maximum value attainable for surface conductivity. Otherwise, flashover should occur before attaining this value.

Here, for the sake of simplicity, this equation is used in order to calculate the surface conductivity during the small fraction of time of arc propagation. The arc channel root radius, r (in cm), is also calculated at each time-step according to Wilkins' empirical model [142]:

$$r = \sqrt{\frac{I_{arc}}{k \pi}} \quad (4.5)$$

in which k is a constant [142]. For an AC arc propagating on an iced surface, k was already determined experimentally and is equal to 0.875 [147]. This value of k was obtained using the peak values of the current [147]. As an approximation, Eq. 4.5 is applied for determination of the arc root radius for all the values of the arc current over the time with $k = 0.875$.

It should be mentioned that Wilkins' approximation was based on the following much more complicated equation [142]:

$$R_{ice} = \frac{1}{2\pi\gamma_e} \sum_{j=-\infty}^{j=+\infty} \frac{1}{2} \log \left[\frac{\left(1 + \cosh \frac{\pi(jw+r)}{2L}\right)^2 + \tan^2 \frac{\pi x}{2L} \sinh^2 \frac{\pi(jw+r)}{2L}}{\left(1 - \sinh \frac{\pi(jw+r)}{2L}\right)^2 + \tan^2 \frac{\pi x}{2L} \sinh^2 \frac{\pi(jw+r)}{2L}} \right] \quad (4.6)$$

A schematic simulation of these two equations (Eqs. 4.3 and 4.6), shows that the validity of this particular approximation is no longer applicable when the arc length, x , tends toward the total length of the conductive layer, L (cf. Fig. 4.7). Typical values for

different parameters as insulator length, ice width, surface conductivity, and arc current were used as indicated.

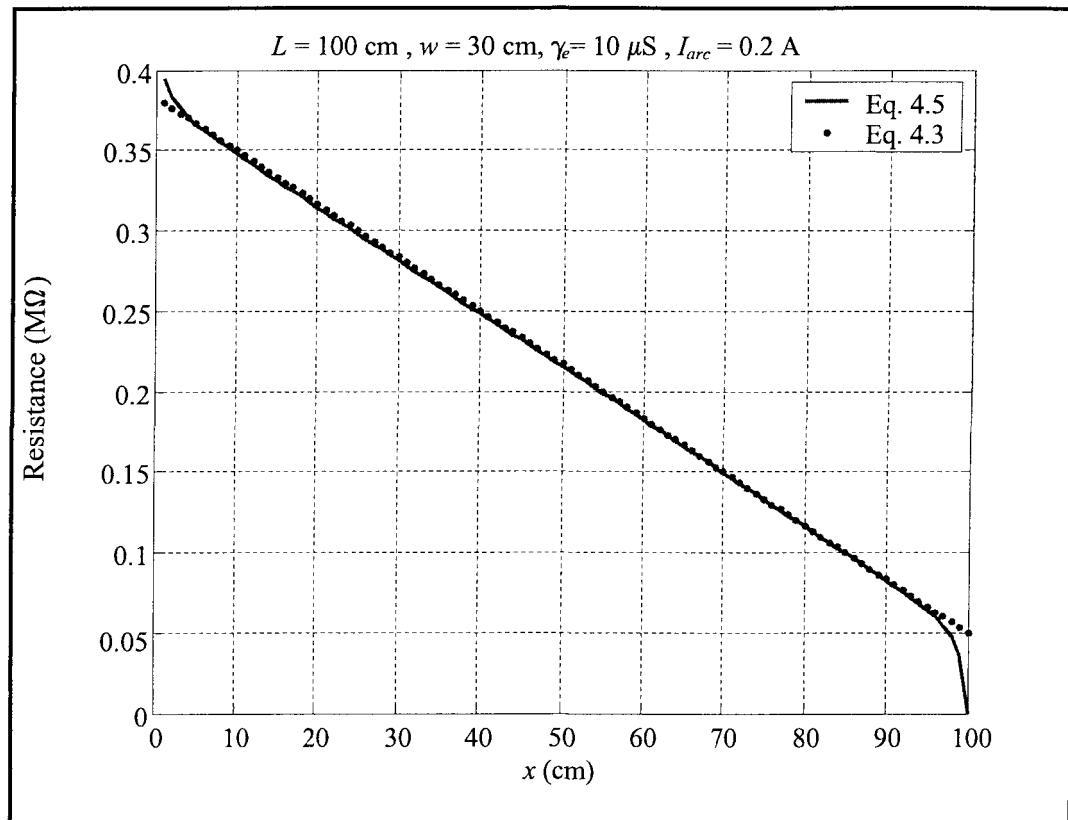


Figure 4.7 Different Wilkins' equations for a resistance of a given specimen.

Therefore, since dynamic modeling lasts up to and including the moment when the arc length, x , becomes equal to the arcing distance, L , the use of Eq. 4.6 rather than Eq. 4.3 is obligatory.

4.4.2 Arc Inductance

In order to determine the inductance of the discharge channel, a simplified model for discharge in air gaps is used similar to the one proposed in [56]. In this model, the end effects are disregarded and the inductance per unit length of the channel l_{arc} (in H/m), is the sum of two inductances. The first part of the simplification is deduced from the electromagnetic energy stored in the channel (or internal inductance) and is provided by:

$$l_1 = \frac{1}{4} \frac{\mu_0}{2\pi} \quad (4.7)$$

while the second part, deduced from the electromagnetic field radiated by the current flowing through the channel, is such that:

$$l_2 = \frac{\mu_0}{2\pi} \left[\ln(D_f/r) \right] \quad (4.8)$$

The channel inductance per unit length is therefore [56]:

$$l_{arc} = \frac{\mu_0}{2\pi} \left[0.25 + \ln\left(\frac{D_f}{r}\right) \right] \quad (4.9)$$

where D_f represents the distance from the discharge axis at which the magnetic field is considered to be zero. If D_f is high enough for transient fields, the fractional error, which is of the order of $1/\ln(D_f/r)$, will be low. For these investigations D_f is set at 100 cm, a typical value already proposed in [56].

4.4.3 Capacitance

Assuming the arc channel to be cylindrical in shape, terminating in a half sphere of radius r (arc radius), the capacitance, C , between the arc tip and the opposite electrode is calculated as follows [56]:

$$C(x,t) = 2\pi\epsilon\alpha[1 + (r/(L-x))] \quad (4.10)$$

where α may be calculated as follows:

$$\alpha = \left(1 - 1/\sqrt{1 + \left[\left(\frac{\phi}{2L} \right) \left(\frac{1}{1-x/L} \right) \right]^2} \right) \quad (4.11)$$

and represents the solid angle between the arc tip and the opposite electrode. The angles α and ϕ are shown in Figure 4.8.

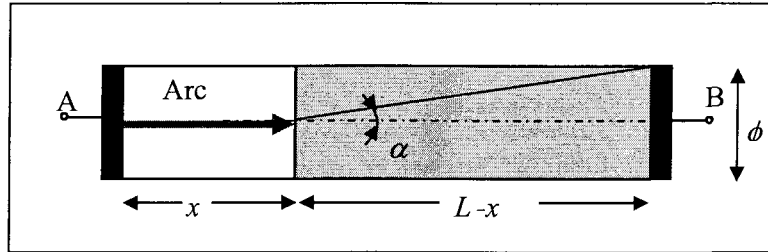


Figure 4.8 Capacitance of the rod and finite plane geometry [56].

4.4.4 Arc Resistance

During the simulation of the second stage, the resistance of the arc is calculated using the following direct relation:

$$R_{arc} = \frac{1-x}{\sigma \pi r^2} \quad (4.12)$$

where x is the axial length of the arc, and r represents its radius.

In a previous study [39], the arc temperature was considered constant during the propagating stage of the arc, as a working hypothesis only, in view of the fact that this consideration is not a true reflection of reality. By increasing the current, much more energy is injected into the channel, and the high speed at which the phenomenon occurs

does not allow any time for heat dissipation. Thus, the arc channel temperature increases rapidly and total flashover takes place.

Based on the physical aspects of the phenomenon, an equation, under certain other assumptions, for calculating the arc resistance has been proposed in [99]. This equation will be used in order to model the propagating stage of the arc in the present model.

The energy balance for the arc channel may be written as follows [91]:

$$r_{arc}I^2 = U + H + \frac{dW}{dt} \quad (4.13)$$

where H is the energy loss per second by heat conduction, U is the radiation loss term, and W is the internal energy stored in the channel. The left hand side of the equation represents the energy injected into the channel as a result of arc current. These parameters depend on the number of electrons, n_e , and if there is a state of thermal equilibrium in the channel, a temperature, T , can be established so that H , W and U , will be functions of it [8].

In order to derive an expression which would connect the electrical conductivity of the channel with the electrical characteristics of the circuit, it may be assumed that the discharge occurs in such a short time that radiation and heat loss by conduction are negligible. Thus Eq. 4.13 becomes:

$$\frac{dW}{dt} = r_{arc}I^2 - H \quad (4.14)$$

Mayr assumed that the arc resistance per unit, r_{arc} , is an inverse function of W , such:

$$\frac{1}{r_{arc}} = f(W) = C \exp(W / W_0) \quad (4.15)$$

where C is a constant and $W_0 = W|_{t=0}$. Thus, the derivation over time of Eq. 4.15 may be written as follows:

$$-\frac{1}{r_{arc}^2} \frac{dr_{arc}}{dt} = \frac{df}{dW} \frac{dW}{dt} \quad (4.16)$$

where:

$$\frac{df}{dW} = \frac{1}{W_0} f = \frac{1}{W_0} \frac{1}{r_{arc}} \quad (4.17)$$

A combination of Equations 4.16 and 4.17 leads to:

$$-\frac{1}{r_{arc}} \frac{dr_{arc}}{dt} = \frac{1}{W_0} \frac{dW}{dt} \quad (4.18)$$

The most important hypothesis formulated by Mayr, was that, during the arc propagation, the heat conduction rate is constant, or $H=P_0$. Then Equations 4.14 and 4.18 may result in a new equation, as follows:

$$\frac{1}{r_{arc}} \frac{dr_{arc}}{dt} = \frac{1}{\tau} \left(1 - \frac{r_{arc} I_{arc}^2}{P_0}\right) \quad (4.19)$$

where $\tau = \frac{W_0}{P_0}$ is the arc de-ionization factor, which may be considered constant at 100 μs for the arcs in air [23, 123 and 131]. The constant P_0 should be determined by a comparison between flashover voltage calculations and the results of the experiments.

4.5 Arc Velocity and Propagation Criterion

Because the velocity of the extension of a partial arc is dependent to a high degree on experimental conditions, the mechanism of extension cannot be explained by a single theory. Discharge velocity is influenced greatly by the applied voltage and controlled by increased ionization and attachment coefficients. The complexity of an electrical discharge increases while the discharge is taking place over an insulating surface.

Under some assumptions it has been shown [120] that there exists a relationship between discharge velocity and its current:

$$v(t) = \frac{I_{arc}(t)}{q} \quad (4.20)$$

where $q = \frac{1}{x} \int_0^t I_{arc}(t) dt$ is the average charge per unit length and can be considered constant for all practical purposes.

In order to achieve a minimum value for critical flashover voltage, Hesketh's criterion [73] during the last period of propagation, is used as follows:

$$dI_{arc}/dx > 0 \quad (4.21)$$

4.6 Recapitulation of Main Points

A self-consistent dynamic model for predicting flashover phenomena was proposed in this chapter, and in order to model the process, a flowchart was also presented. Based on an electrical equivalent circuit, a number of relationships were chosen to determine different variables involved in the arc phenomenon. The duration of the propagation, Δt , was assumed to be 1.1 ms, when the applied voltage is $\pm 98\%$ of its peak value and then the applied voltage was considered constant during the last stage of arc propagation. The arc resistance during the propagating stage was considered to vary in accordance with the Mayr equation. Initial arc temperature was assumed to be a maximum attainable value, 4550 °K, while initial arc length needs to be determined from the experiments for initializing the model. The heat dissipation rate in the Mayr equation will be determined based on the minimum flashover voltage obtained by experiment. The surface conductivity at the time of flashover was calculated using an already existing relationship. The input data to the model are insulator length, ice width and applied water conductivity. The model is formulated in such a way to predict and determine the critical flashover voltage and the variation of arc current and velocity over time during the propagation stage. If the surface conductivity and arc length and temperature are known, this model is also able to simulate the arc current for any given cycle before propagation.

CHAPTER 5

DESCRIPTION AND IMPLEMENTATION OF EXPERIMENTS

CHAPTER 5

DESCRIPTION AND IMPLEMENTATION OF EXPERIMENTS

The necessity for designing several experiments to measure a number of different parameters was justified earlier in the text. The initial arc length and the value of the heat dissipation rate P_0 , are among those parameters which should be determined from experimental results. The constant, P_0 , may be calculated by comparing experimental flashover test results with those of the simulations.

Several series of flashover tests were proposed in order to obtain the desired data. Two different lengths of glass tubing cylinder, 40 and 80 cm, respectively, each with three values of applied water conductivity, σ_w , set at 30, 65 and 100 $\mu\text{S}/\text{cm}$, were the test parameters imposed. Such a setup thus involves 6 different flashover test series. In order to evaluate greater insulator lengths and to compare test data with those using real-shape insulators, 2 more test sets (each containing three series) were carried out on one unit of standard post type insulator, where the first set was applied to a total insulator length, 103 cm, and the second set was applied to a little over half that length, or 54 cm, with both series having the same three applied water conductivity values. The wet-grown ice used in the experiments was accumulated without applied voltage. The method of maximum withstand, V_{WS} , (and minimum flashover, V_{MF}) voltage calculation is the same as described in the standard IEC60507 guidelines (International

Electrotechnical Commission) [79] and recommended in [40]. A data acquisition system was used for the purpose of gathering current and voltage signal values. In the following section, test facilities, test objects, and test results will all be introduced in the relevant sequence.

5.1 Test Facilities

In order to carry out flashover experiments on ice-covered insulators, several facilities should be prepared in advance. Besides the high voltage test sets and the data acquisition system (DAQ), ice-making procedures require special equipment.

5.1.1 High Voltage Equipment

Considering the low estimated voltage needed for these particular experiments, a single-phase test voltage transformer of 120 kV (maximum), 240 kVA and 60 Hz was used. The input voltage of this equipment is 600 V. A regulator is used to make it possible to vary the output voltage from 0 to 120 kV. The voltage increase may be affected either manually or automatically at an approximately constant rate of 3.9 kV/s. Since high voltage experiments on ice-covered insulators are carried out in a closed area, and the transformer is kept outside that area, the security system set in place for this type of experiment is of vital importance. Two circuit-breakers and an accurate relay which interrupts the voltage instantaneously on demand are a part of this security system. The system may be adjusted to cut off the voltage and de-energize automatically in the case of all personnel entering any of the test areas. High voltage bushing conducts the applied voltage through the walls of the cold climate room.

5.1.2 Climate Room

Wet-grown ice, known as the most dangerous type [43 and 45], was used for the experiments carried out in the present study. The ambient characteristics required to produce this type of ice in the laboratory are shown in Table 5.1.

Table 5.1 Ice-making specifications.

Ice Type	Glaze
Air Temperature	-12 °C
Droplet Size	80 μm
Time Duration	75 min
Ice Thickness <i>on rotating monitoring cylinder</i>	1.5 cm
Rate of Water Flow	200 ml/s/nozzle
Wind Velocity	3.3 m/s
Air Pressure	10 psi (70 kPa)

One of CIGELE climate rooms was used for creating the ice accumulation and for carrying out the designated tests. This climate room is a thermally isolated room, measuring 5.8 m×6.3 m×3.9 m, which is deemed sufficient to meet the standard clearances required by the standard IEC60507 [79]. The room temperature is controlled by a proportional-integral-differential (PID) controller with a precision rate of within ± 0.2 °C. This climate room is equipped with such appropriate facilities as a wind generator and a water-droplet spray system. Super-cooled droplets are generated by oscillating nozzles which are of the air-atomizing type. Each nozzle produces a mix of water droplets and compressed air. The air pressure is controlled and set to remain constant. The water flow is also controlled by flow meters. Each nozzle tip is heated by a heating element to avoid ice blockages during ice-accumulation.

The water used to produce the droplets, and ultimately the ice, is produced by filtration and demineralization of drinking water or regular tap water. This filtered water

is stored in tanks before starting the accumulation process. This enables the researcher not only to regulate the water conductivity to reflect a desired value, but also to ensure in advance that there is enough prepared water for each test.

The wind generators are adjustable electrical fans. A high-performance frequency-control electronic drive makes it possible to achieve the desired wind velocity behind the nozzles (see Fig. 5.1).

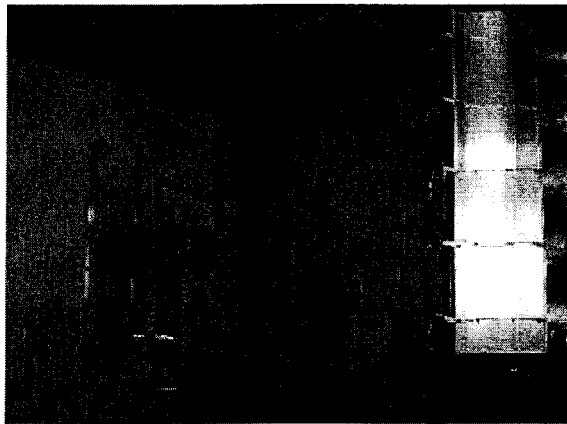


Figure 5.1 Climate room.

5.1.3 Test Objects

In order to perform the experiments and to obtain the desired data, a standard post insulator unit and a cylindrical model similar to that used in previous studies at CIGELE [17 and 39] were chosen. Figures 5.2 and 5.3 represent a schematic diagram of the models. The cylindrical object is constituted of three separate parts, two identical electrodes and a glass tube. This makes it possible to do experiments on different lengths of tube using the same electrodes. The type of glass tube used was chosen so as to be sufficiently resistant to overheating from the burning arc.

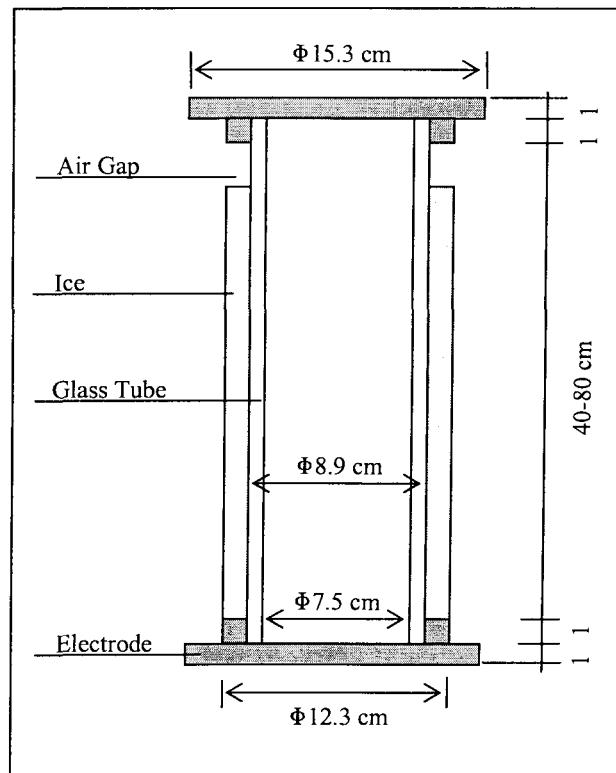


Figure 5.2 Cylindrical model used for experiments.

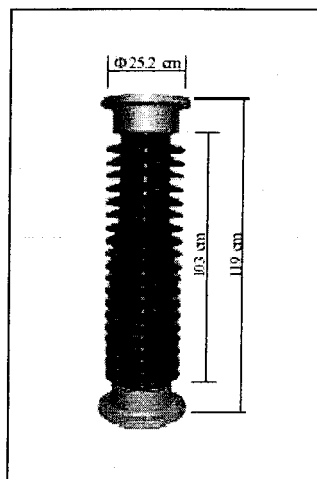


Figure 5.3 Post insulator unit.

5.1.4 Data Acquisition System

Dynamic modeling of the arc leads to the temporal evolution of a number of parameters. In order to be able to compare these curves with the ones produced experimentally, the laboratory data should be acquired at a relatively rapid frequency. A **LabVIEW** graphical software program was used to acquire high quality data. The voltage signal was attenuated by using a capacitive voltage divider. The current signal was transferred to a voltage signal using a low resistance shunt of $10\ \Omega$. The test signals were connected to a measuring set through a conditioning box providing protection and insulation. A NI-DAQ device, model PCI-6035E, was used for this purpose.

Using the **LabVIEW** user-interface features, a visual program was specifically designed and developed for these experiments to acquire and save data under the desired extension. This multi-layer program takes all the necessary test data and saves them together in the form of numerical signal data (cf. Figs. 5.4 and 5.5).

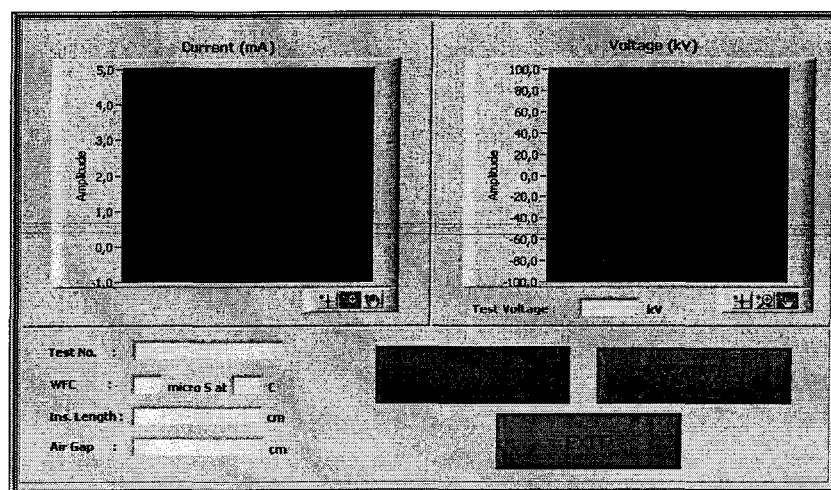


Figure 5.4 Main program menu.

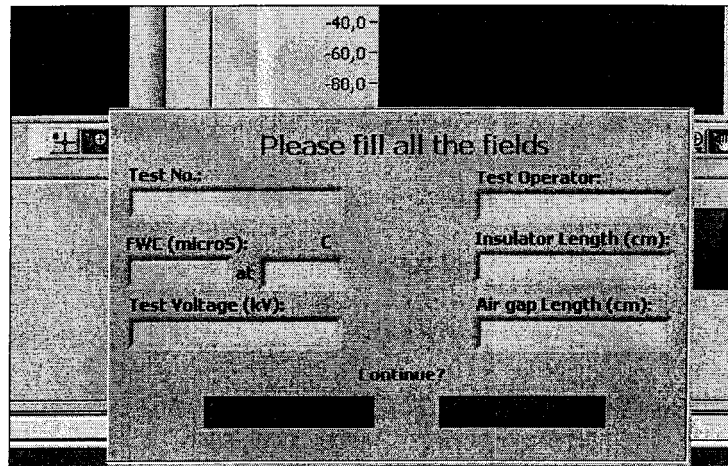


Figure 5.5 Test data loading menu.

During the acquisition time, to prevent loss of data, it is stored in a buffer and indicators show the effective values of current and voltage. The acquisition period is not time-limited and proceeds continuously (cf. Fig. 5.6).

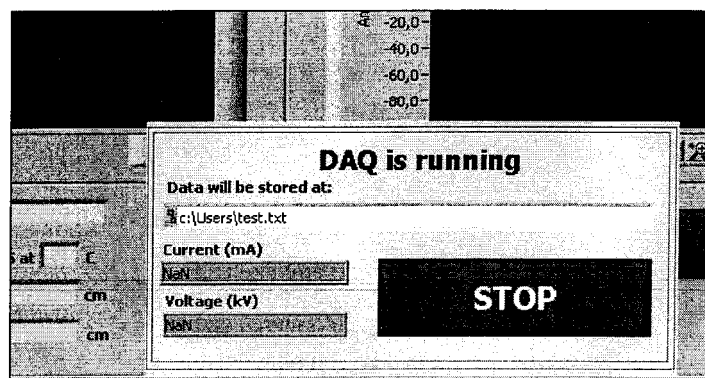


Figure 5.6 DAQ period of program.

A further feature of the program is the ability to display data and to analyse them visually. Current and voltage curves may be presented in the same figure and both signals may be observed simultaneously (cf. Fig 5.7)

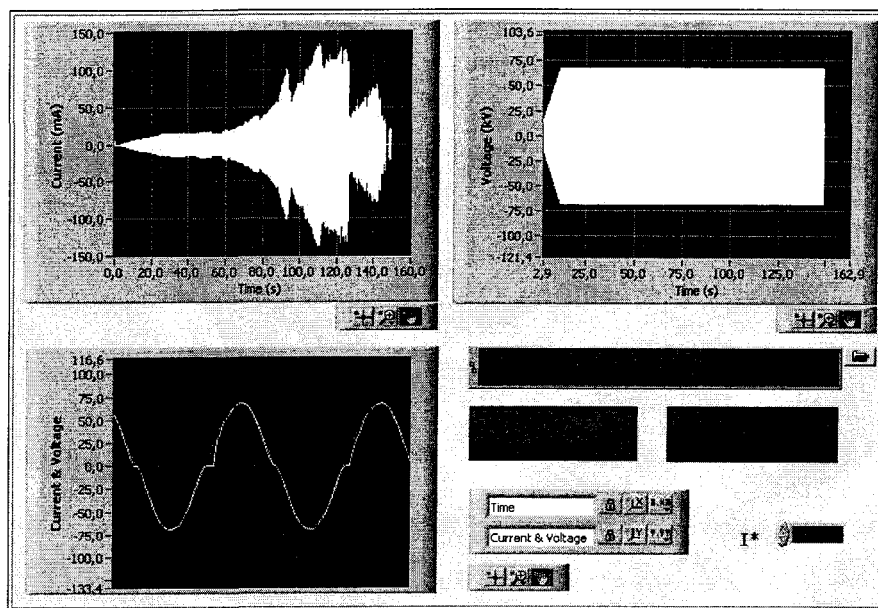


Figure 5.7 Data analysis program session.

5.1.5 High-Speed Camera

A high-speed camera was used to study arc behavior during the pre-flashover stage and to measure arc-propagation velocity during the flashover period. This camera is able to take photos at a high velocity of up to 1000 images per second. In this mode, the maximum time for data-saving is 3 seconds.

A schematic diagram of the entire test circuit is shown in Figure 5.8.

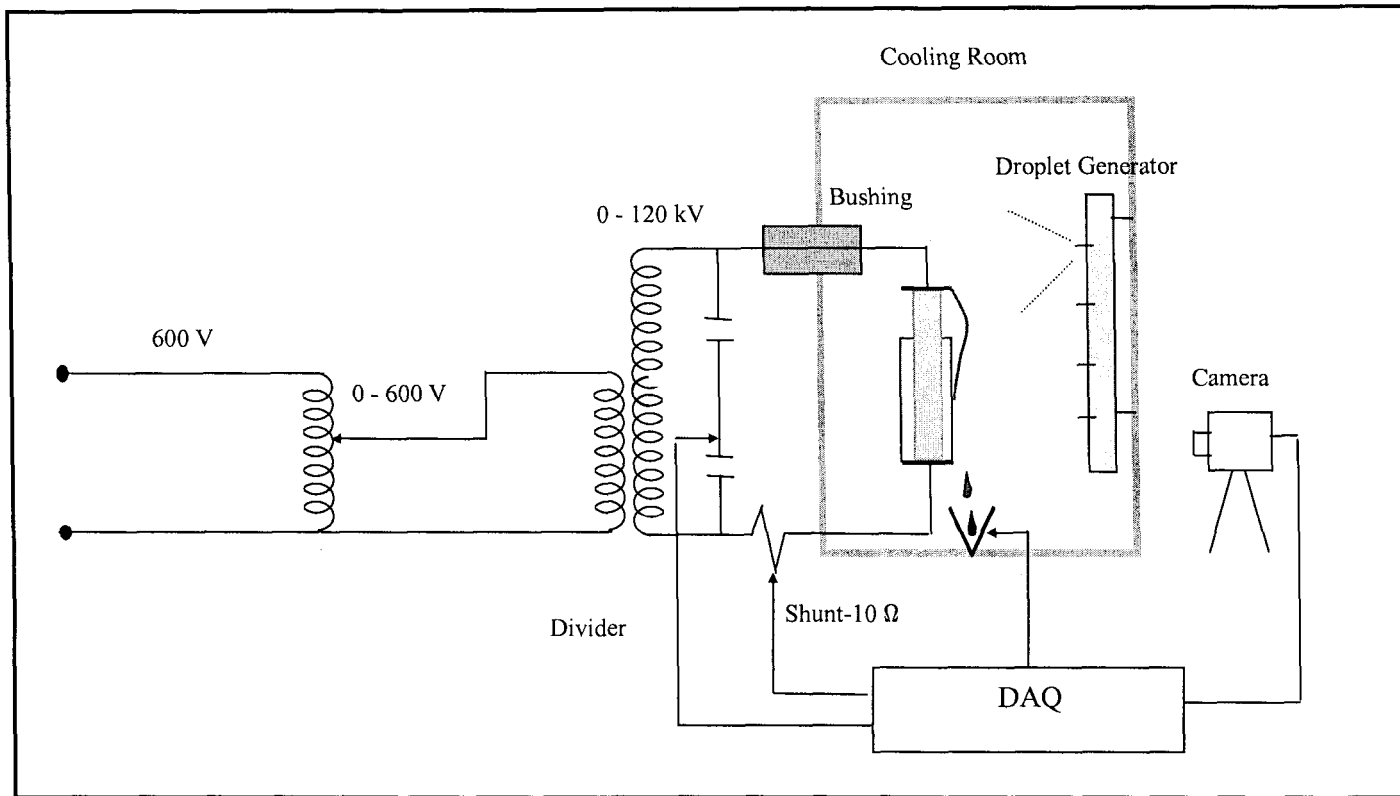


Figure 5.8 Schematic diagram of test circuit.

5.2 Test Procedure

Ice was accumulated without applied voltage, and the test object was not rotated to simulate natural conditions. After installing the test object in front of the nozzles, an accumulation time of 70 min was allowed for. This time duration was long enough to produce an ice thickness of about 1.5 cm on monitoring cylinder. Four nozzles were used and the rate of flow was 200 ml/s per nozzle. The air pressure behind the nozzles was set at a constant 10 psi. Since the room and the test object must be in thermal equilibrium at accumulation temperature, it was necessary to turn on the cooling system several hours before starting the test. The water conductivity was set by adding sodium chloride NaCl, to de-ionized water. This parameter was verified before and after each test. Twelve series of tests were proposed involving two different insulator lengths and three different conductivities for two different types of insulators.

Immediately after ice-accumulation, an artificial air gap of 7-8 % of the total length of the insulator was created (cf. Fig. 5.9). The mean ice width, w , was approximately 39 cm and 44 cm for the cylinder and the post insulator, respectively.

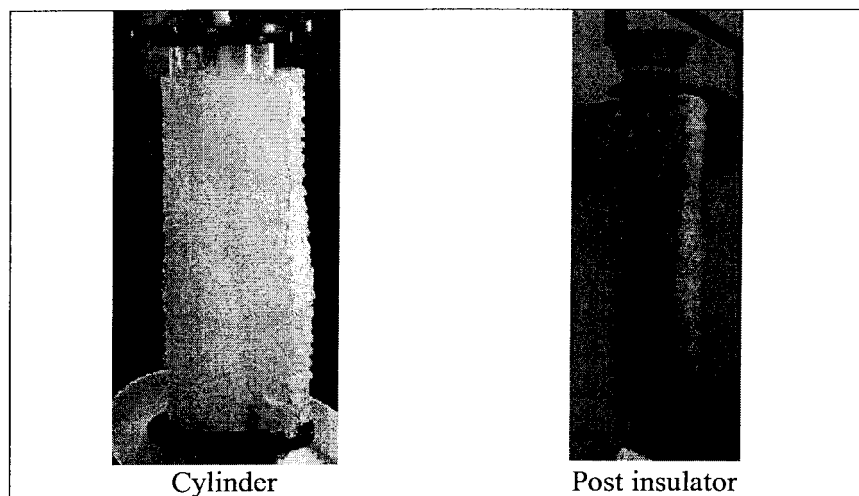


Figure 5.9 Complete samples of ice and initial air gap, before applying the voltage.

The test voltage was then applied to the test object. The whole test was carried out at the same temperature as the room (-12°C). Operational restrictions made it necessary to increase the voltage at the rate of 3.9 kV/s . In order to evaluate minimum flashover voltage, V_{MF} , the same method as previously used at CIGELE [40] was employed. In this method, after the first useful flashover result, the voltage was decreased by less than 5% of the nominal voltage, and then after any withstand or flashover result, the voltage was increased or decreased once more by the same value, or else it was maintained. Based on this method, the maximum withstand voltage is the maximum level of applied voltage at which flashover does not occur for a minimum of 3 tests out of 4, under similar experimental conditions. For each withstand test, the insulator is kept at the test voltage for a period of at least 15 min to ensure that no flashover occurs during this period. The V_{MF} then corresponds to a voltage level $\sim 5\%$

higher than the maximum withstand voltage at which 2 flashovers out of a maximum of 4 tests is produced. Clearly, for each series, at least 5 tests are required.

During each test, when the arc is strong enough, the current and voltage signals were captured by the DAQ system and arc behavior was filmed by a high-speed camera. The camera takes the photographs uninterruptedly and when flashover occurs the filming process may be brought to a halt, and according to the functional mode, the camera retains the last 3 seconds of data recorded. Meanwhile, the dripping water due to melting ice is collected for subsequent surface conductivity measurements to be used in the final model.

A further series of tests was carried out to study the effects of air gap length on flashover voltage. This series was done on a 40 cm long cylinder with the same three conductivities as used previously. The initial air gap length is 6 cm for this series.

5.3 Test Results

According to a large quantity of test data, the process of the AC flashover phenomenon on ice-coved insulator surface occurs as follows:

After applying the test voltage, several violet discharges appear. The rate and amount of dripping water increases and the arc becomes stronger while the current increases as well. When the peak current level reaches about 25 mA, there are no more violet discharges and a white arc is formed. The length of arc at this moment can reach about 15-20% of total length of the insulator. Then, the white arc lengthens gradually and its maximum length varies under different test conditions. Maximum arc length generally reaches about 45-60% of the total insulator length, for both types of insulators tested, before leading to flashover (cf. Fig. 5.10). The value of this maximum length is

independent of the first air gap length. In fact, the initial air gap length is important only prior to the formation of the white arc. Several cycles before jumping toward the second electrode, arc length remains constant at this maximum length. Meanwhile, water flow increases as a result of ice melting. The conductivity of melting water reaches a certain value, and flashover takes place abruptly once the applied voltage approaches its peak value. Before the last propagating stage, the intensity of arc channel luminosity oscillates with the intensity of the current, whereas the length of the arc appears to remain constant. This means that the arc is maintained, and it flows continuously through a volume of air.

A few cycles before arc propagation, the amount of melted water dripping from the insulator increases gradually. The conductivity of this water is not constant and varies according to several parameters. At the very moment of flashover, the conductivity of dripping water reaches its maximum value, when, the arc current increases as well and reaches several hundred mA. It was also observed that this maximum conductivity for flashover tests is higher than withstand results, possibly due to the more rapid melting of ice. Also, in general, time to flashover was lower for higher conductivities, than for lower ones.

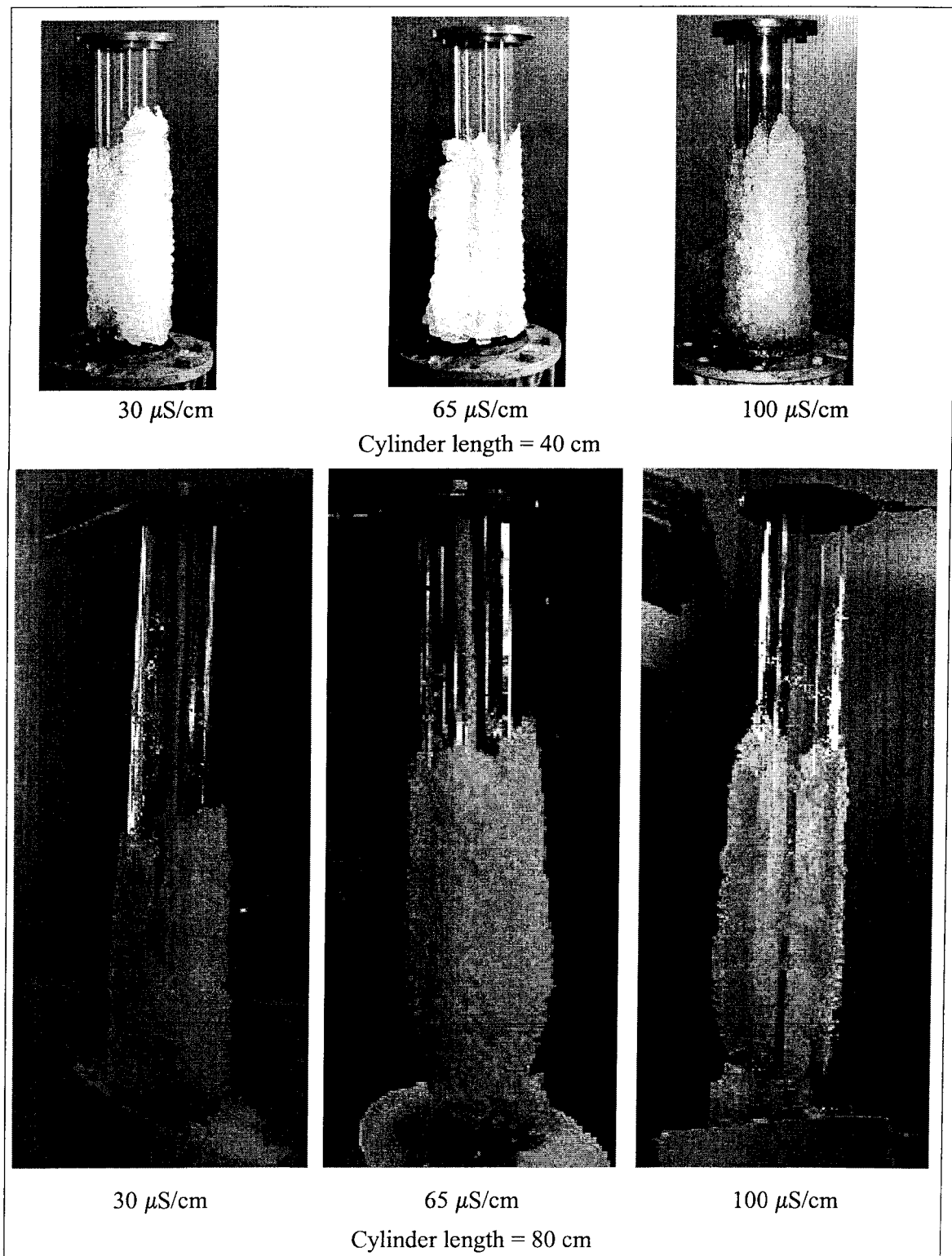
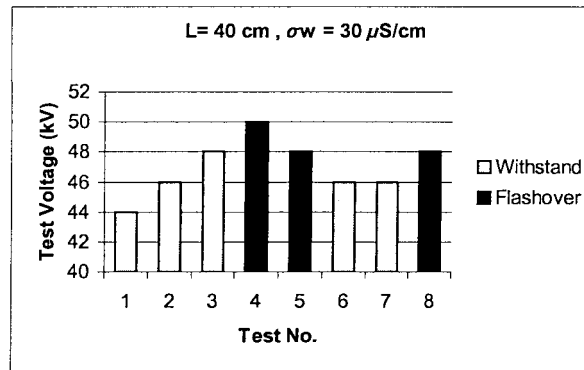


Figure 5.10 Ice geometry immediately after flashover.

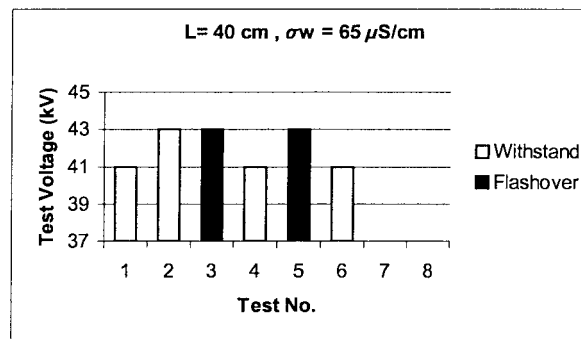
The results of flashover experiments, as well as typical curves for current and voltage, will be discussed and presented in the following sections. These results will be used later to complete and to verify the mathematical model presented.

5.3.1 Flashover Results

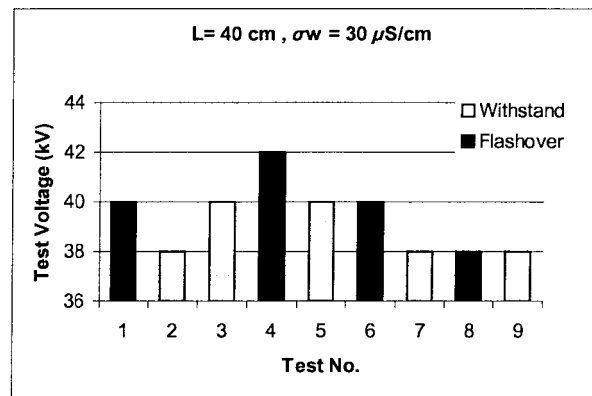
The flashover test results were obtained from 6 different series of experiments on cylinders of 2 different lengths, 40 and 80 cm each, and a further 6 series on standard post insulators of lengths 54 and 103 cm. Three different applied water conductivities of 30, 65 and 100 $\mu\text{S}/\text{cm}$ were applied. According to the evaluation method, each series was constituted of at least 5 tests, which, under optimum conditions, contain 2 flashovers and 3 withstands. The results are shown in Figures 5.11 to 5.14, and then in summary form in Table 5.2. The mean ice width, w , on cylinder and post insulator was 39 and 44 cm, respectively. Due to the uniform ice formation on cylinder and tested post insulator, the arcing distance of accumulated ice was almost the same as dry arcing distance of insulators. Therefore, hereafter, L represents whether the insulator length or arcing distance.



$$V_{MF} = 48 \text{ kV}$$



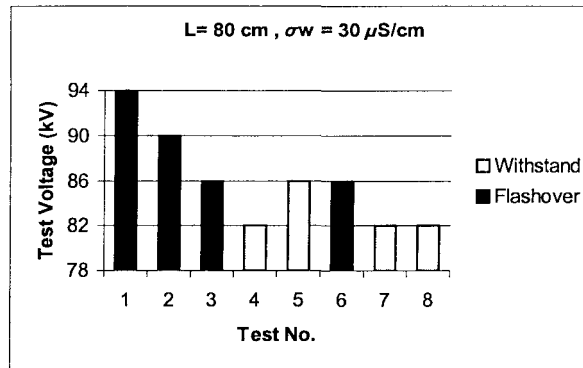
$$V_{MF} = 43 \text{ kV}$$



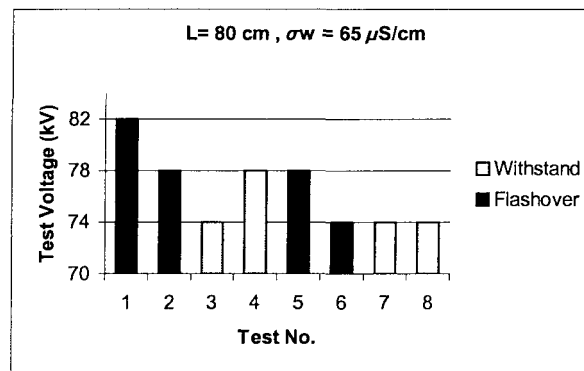
$$V_{MF} = 40 \text{ kV}$$

$L = 40 \text{ cm}$

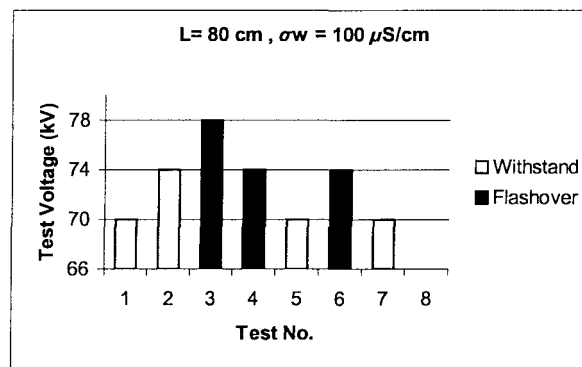
Figure 5.11 Flashover test results for $L = 40 \text{ cm}$ on a cylindrical insulator and different applied water conductivities.



$$V_{MF} = 86 \text{ kV}$$



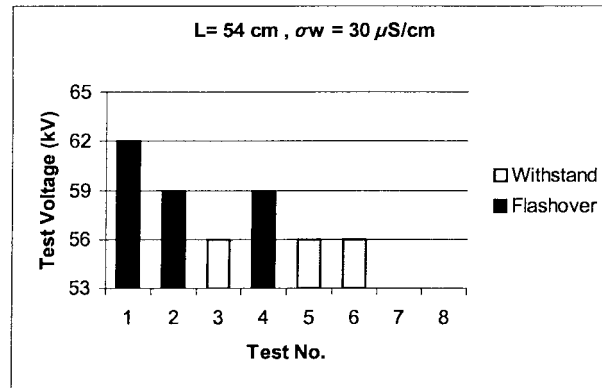
$$V_{MF} = 78 \text{ kV}$$



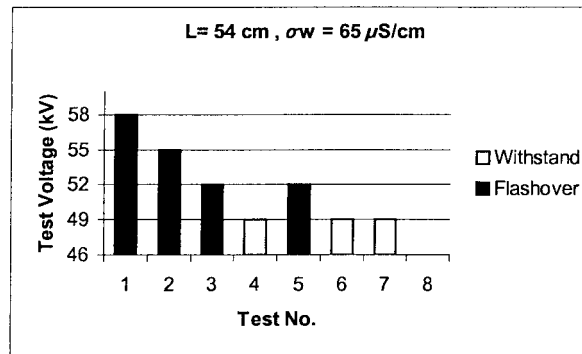
$$V_{MF} = 74 \text{ kV}$$

L = 80 cm

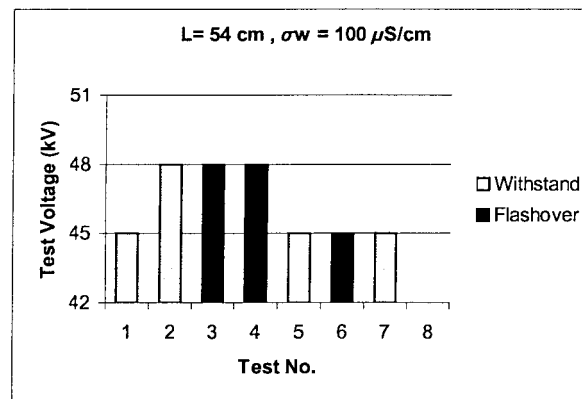
Figure 5.12 Flashover test results for $L = 80 \text{ cm}$ on a cylindrical insulator and different applied water conductivities.



$$V_{MF} = 59 \text{ kV}$$



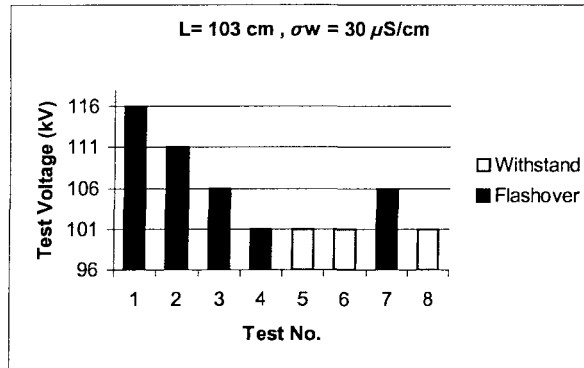
$$V_{MF} = 52 \text{ kV}$$



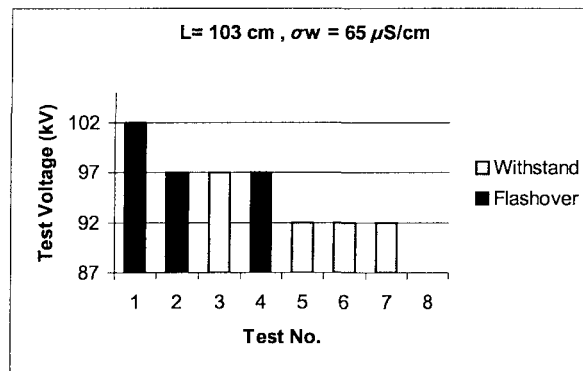
$$V_{MF} = 48 \text{ kV}$$

$L = 54 \text{ cm}$

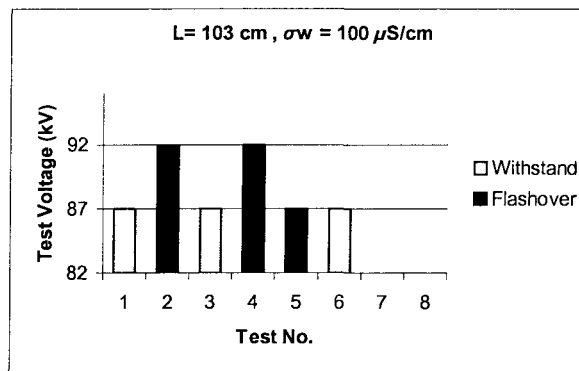
Figure 5.13 Flashover test results for $L = 54 \text{ cm}$ on a post insulator and different applied water conductivities.



$$V_{MF} = 106 \text{ kV}$$



$$V_{MF} = 97 \text{ kV}$$



$$V_{MF} = 92 \text{ kV}$$

$L = 103 \text{ cm}$

Figure 5.14 Flashover test results for $L = 103 \text{ cm}$ on a post insulator and different applied water conductivities.

Table 5.2 Minimum flashover voltages (kV) for cylinder and post insulator.

		30 $\mu\text{S/cm}$	65 $\mu\text{S/cm}$	100 $\mu\text{S/cm}$
Cylinder	$L = 40 \text{ cm}$	48	43	40
	$L = 80 \text{ cm}$	86	78	74
Post Insulator	$L = 54 \text{ cm}$	59	52	48
	$L = 103 \text{ cm}$	106	97	92

5.3.2 Effects of Initial Air Gap Length

Three additional series of tests were done on a cylinder to study the effects of the initial air gap on V_{MF} . These series were carried out on a 40 cm length insulator and three different applied water conductivities of 30, 65 and 100 $\mu\text{S/cm}$. The air gap was artificially created so as to encompass 15% of the total insulator length. The results are shown in Table 5.3.

Table 5.3 Flashover results for a 40 cm cylinder and longer initial air gap in kV.

	30 $\mu\text{S/cm}$	65 $\mu\text{S/cm}$	100 $\mu\text{S/cm}$
Initial Air Gap = 6 cm	47	43	44

A comparison of these results with those of previous tests was made in Figure 5.15. It may be seen that, for conductivities of 65 and 100 $\mu\text{S/cm}$, the flashover voltage is the same as the flashover voltage of a 65 $\mu\text{S/cm}$ ordinary test, where the initial air gap length is 7-8% of the total insulator length.

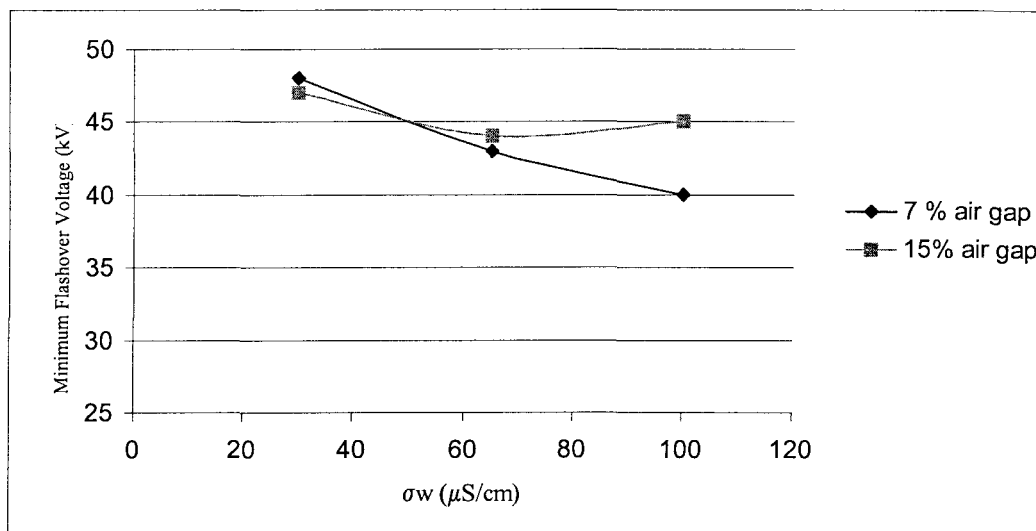


Figure 5.15 Comparison of different flashover results for different initial air gap lengths, and different applied water conductivities, σ_w .

For higher conductivity (100 $\mu\text{S/cm}$), when the voltage was less than the flashover value of 65 $\mu\text{S/cm}$, no discharge was observed and when it was higher or equal to this value, a sudden flashover occurred. This confirms that the flashover voltage obtained is, in fact, the level of threshold voltage for longer artificial air gaps. This means that the only effect of the initial air gap length is to increase the threshold voltage for breaking down the air gap. Then, after establishing the arc along the air gap and when melting water is present on the insulator surface, this length has no more effect on discharge phenomena.

5.3.3 Current and Voltage Curves

When flashover takes place, current increases and goes toward short circuit current. The study of current and voltage curves shows that the current curve contains strong harmonics and is not purely sinusoidal, but also that after the appearance of the

white arc, the peak moments of voltage and current occur almost simultaneously. The distortion of the current curve may be due to the nonlinearity of both arc and surface-water resistances (see Fig. 5.16).

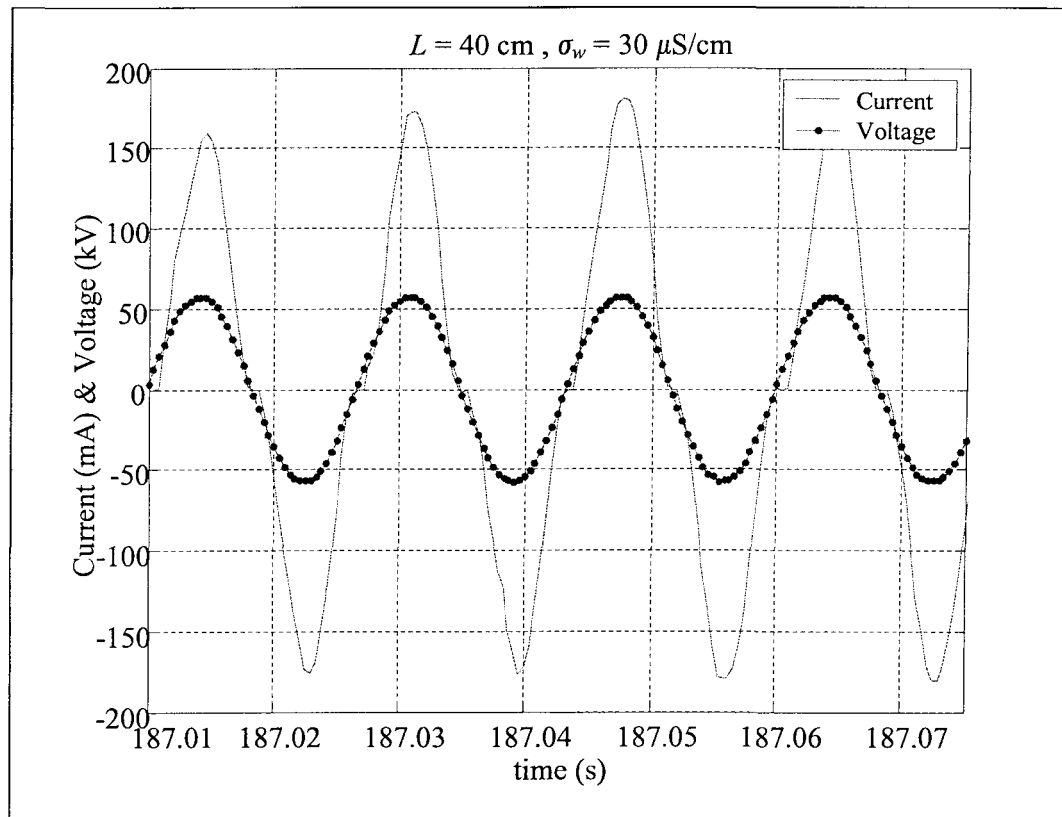


Figure 5.16 Typical current and voltage signals.

In all experiments, flashover occurred when the voltage signal was nearly its maximum value. When a complete flashover occurs, the current increases while the voltage drops to zero (cf. Fig. 5.17).

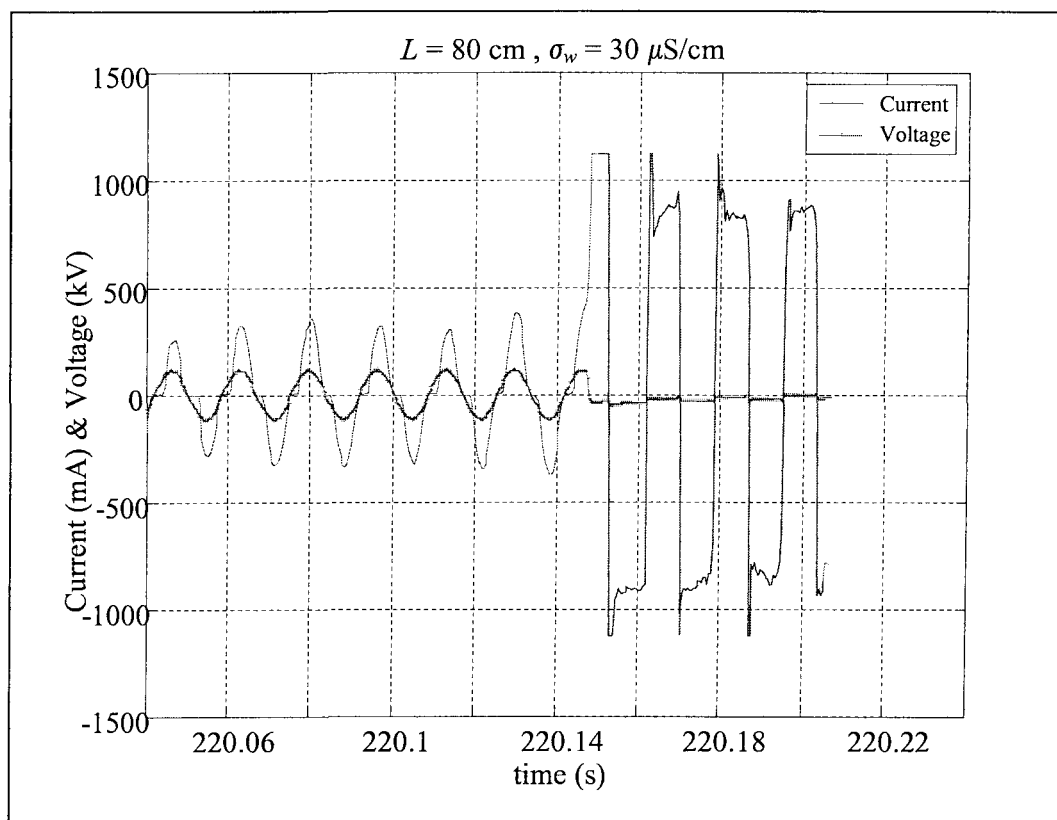


Figure 5.17 Typical current and voltage signals for a flashover test.

In almost all of the experiments, the flashover (current increase) occurs within three acquired points, which by considering a frequency of acquisition of 2400 Hz, leads to $t = 3/2400 \text{ s}$ or almost 1.25 ms. Thus, the duration of this stage, Δt , is assumed to be 1.25 ms, based on the requirement of obtaining the best curve-fitting as compared to the experimental current curve. However, the results of next section show that this duration is less than 1 ms.

5.3.4 Arc Length Observations

The arc behavior during the final propagation stage was observed using a high speed camera. The filming speed was 1000 images per second which makes it possible

to take approximately four images every quarter cycle. This filming rate was not sufficient to measure the velocity of arc propagation, particularly during the propagation stage, where the flashover takes place in less than 1 ms and can not be filmed using our equipment. Therefore the arc velocity was not measured during the experiments.

Figure 5.18 shows a typical last cycle before flashover for a tested insulator. It will be observed that, before flashover, for almost the entire period, arc length remains constant at the same length.

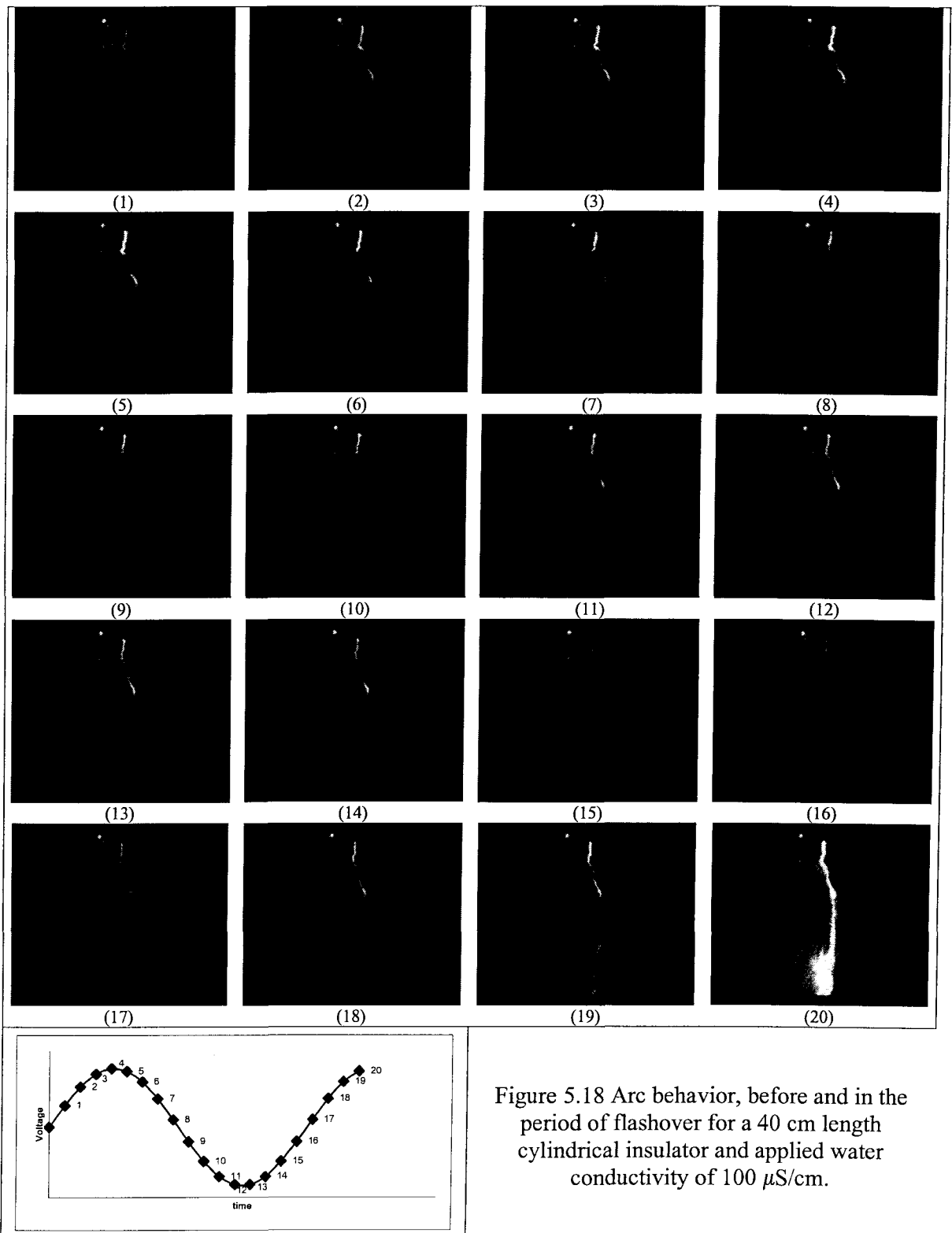


Figure 5.18 Arc behavior, before and in the period of flashover for a 40 cm length cylindrical insulator and applied water conductivity of $100 \mu\text{S}/\text{cm}$.

5.4 Recapitulation of Main Points

A number of experiments were carried out in order to obtain minimum flashover voltage as well as current and voltage variation on different ice-covered insulators, where cylindrical, as well as a post-type, insulators were involved. Two lengths and three applied water conductivities were tested resulting in 12 series of tests. The arc behavior during the pre-flashover stage was observed using a high-speed camera, however, the capacity of the camera used (1000 images per second) was not sufficient in order to measure the arc velocity during its propagation period of time. The duration of propagation, Δt , seems to be 1.25 ms. The arc was observed to be stationary for several seconds over a length of 45-60 % of the total insulator length before flashover occurred. The latter variable is independent of initial air gap length. The flashover seems to occur when the dripping water conductivity reaches its maximum value and applied voltage is in vicinity of its peak value within a cycle. The maximum conductivity of dripping water for flashover tests is higher than withstand results. The peak moments of arc current and applied voltage seem to be coincidence. Time to flashover was lower for higher conductivities, than for lower ones.

CHAPTER 6

TEST DATA ANALYSIS AND NUMERICAL SIMULATIONS

CHAPTER 6

TEST DATA ANALYSIS AND NUMERICAL SIMULATIONS

As mentioned in previous chapters, the arc heat dissipation rate, P_0 , in Eq. 4.19 should be based on the analysis of test result data. This chapter contains an analysis of the test data used to calculate the above-mentioned parameter; it also includes simulation results covering a few seconds of the pre-flashover stage; and results of the flashover stage itself.

6.1 Pre-flashover Stage Simulation

As already defined, the second stage of arc development begins at the very moment that a white arc is established and lasts up to the moment of arc propagation inception. The mechanism of water film formation on the ice bulk surface and the major role it plays in the inception of the discharge phenomenon was explained in an earlier chapter. This water film is also a main factor in determining the resistance of the ice layer. In fact, a study of the above phenomenon of water film evolution shows a dynamic change in the conductivity of the surface water which is a multi-faceted function of (a) ambient temperature, (b) the freezing process, (c) applied water conductivity, and (d) Joule heat injected by arc burning,

among several other factors. The surface-water conductivity also changes as a function of the applied electric field and the current which passes through the ice. All of the preceding points make it a laborious process to identify the temporal evolution of this parameter during the ice-melting period in the second stage. Thus, it is only by using the exact values of different variables such as arc length, arc temperature and surface conductivity, that the arc current may be simulated, otherwise, predicting the arc current during this stage cannot be accomplished (cf. Section 4.3.1).

In order to simulate arc current under certain known conditions during a given cycle in this stage, the same model as shown in Figure 4.3 is applied, then Eqs. 4.5 through 4.12 are used for calculating different circuit parameters. These equations are repeated here for ease of consultation:

$$L_{arc} = \frac{\mu_0 x}{2\pi} \left[0.25 + \ln\left(\frac{100}{r}\right) \right] \quad (6.1)$$

$$C(x, t) = 2\pi\epsilon\alpha \left[1 + (r/(L - x)) \right] \quad (6.2)$$

$$\alpha = \left(1 - 1/\sqrt{1 + \left[\left(\frac{\phi}{2L}\right) \left(\frac{1}{1 - x/L}\right) \right]^2} \right) \quad (6.3)$$

$$R_{arc} = \frac{1}{\sigma} \frac{x}{\pi r^2} \quad (6.4)$$

$$r = \sqrt{\frac{I_{arc}}{0.87\pi}} \quad (6.5)$$

$$R_{ice} = \frac{1}{2\pi\gamma_e} \sum_{j=-\infty}^{j=+\infty} \frac{1}{2} \log \left[\frac{\left(1 + \cosh \frac{\pi(jw+r)}{2L}\right)^2 + \tan^2 \frac{\pi x}{2L} \sinh^2 \frac{\pi(jw+r)}{2L}}{\left(1 - \sinh \frac{\pi(jw+r)}{2L}\right)^2 + \tan^2 \frac{\pi x}{2L} \sinh^2 \frac{\pi(jw+r)}{2L}} \right] \quad (6.6)$$

Figures 6.1 to 6.4 are presented here to illustrate model performance in predicting a typical current cycle as it occurs a few cycles before flashover moment on cylinders and post insulators covered with ice. The simulated current is also compared to the one obtained from experiments.

The value of the surface conductivity may be considered constant from a few cycles before propagation stage to the moment of flashover. This may be ascribed to the much higher speed of the flashover mechanism, when compared to the speed of the heat transfer phenomenon on the ice surface. Thus, surface conductivity was determined using Eq. 4.4 which reads as follows [51]:

$$\gamma_e = 0.0675\sigma_w + 2.45 \quad (6.7)$$

while the arc temperature was considered to be 4500 °K ($\sigma = 0.0005 \text{ 1}/\Omega\text{cm}$) which is close to its maximum attainable value. It was observed from the experiments (cf. Section 5.3) that the maximum arc length before the propagation stage attains 45-60% of the total insulator length. A shorter arc length results in a higher arc current due to higher arc resistance per unit as compared to that of ice during the second stage. Then higher arc current in turn results in lower arc resistance per unit. The arc length was considered to be 45% of total insulator length as a typical value for the simulations in this section. Ice layer

resistance was calculated using Eq. 6.6, where the mean ice width was $w = 39$ cm for a cylinder, and $w = 44$ cm for a standard post insulator.

The non-linearity of arc resistance and inductance causes a deformation in the arc current wave when the current passes through zero. The phase difference between simulated and experimental results involves the necessity for correcting the inductance relationship. In fact, using Eq. 6.1 produces very small values for arc inductance so that this factor becomes negligible compared to the resistance of the arc. This phase difference confirms that the real inductance of the arc should be higher than the one obtained using Eq. 6.1, at least with regard to insulator lengths of less than 1 m. The disparity between the results of the simulated and experimental current, when the arc current approaches zero, may be due to the use of the arc root radius equation. This equation was derived from peak values of the current [147] and may possibly not be applicable to all instants of a cycle.

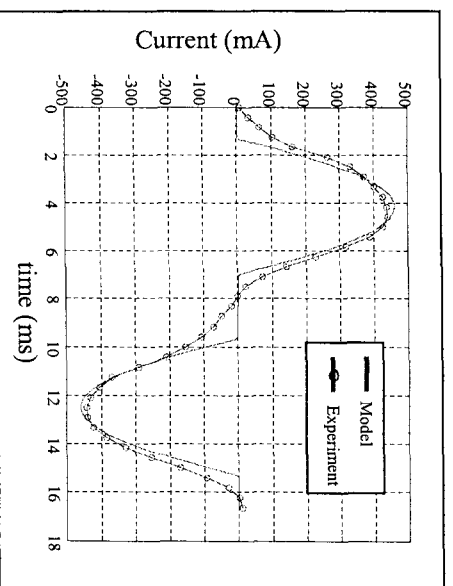
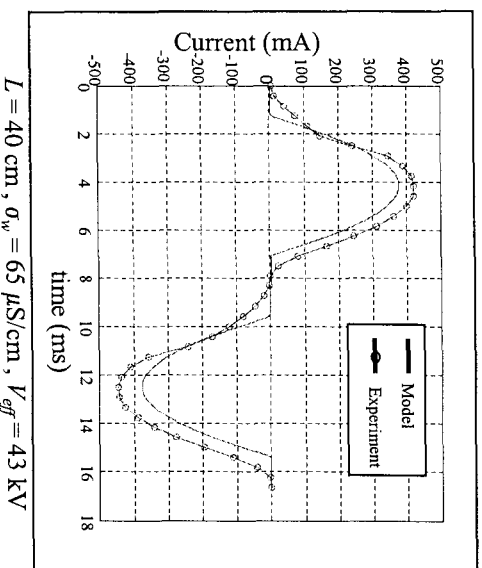
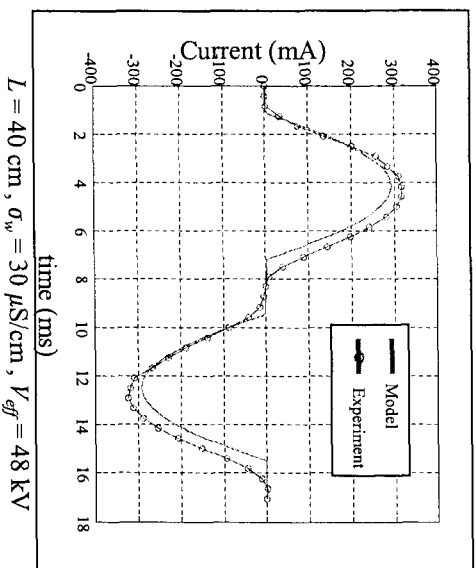
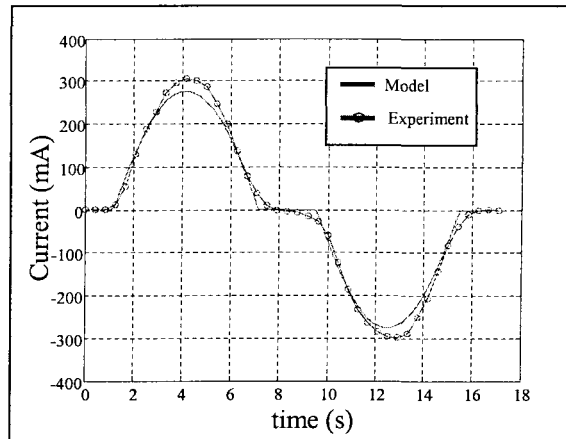
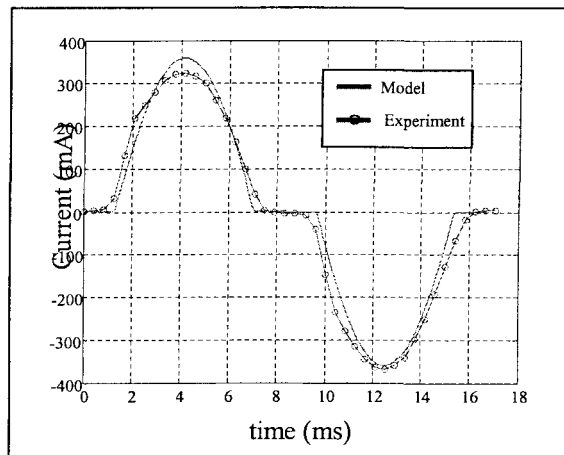


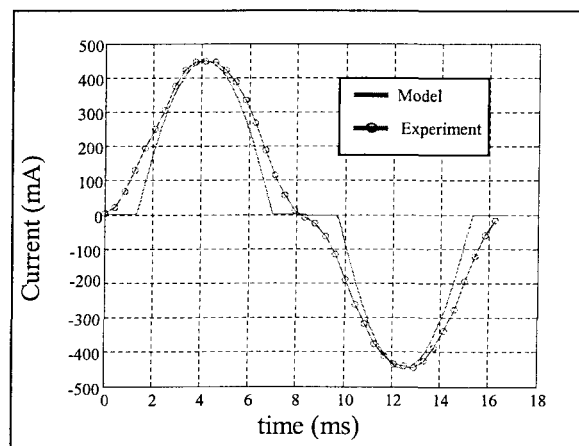
Figure 6.1 Arc current during second stage for iced cylinder and $L = 40 \text{ cm}$.



$L = 80 \text{ cm}, \sigma_w = 30 \mu\text{S/cm}, V_{eff} = 86 \text{ kV}$

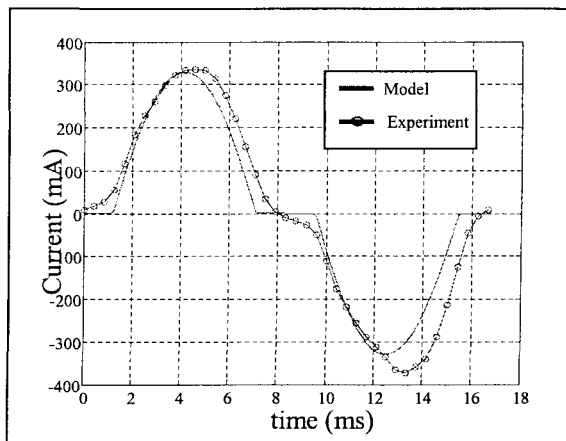


$L = 80 \text{ cm}, \sigma_w = 65 \mu\text{S/cm}, V_{eff} = 78 \text{ kV}$

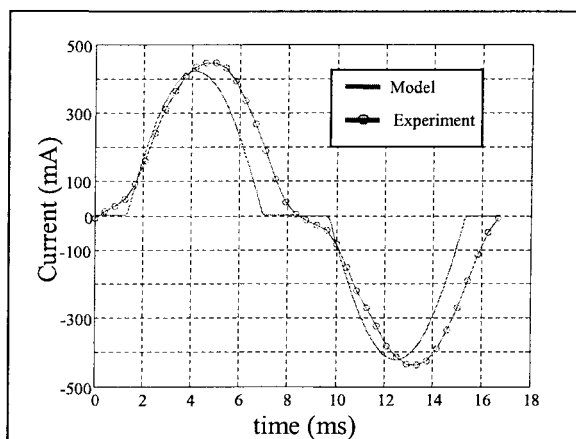


$L = 80 \text{ cm}, \sigma_w = 100 \mu\text{S/cm}, V_{eff} = 74 \text{ kV}$

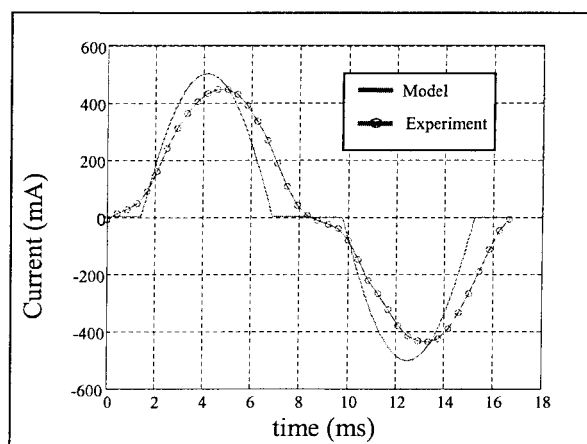
Figure 6.2 Arc current during second stage for iced cylinder and $L = 80 \text{ cm}$.



$L = 54 \text{ cm}, \sigma_w = 30 \mu\text{S/cm}, V_{eff} = 59 \text{ kV}$

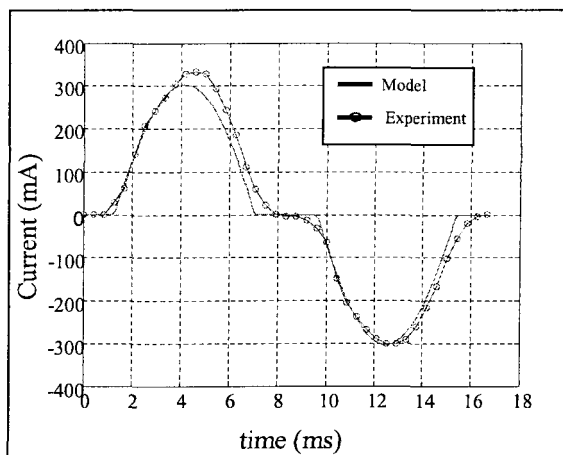


$L = 54 \text{ cm}, \sigma_w = 65 \mu\text{S/cm}, V_{eff} = 52 \text{ kV}$

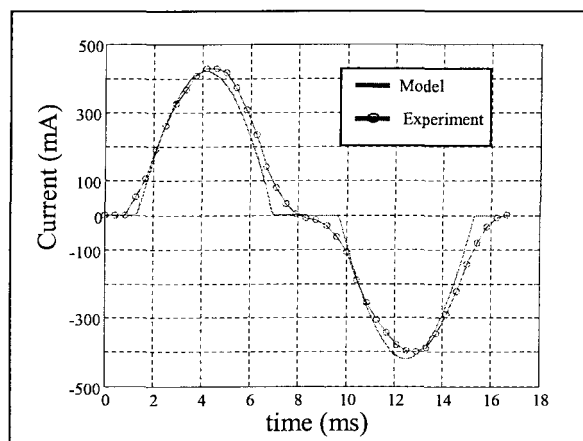


$L = 54 \text{ cm}, \sigma_w = 100 \mu\text{S/cm}, V_{eff} = 48 \text{ kV}$

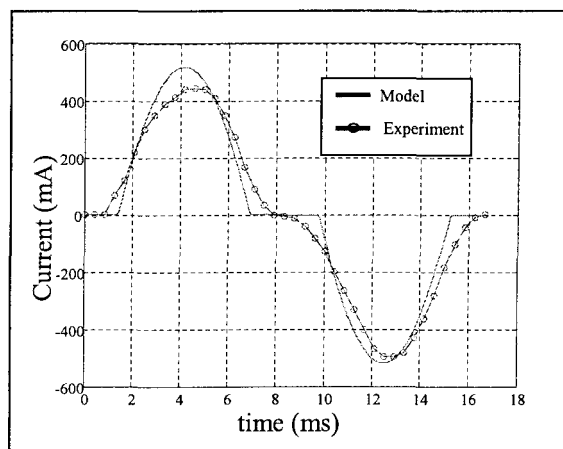
Figure 6.3 Arc current during the second stage for tested post insulator and $L = 54 \text{ cm}$.



$L = 103 \text{ cm}, \sigma_w = 30 \mu\text{S/cm}, V_{eff} = 101 \text{ kV}$



$L = 103 \text{ cm}, \sigma_w = 65 \mu\text{S/cm}, V_{eff} = 97 \text{ kV}$



$L = 103 \text{ cm}, \sigma_w = 100 \mu\text{S/cm}, V_{eff} = 92 \text{ kV}$

Figure 6.4 Arc current during the second stage for tested post insulator and $L = 103 \text{ cm}$.

Figure 6.5 shows a typical current cycle before flashover moment on a post insulator of $L = 103$ cm, $w = 44$ cm, and applied water conductivities ranging from 30 to 100 $\mu\text{S}/\text{cm}$. It may be concluded from the figure that higher applied water conductivities result in higher arc currents before flashover. This is clearly due to the decrease in the surface resistance.

The applied voltage here was considered constant at 105 kV per one meter of dry arcing distance, therefore $V_{eff} = 108.2$ kV. It should be mentioned that higher applied water conductivities lead to lower minimum flashover voltages [40]. Thus, under flashover voltage, the difference between peak values of the current should be lower than those observed in Figure 6.5.

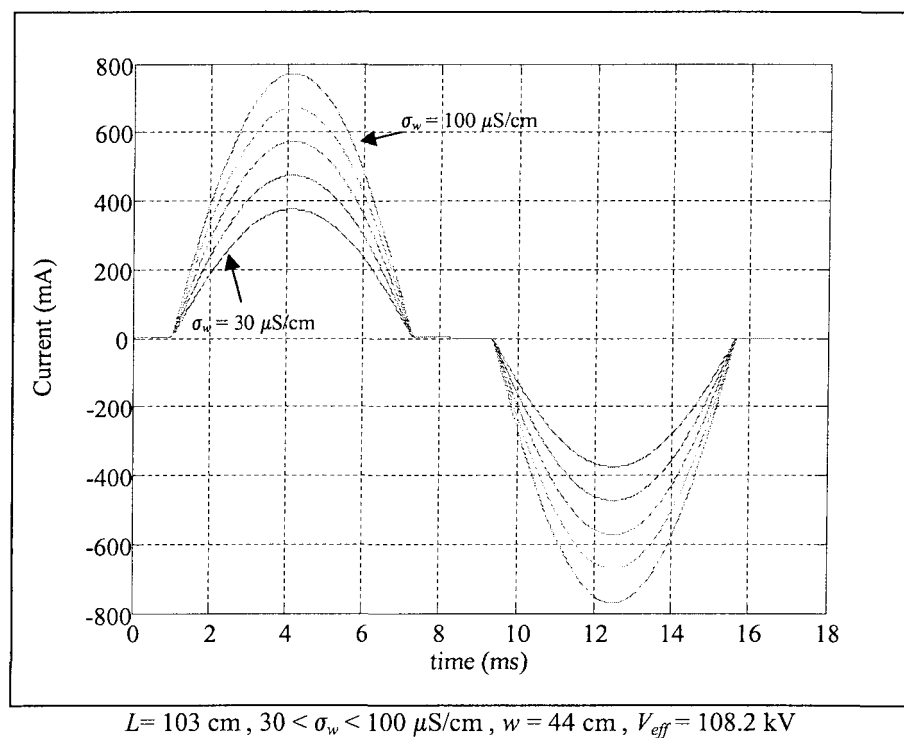


Figure 6.5 Effect of applied water conductivity, σ_w , on typical arc current cycle.

Figure 6.6 shows a typical current cycle before flashover moment on a post insulator of $L = 103$ cm, $\sigma_w = 65 \mu\text{S/cm}$, and ice widths ranging from 40 to 60 cm. It may be concluded from the figure that higher ice widths result in higher currents before flashover. This is also due to the decrease in the surface resistance.

The applied voltage, here too, was considered constant at $V_{eff} = 108.2$ kV. Since greater ice widths result in lower minimum flashover voltages [13], the differences between the currents, under flashover voltage conditions, should be less than those observed in Figure 6.6.

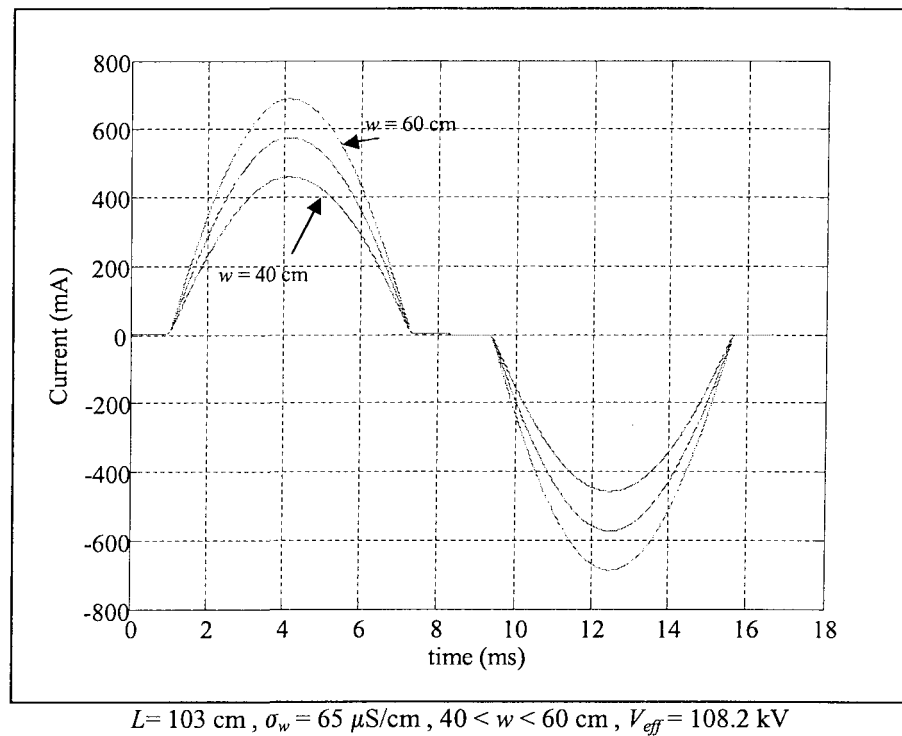


Figure 6.6 Effect of ice width, w , on typical arc current cycle.

Figure 6.7 shows a typical current cycle before flashover on a post insulator for $w = 44$ and $\sigma_w = 65 \mu\text{S/cm}$, and insulator lengths ranging from 50 to 150 cm. The applied voltage was considered constant at $V_{eff} = 105 \text{ kV}$ per meter of dry arcing distance, thus causing the discharge current to remain constant.

It was observed that the minimum flashover voltage per unit decreases when insulator lengths increase [40]. Therefore, under flashover voltage conditions, longer insulator lengths should result in lower initial currents than for shorter insulators.

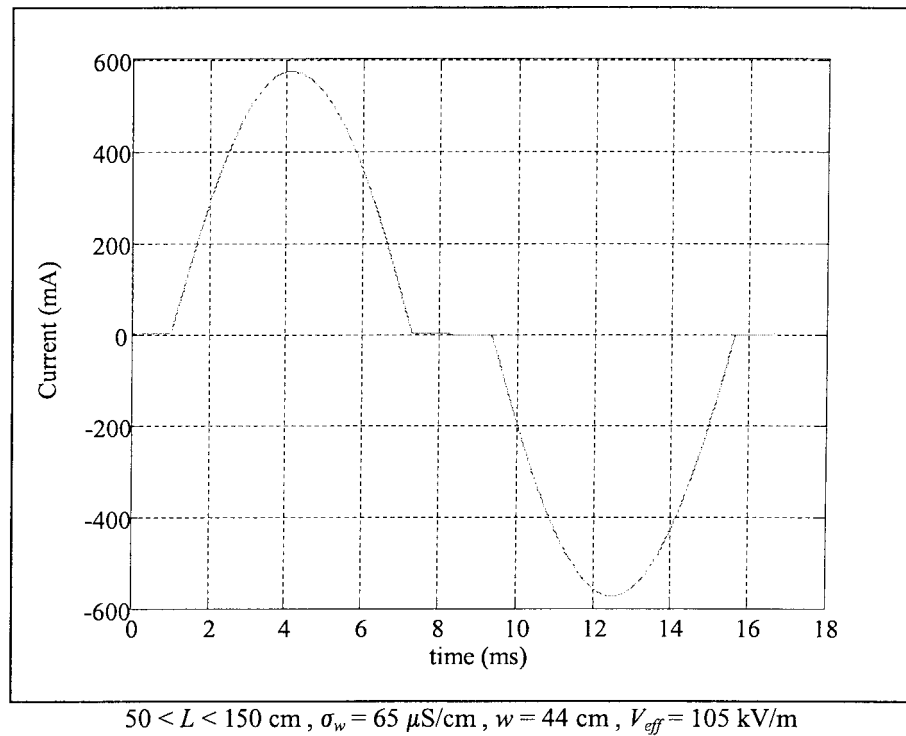


Figure 6.7 Effect of insulator length, L , on typical arc current cycle.

6.2 Heat Dissipation Rate Calculations

The value of the heat dissipation rate, P_0 , should be determined by comparing the critical flashover voltage, as calculated using the model, with results obtained by experiment (cf. Section 4.4.4). In order to calculate this parameter, the model in Figure 4.3 and the same procedure as shown in Figure 4.5 are applied. The arc resistance is calculated here using Eq. 4.19 as follows:

$$\frac{1}{r_{arc}} \frac{dr_{arc}}{dt} = \frac{1}{\tau} \left(1 - \frac{r_{arc} I_{arc}^2}{P_0}\right) \quad (6.8)$$

A large number of simulations using different test characteristics produce different values for P_0 . Table 6.1 shows these values in VA/cm, for different test results, where L is indicated in centimeters and σ_w in $\mu\text{S/cm}$.

Table 6.1 Values of P_0 obtained by comparing experimental results with those of simulations.

		$\sigma_w = 30 \mu\text{S/cm}$	$\sigma_w = 65 \mu\text{S/cm}$	$\sigma_w = 100 \mu\text{S/cm}$
$w = 39 \text{ cm}$	$L = 40 \text{ cm}$	235	270	315
	$L = 80 \text{ cm}$	260	325	350
$w = 44 \text{ cm}$	$L = 54 \text{ cm}$	225	270	295
	$L = 103 \text{ cm}$	275	350	390

From Table 6.1, it may be concluded that:

- the greater the length, the higher the P_0 ,
- the higher the applied water conductivity, σ_w , the higher the P_0 ,

This increase in P_0 occurs in the view of the fact that longer insulator lengths produce colder ambient temperatures which in turn accelerate the process of heat dissipation, and also the fact that higher σ_w results in higher arc currents and temperatures, thus resulting in higher heat dissipation rates. The average of the values indicated in Table 6.1 is 296.7 VA/cm. Therefore, hereafter, P_0 is considered to be constant at this value for cylinder and post insulators.

The input data for this model are insulator length, L , applied water conductivity, σ_w , and ice width, w . Accordingly, the ice-covered insulator under investigation will be considered as a rectangular ice volume covered with a conductive surface as was considered earlier in [13, 17, 51 and 146-148] (cf. Section 4.4.1). It should be remembered that insulators of a greater diameter tend to accumulate ice of greater width, and thus the ice-width effect will tend to reflect the insulator diameter effect [147]. This also implies that insulator geometry is of no great significance in calculating ice resistance, and that the only influencing parameters are insulator length and insulator radius. The specific model parameters are: duration of propagation, Δt ; initial arc temperature, T_0 ; and initial arc length, L_{arc0} . The output of the model includes the critical flashover voltage and the temporal evolution of different circuit parameters such as arc current and velocity. It was observed from the experiments that initial arc length lies between 45-60 % of the total insulator length and that duration of propagation is almost 1.25 ms (cf. Section 5.3). It was also mentioned that the maximum attainable initial arc temperature is 4550 °K [2].

Figures 6.8 and 6.9 each shows the effect of variations in L_{arc0} and T_0 on the critical flashover voltage calculated. Simulation results show that even a 30% variation in the

duration of propagation, Δt , will have no effect on critical voltage calculation. The simulation input data are tabulated as follows:

Table 6.2 Simulation input data.

	L (cm)	w (cm)	σ_w ($\mu\text{S}/\text{cm}$)	$T0$ ($^{\circ}\text{K}$)	L_{arc0}/L (%)
Figure 6.8	100	44	80	4550	45-60
Figure 6.9	100	44	80	4400-4700	45

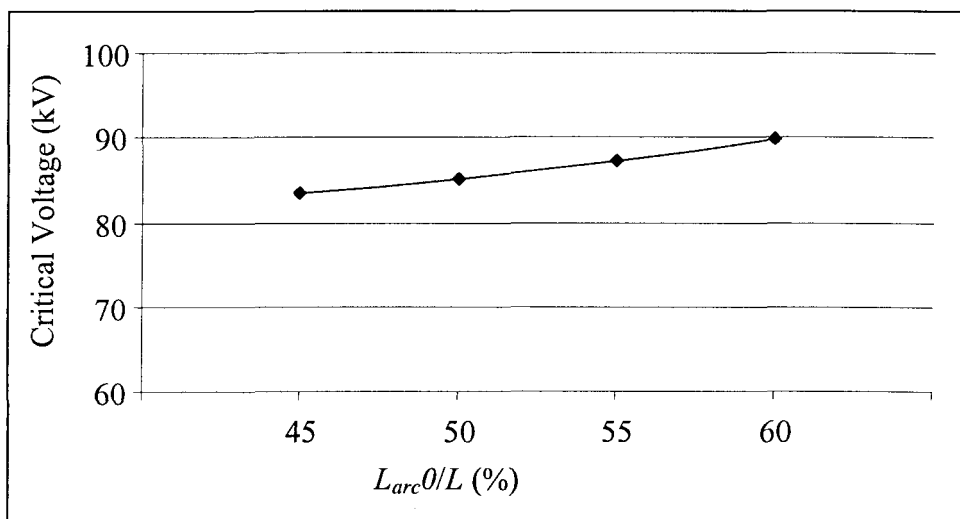


Figure 6.8 Effect of variations in L_{arc0} on the calculation of flashover voltage.

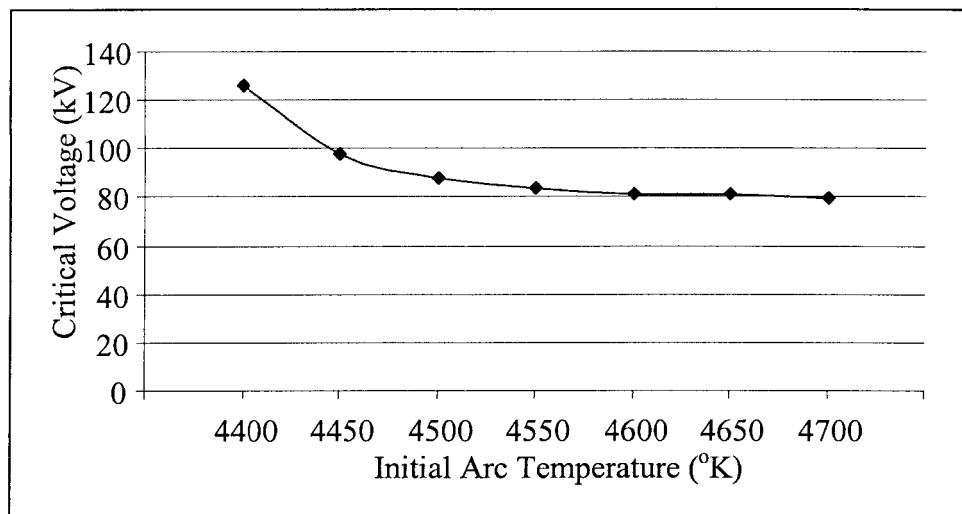


Figure 6.9 Effect of variation of T on the calculation of flashover voltage.

It may be concluded from Figures 6.8 and 6.9 that a decrease in initial arc length or an increase in initial arc temperature causes a corresponding decrease in critical flashover voltage. This effect is a result of the decrease in initial arc resistance. A shorter arc length results in a higher arc current due to higher arc resistance per unit as compared to that of ice during the second stage. Then higher arc current in turn results in lower arc resistance per unit. From now on in the text, the initial arc length will be considered at 45% of the total insulator length, based on the conclusions emerging from Figure 6.8, since this value results in a minimal value for the critical flashover voltage. In the case of this particular simulation, the variation of the critical voltage is less than 6% due to a variation of initial arc length. From Figure 6.9, it may be seen that the increase in initial arc temperature has no significant effect on flashover voltage after a certain value ($T_0 = 4550$ °K). This value

relates to the maximum air temperature attainable by the arc [2]. In general, the model is robust in the range of the desired test data.

6.3 Calculation of Flashover Voltage

6.3.1 Comparison of the Model and Experiments

Figures 6.10 to 6.13 compare the critical flashover voltage values, V_c , obtained by the model, with those emerging from the experiments. The error bars indicate the percentage of error between the experimental points and the corresponding model results. The figures show that these results are in satisfactory concordance, although the percentage of error tends to increase for smaller lengths and lower conductivities or greater length and higher conductivities.

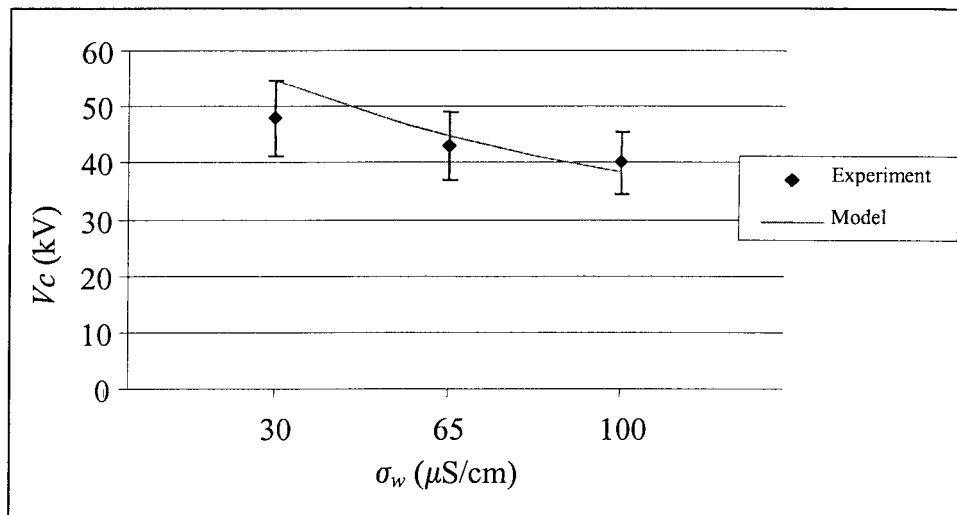


Figure 6.10 Flashover results for a 40-cm iced cylinder and different applied water conductivities with 13.6% difference.

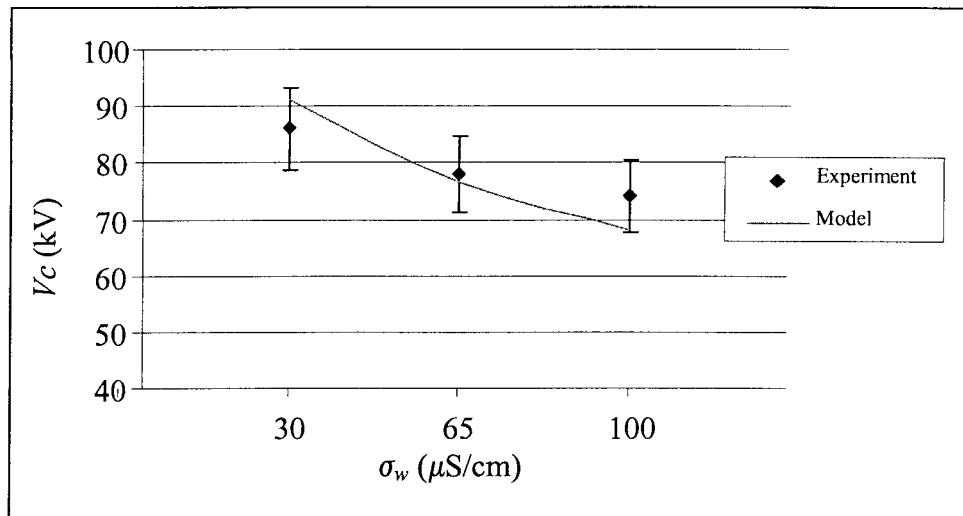


Figure 6.11 Flashover results for an 80-cm iced cylinder and different applied water conductivities with 8.9% difference.

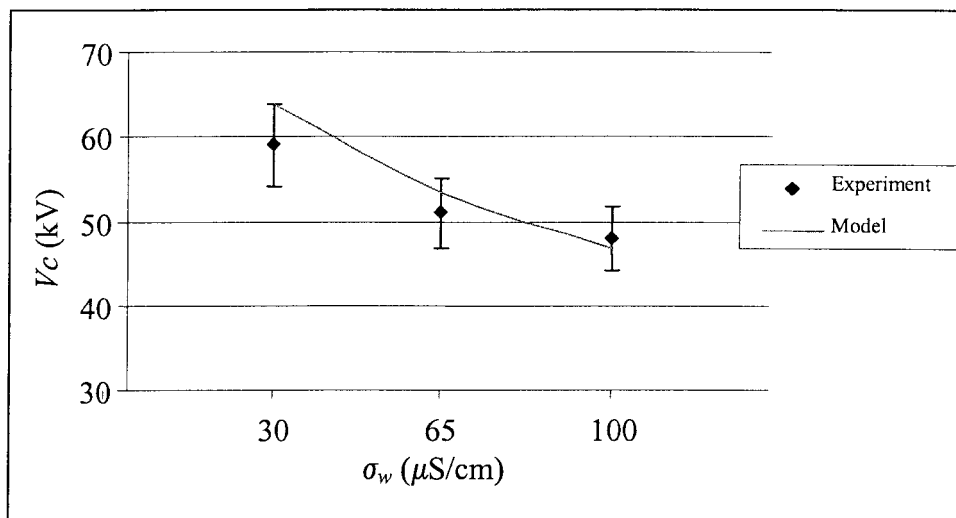


Figure 6.12 Flashover results for a 54-cm post insulator and different applied water conductivities with 8.1% difference.

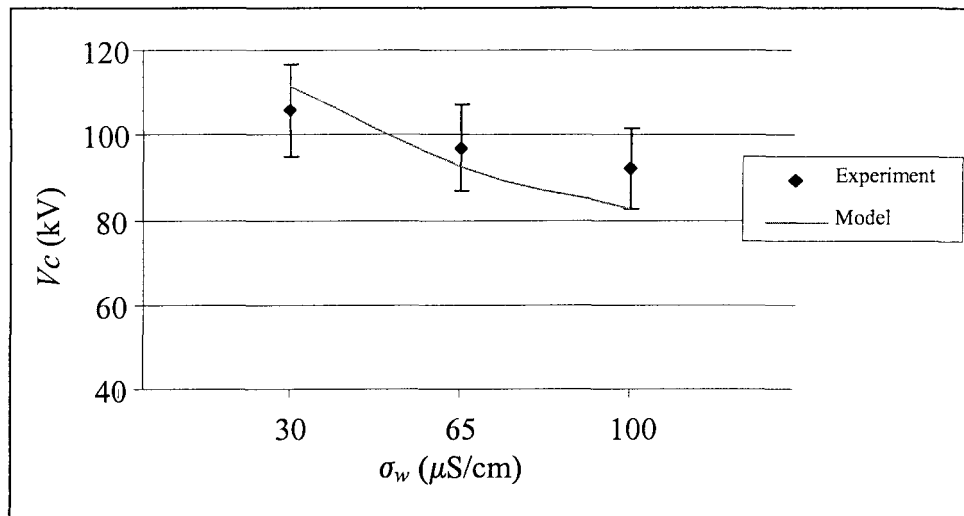


Figure 6.13 Flashover results for a 103-cm post insulator and different applied water conductivities with 10.3% difference.

The error in the calculation obviously is the result of assuming a constant value for P_0 , since this parameter showed a considerable variation as a reason of variation in insulator lengths, and in applied water conductivities (cf. Table 6.1). A part of the variation in calculation of P_0 may be due to the use of Eq. 6.7 for calculating surface conductivity, since the equation was based on the experimental results from a relatively short test object [51]. This relation (Eq. 6.7) was obtained by assuming equality between the surface resistance measured and its analytical relation, displaying a relatively high degree of error, up to 50% [51]. This deviation confirms that the surface conductivity at the moment of flashover is not only a function of applied water conductivity but also of further parameters. During the experiments carried out in the context of this study, it was observed that, at the moment of flashover, the conductivity of dripping water changes as a result of changes in insulator length. On the other hand, this relationship is based on a concept that water film

thickness is constant. If the length of the insulator is increased, this concept may no longer be applicable. Thus, for more accurate calculation this relationship (Eq. 6.7) needs to be investigated in much greater detail.

6.3.2 Present Model and Experiments Performed by Other Researchers

In order to assess the performance of the present model, it was first submitted to a variety of test characteristics used by other researchers. The results of each of these tests were then compared with each other.

The specific tests which were carried out within the context of this research project encompassed a range of test characteristics relating to insulator length and applied water conductivity. Thus model performance was only compared with the results of other researchers when their test characteristics lay outside those of this thesis project. It will be observed from Figures 6.14 to 6.18 that this new model displays acceptable performance qualities.

6.3.2.1 Cylinder and Post Insulator

Figure 6.14 shows a comparison between the results obtained by the present model and those of the experiments [17] on a relatively small cylinder covered with a wet-grown ice layer. The parameters submitted to testing were the insulating cylinder length, $L = 30$ cm, the ice width assumed to be $w = 39$ cm, and various applied water conductivities between 40 and 120 $\mu\text{S}/\text{cm}$. The maximum error for this curve is 6.4%.

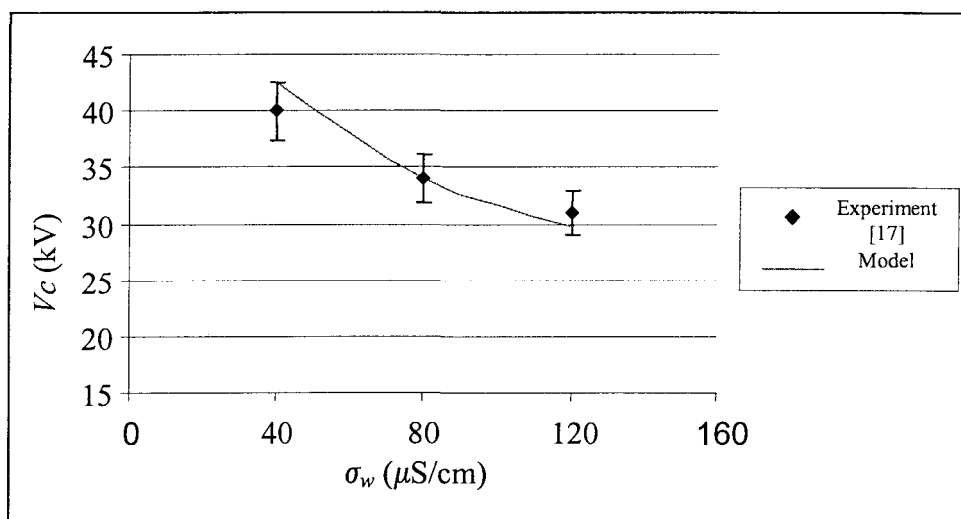


Figure 6.14 Flashover results for a 30-cm iced cylinder and various applied water conductivities.

Figure 6.15 shows a comparison between the results obtained by the model and those of the experiments [17] on a cylinder covered with wet-grown ice. The applied water conductivity was $\sigma_w = 80 \mu\text{S}/\text{cm}$, the ice width was assumed to be $w = 39 \text{ cm}$, and different cylinder lengths were applied. The maximum error for this curve is 5.7%.

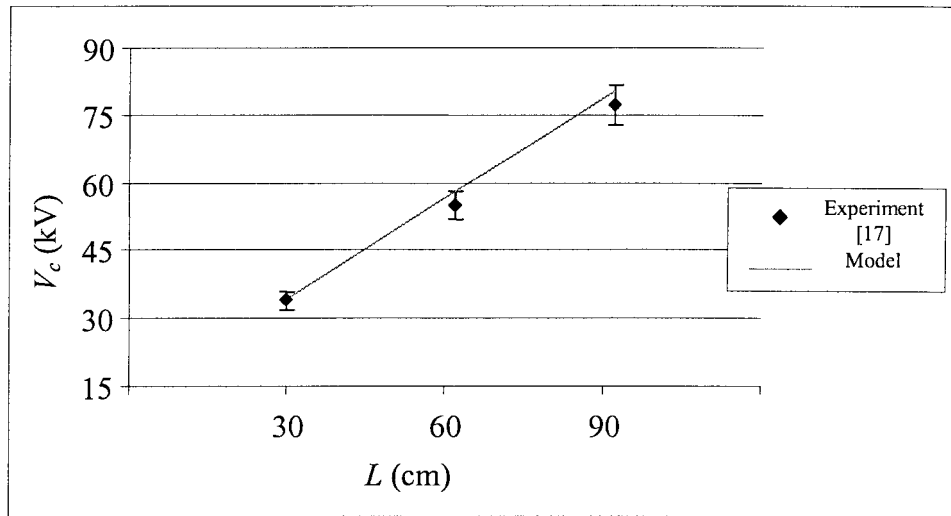


Figure 6.15 Flashover results for applied water conductivity of $80 \mu\text{S}/\text{cm}$ and different cylinder lengths.

6.3.2.2 IEEE Standard String Insulators

This section outlines the results of variation in critical flashover voltages due to the varying of different test parameters such as insulator length, L , applied water conductivity, σ_w , and wet-grown ice width, w , on IEEE standard insulator strings with an outer diameter of 25.4 cm. The model results are also compared with the results of experiments performed by other researchers and those of a static model [147]. In this static model, the arc constant in the re-ignition condition, K , (cf. Section 3.2.2) was experimentally established earlier at 1118 [51]. Other arc constants, A , n and b , were set at 204.7, 0.5607 and 0.5277, respectively [51].

Two ice samples, identical in length and width, occurring on a post insulator and on standard insulator strings, lead to a lower minimum flashover voltage on the insulator string. This information was compiled from a comparison between the data available in [31] and [45]. Thus, the heat dissipation rate, P_0 , for insulator strings should be lower than the rate obtained for post insulators. This may be due to the fact that arcs on post insulators burn in an air-and-vapor medium which increases the heat exchange rate between the arc and the medium itself. On the other hand, arcs on string insulators burn from beneath the ice sample, so the vapor around the arc space is much less intense, causing the heat exchange rate to be lower. A large number of simulations showed that the heat dissipation rate, P_0 , for this type of insulator should be considered at 191.2 VA/cm which will be used throughout this section. It should be mentioned that all experimental results here were obtained from wet-grown ice accumulated under 105 kV/m of electric stress.

Effects of L : Figure 6.16 shows the simulation results of critical flashover voltages for different dry arcing distances on an ice width of $w = 46.2$ cm (cf. [51]), and $\sigma_w = 80$ $\mu\text{S}/\text{cm}$. The experimental results were taken from [44], where 1 to 6 units of IEEE insulator strings were tested under uniform wet-grown ice.

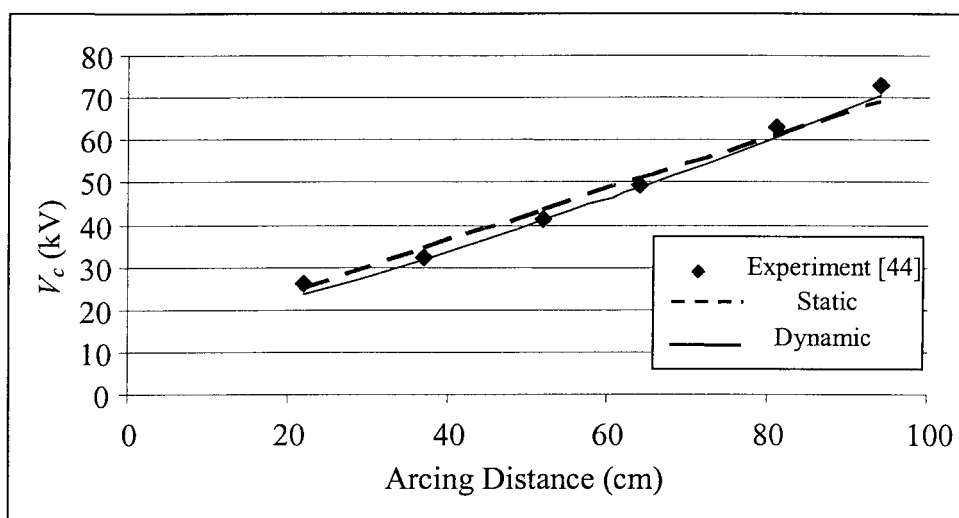


Figure 6.16 Calculated and experimental critical voltages of 1 to 6 units of IEEE standard strings for $w = 46.2$ cm and $\sigma_w = 80$ $\mu\text{S}/\text{cm}$.

Effects of σ_w : The model was also applied to a string of 5 units of IEEE standard insulators where different applied water conductivities were tested. The wet-grown ice layer was considered to be 46.2 cm wide and the arcing distance, L , was considered to be 80.9 cm [51]. The experimental results as well as the values calculated by the static model are presented in Figure 6.17.

A noticeable decrease in the flashover voltage resulting from an increase in the applied water conductivity may be observed for conductivities of less than 100 $\mu\text{S}/\text{cm}$, whereas for higher values, the effect of the variation of this parameter is less significant.

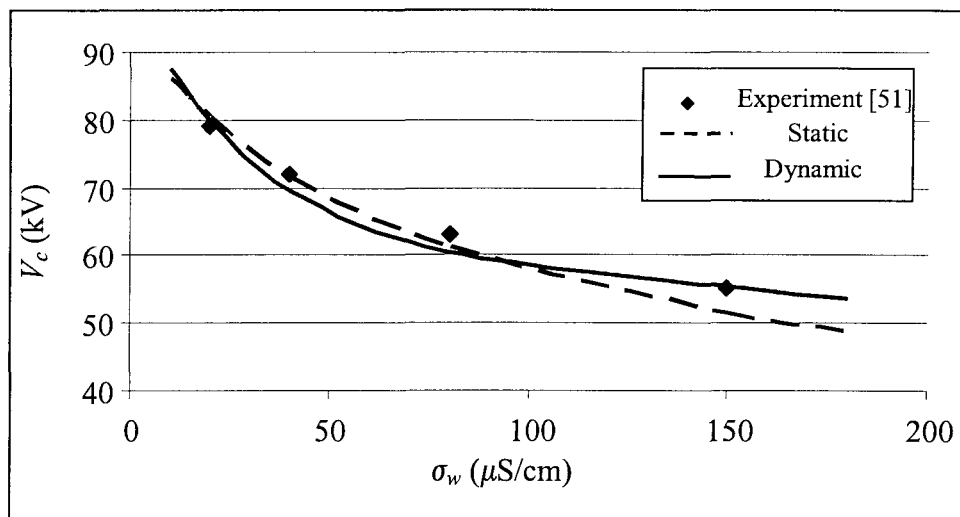


Figure 6.17 Calculated and experimental critical voltages for 5 units of IEEE standard insulators and different applied water conductivities.

Effects of w : Figure 6.18 shows the simulation results of different wet-grown ice widths on 5 units of IEEE standard insulators with a length of $L = 80.9$ cm, and $\sigma_w = 80$ $\mu\text{S}/\text{cm}$. The results of the dynamic model are presented together with static and experimental results [13].

An observable decrease in the flashover voltage with an increase in ice width may be seen for w of less than 30 cm, whereas this decrease becomes less significant for higher values of w . It should be remembered that the parameter w is proportional to the insulator diameter, and that an increase in w reflects an increase in insulator diameter.

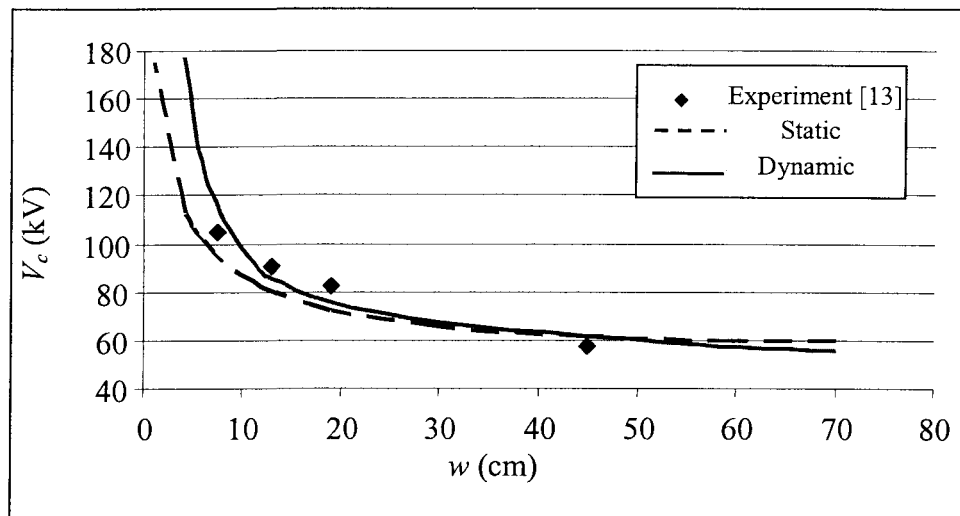


Figure 6.18 Calculated and experimental critical voltages of 5 units of IEEE standard insulator strings and different ice widths.

6.4 Simulation of the Propagation Stage

6.4.1 Arc Current Comparison

This section outlines the comparison between experimental measurements of arc current and those obtained by the model during the last quarter cycle. A study of experimental results showed that, in most cases, the arc starts to propagate and flashover takes place when the applied voltage approaches its peak value (cf. Section 5.3.3). Before this moment, which belongs in the second stage, the simulation is being run under the same assumptions as those prevailing in Section 6.1, except that the arc temperature is assumed to be at its maximum possible value of $T = 4550^{\circ}\text{K}$ ($\sigma = 0.0006 \text{ 1}/\Omega\cdot\text{cm}$). Then, when the voltage begins to approach its peak value, the current is calculated using the same assumptions as those explained in Section 6.1. The duration of this final propagation stage was assumed to be 1.25 ms (cf. Section 5.3.3). The reason for choosing this time value was based on the requirement of obtaining the best curve-fitting as compared to the experimental current curve. Also, as mentioned earlier, a $\pm 30\%$ variation of this parameter has no influence on flashover voltage calculations.

Figures 6.19 and 6.20 show a number of comparisons between the measured and simulated currents occurring in the last quarter cycle. In each case, the first part of the curve ($t < 3.54 \text{ ms}$) belongs in the second stage, up to the moment that the applied voltage rises to 97.2% of its peak value, or $t \cong 3.54 \text{ ms}$, while the second part of the curve ($3.54 \text{ ms} < t < 4.79 \text{ ms}$) belongs in the third stage or arc propagation stage.

A satisfactory agreement will be observed between the simulated and experimental currents shown in the figures, although the voltage applied in the simulation was considered to be the flashover voltage obtained from the model for those particular test characteristics.

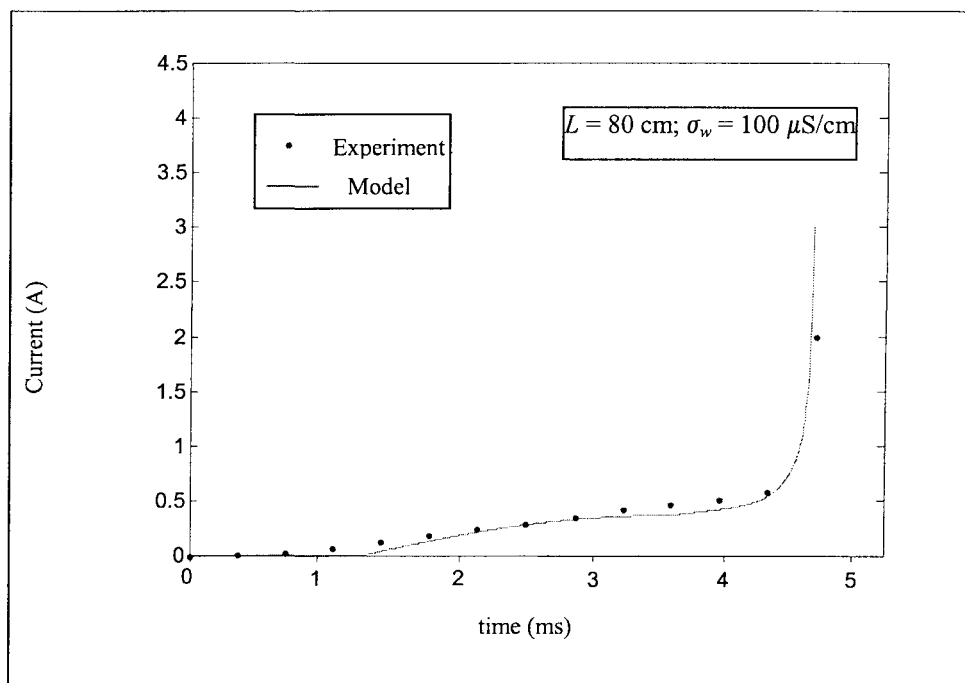
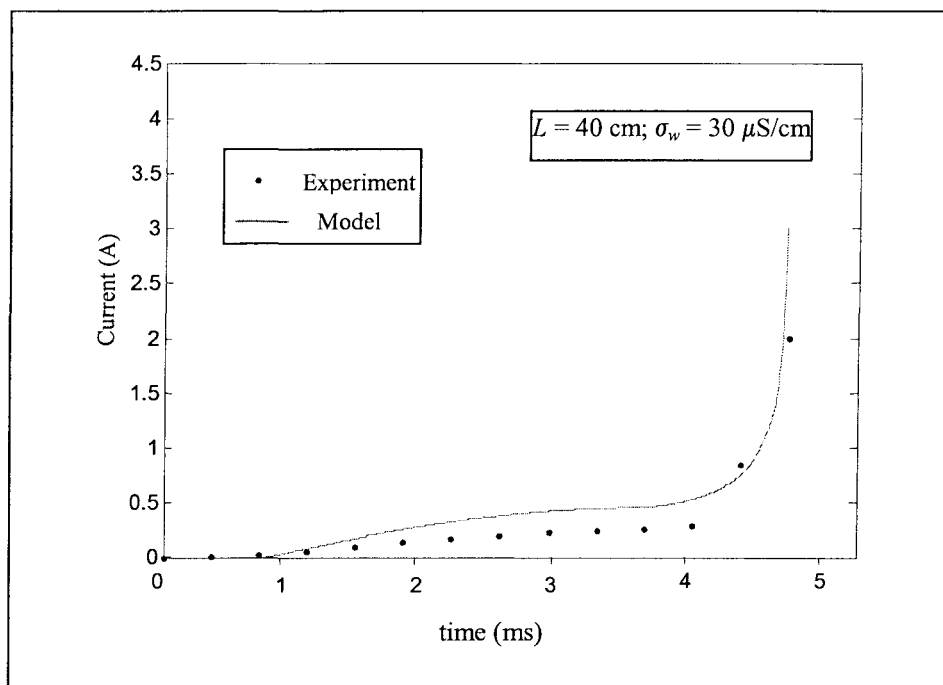


Figure 6.19 Experimental and calculated last quarter cycle of the current for an iced cylinder.

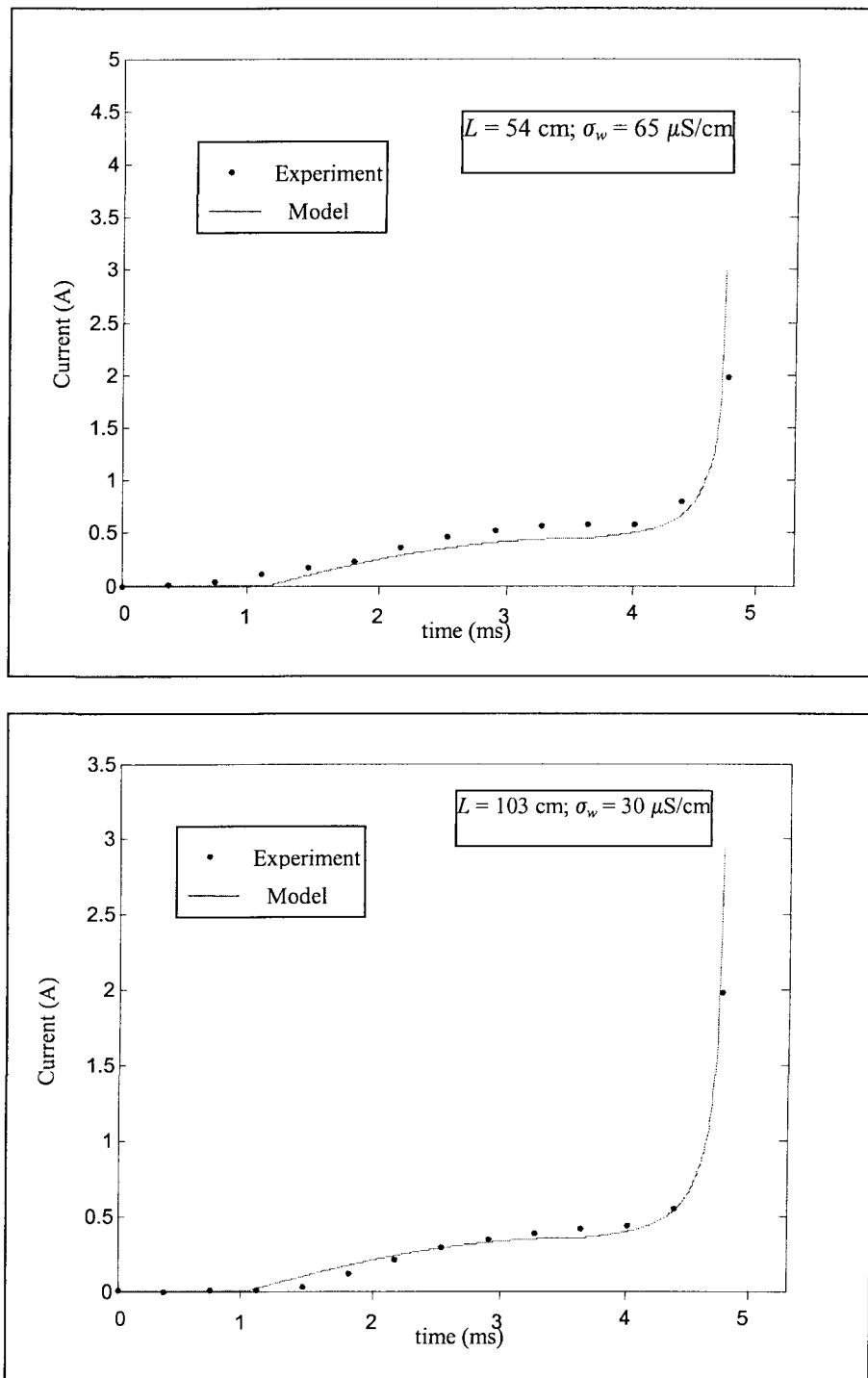


Figure 6.20 Experimental and calculated last quarter cycle of the current for a post insulator.

6.4.2 Propagating Arc

In this section, three different series of simulations are carried out, where each series is run for the purpose of studying the effects of one out of the three main parameters (L , w or σ_w) on arc dynamic characteristics. These characteristics are current, velocity, resistance per unit, and temperature of the arc during the propagation stage. The test object is a post insulator covered with wet-grown ice. Test settings are indicated in Table 6.3.

Table 6.3 Test settings for different series of simulation.

	L (cm)	w (cm)	σ_w ($\mu\text{S}/\text{cm}$)
Series 1	50-100	44	80
Series 2	100	20-50	80
Series 3	100	44	30-120

It should be mentioned here that the simulation is run under the assumption that there is no external impedance in the test circuit of the arc, and that the voltage source may deliver currents of up to several amperes without any significant effect on applied voltage. Also, each simulation was carried out under the critical flashover voltage obtained by the model for those particular test characteristics. Fresh direction indicates the increase in tested variable.

6.4.2.1 Arc Current

Figure 6.21 shows the effects of the three above-mentioned parameters on arc current during the propagation stage. It may be concluded from the figure that, for the range of characteristics tested, longer insulator lengths result in a higher current during propagation. This tendency was also observed for electrical breakdown in air gaps [114]. Such an effect may result from using a constant value for the heat dissipation rate. It was observed (cf. Section 6.2) that longer insulators lead to higher values of the heat dissipation rate. Therefore, using a constant value for different insulator lengths will result in a low heat dissipation rate for longer insulators. This in turn will result in higher currents.

An increase in the arc current with an increase in applied water conductivity and ice width (or insulator radius) may also be observed. This is obviously due to a decrease in the resistance of the unbridged ice layer.

The effect of variation in the ice width will be seen to be less when compared to that of variation in applied water conductivity. Such an effect is due to a lower variation in the resistance of the residual ice layer. In fact, for a particular value of current and arc length, the variation of ice width of 20 to 50 cm has much less effect than the variation of applied water conductivities of 30 to 120 $\mu\text{S}/\text{cm}$ on the resistance of this layer.

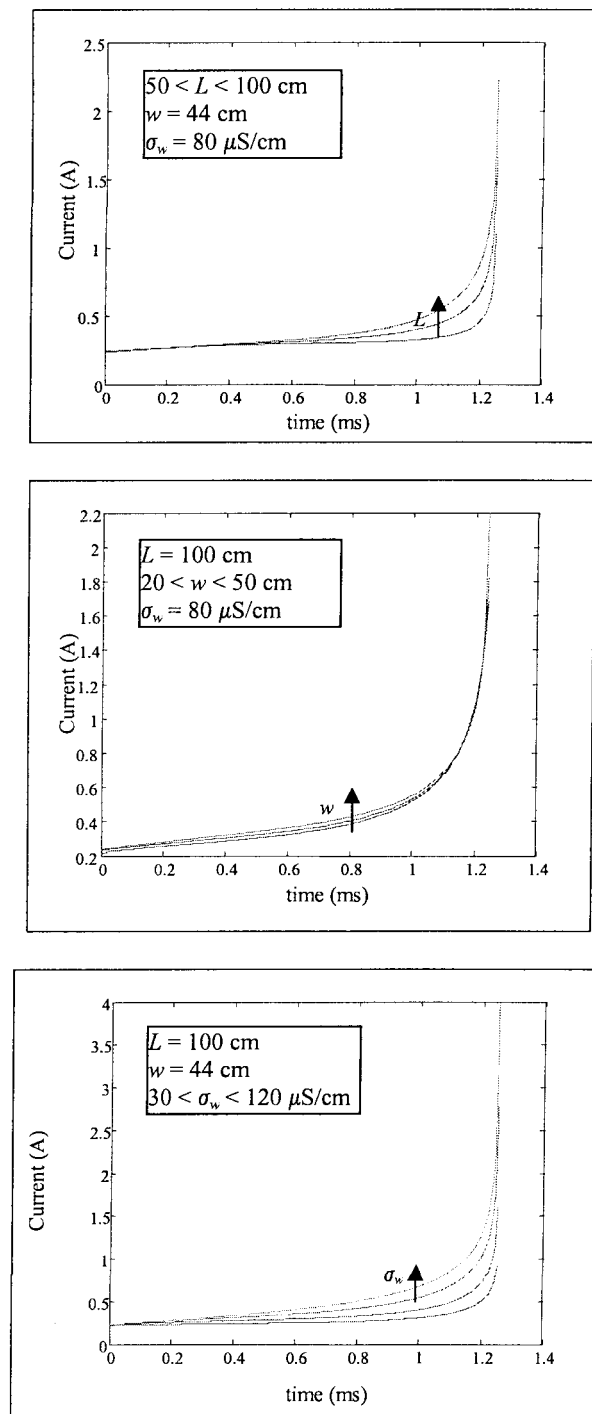


Figure 6.21 Arc current for different simulation series.

6.4.2.2 Arc Velocity

Figure 6.22 indicates the effects of the above-mentioned parameters on arc velocity, from which it may be concluded that, for the range of characteristics tested, longer insulator lengths result in higher maximum velocities during arc propagation. This tendency was also observed for electrical breakdown in air gaps [114]. Wider ice bands and higher applied water conductivities will also result in higher maximum velocities.

It should be noted that, on the basis of the model flowchart, the arc propagation period is to be considered constant for all of the simulations carried out. Also, based on the relationship used for arc velocity calculation (Eq. 4.20), this velocity is proportional to the arc current during its propagation. The factor of proportionality is adjusted by the model in such a way as to cause the arc to reach the other electrode within the desired period.

The variation in arc velocity may be explained on the basis of the above-mentioned concepts. Where greater insulator lengths are concerned, not only is the arc current higher than for shorter insulators, but also the arc must propagate more rapidly in order to cover a greater distance within the same time interval. In the case of similar lengths, as in series 2 and 3, the higher arc current at the end of arc propagation will lead to higher velocities; therefore the arc velocity must be less at the beginning of the propagation, in order to compensate for this effect.

In practical cases, a camera speed of at least 6000-8000 frames per second is required for recording arc behavior to measure the arc velocity, even though the applied voltage drops to zero when the arc length reaches approximately to the total insulator length.

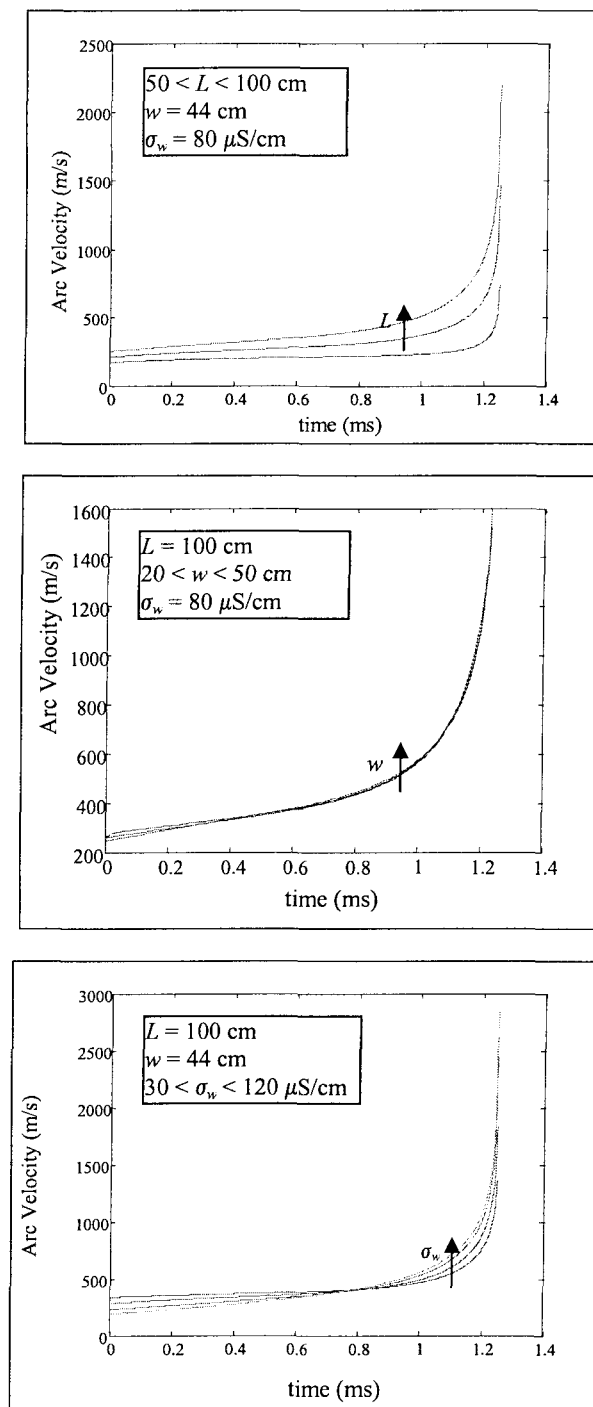


Figure 6.22 Arc velocities for different simulation series.

6.4.2.3 Arc Resistance per Unit

The effects of the various parameters on arc resistance per unit are shown in Figure 6.23. It should be noted that the initial arc resistance per unit is a function of a number of parameters (cf. Section 4.4.4). Generally speaking, lower applied voltages, greater insulator lengths, lower applied water conductivities, and lower ice widths will each result in lower initial arc currents. A lower initial arc current results in a higher initial arc resistance considering that the initial arc temperature was assumed to be constant. This tendency will be observed in the figure for the range of characteristics tested. Then, as a result of applying the Mayr equation, higher arc currents will result in a further decrease in arc resistance per unit during arc propagation. In view of the results shown in Figure 6.21, it may be concluded that longer insulator lengths, higher applied water conductivities, and greater ice widths, should result in a further decrease in arc resistance per unit, as will be seen in Figure 6.23.

As may also be observed, applying various test characteristics for a relatively wide range of data will result in an initial arc resistance per unit of between 6000-7000 Ω/cm . Approximate median values, lying in the central range of the quoted parameter, have already been used by other researchers for the simulation of arc behavior on polluted surfaces in dynamic models [24].

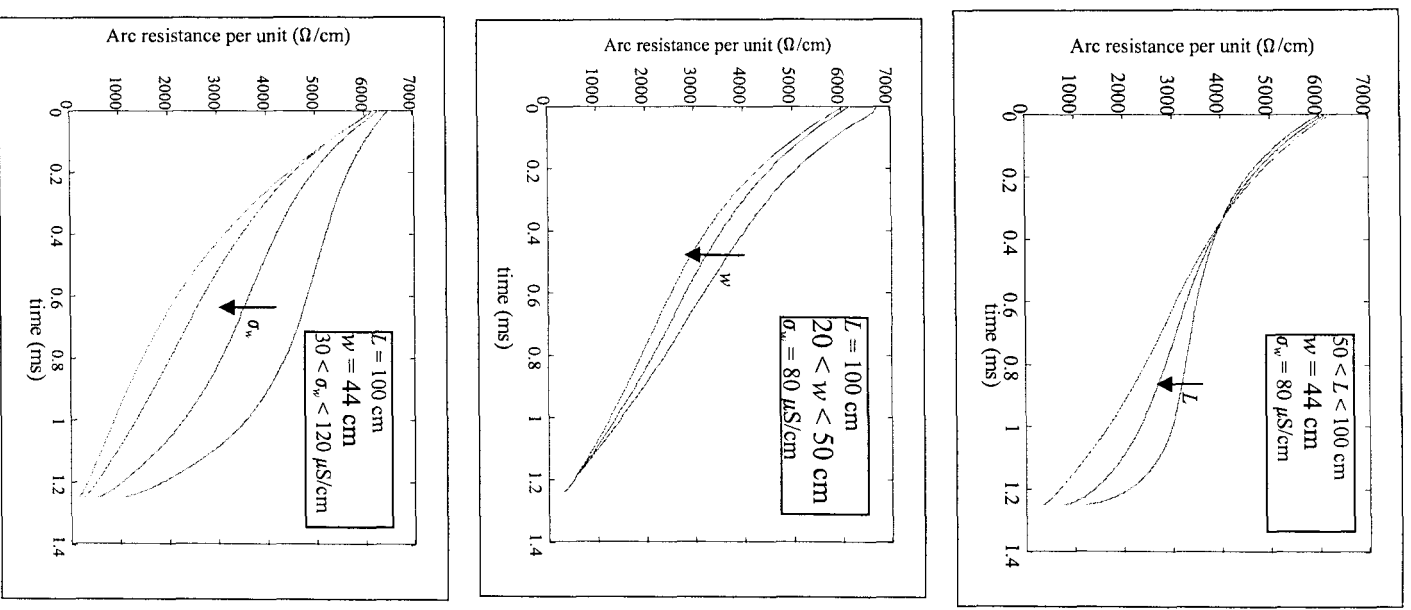


Figure 6.23 Arc resistances per unit for different simulation series.

6.4.2.4 Arc Temperature

During the propagation stage, the arc temperature is assumed to start from an initial value of 4600°K. Considering the classical equation for arc resistance, $R_{arc} = \frac{1}{\sigma} \frac{x}{\pi r^2}$, together

with the one for arc radius, $r(t) = \sqrt{\frac{I_{arc}}{0.875\pi}}$, a relationship for calculating equivalent arc

conductivity may be obtained as follows:

$$\sigma_{eq} = \frac{0.875}{r_{arc} I_{arc}} \quad (6.9)$$

This equivalent conductivity may be calculated using the already-obtained values of arc resistance per unit, r_{arc} , and arc current, I_{arc} . The arc temperature during this stage may then be estimated on the basis of Figure 4.4.

The values of arc current and arc resistance per unit will determine the value of arc temperature based on Eq. 6.9. It is expected that higher arc currents, however, will lead to higher arc temperatures due to the higher energy injected into the channel. This increase in temperature may be seen in Figure 6.24 for the range of data tested.

The decrease in arc temperature, when the arc length approaches the total insulator length, i.e. when flashover takes place and the current goes towards infinity, may be a result of applying Eq. 6.5. Based on this equation, the radius of the arc channel is proportional to the square root of the arc current. Thus, for very high currents, this relationship will lead to very high arc radii, while the energy injected into the channel may no longer be sufficient to maintain the arc temperature at high values. It should be mentioned that Eq. 6.5, which is

the equation of arc radius, was derived from the peak values of arc current [147], and may thus not be applicable to all instants of a cycle.

It should be noted that, at the particular time interval under discussion, the arc temperature decreases, although the arc current increases. Thus, the decrease in arc temperature does not affect the arc propagation criterion, since arc resistance per unit is already at very low values. With regard to the range of the data tested, it will also be observed that the arc temperature is limited to values of less than 5000°K for the entire propagation period.

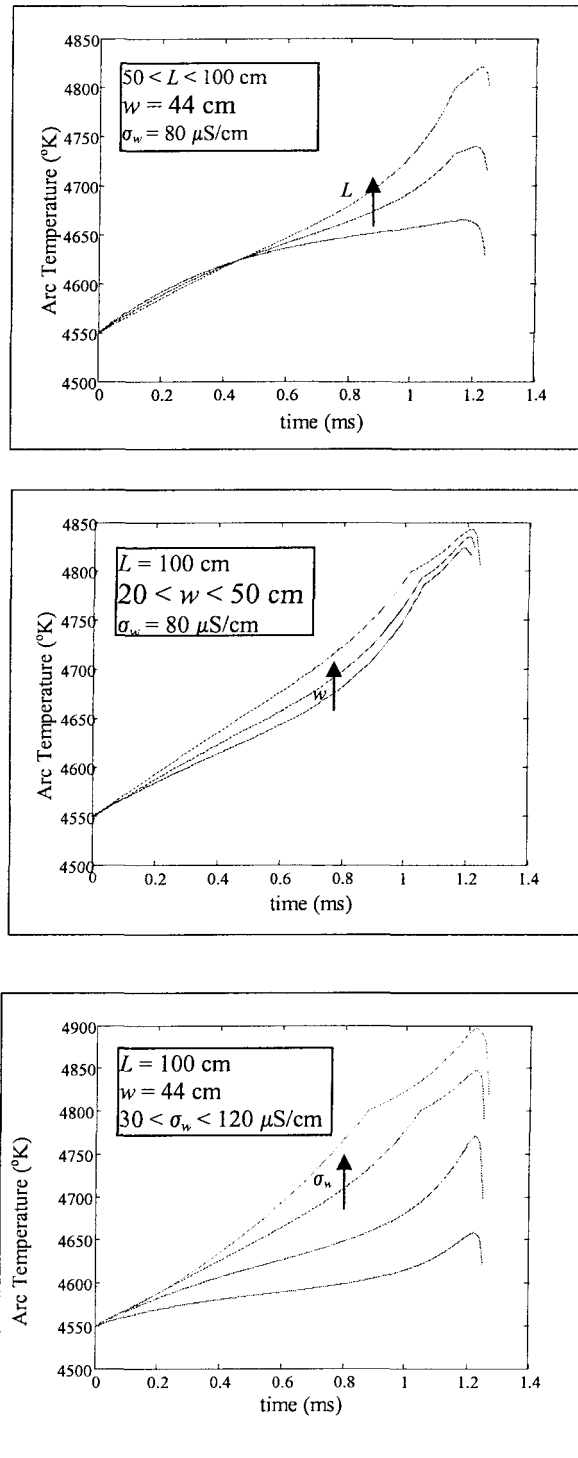


Figure 6.24 Arc temperatures for different simulation series.

6.4.2.5 *E-I Arc Characteristics*

It would be useful to evaluate the arc gradient against the arc current using simulated data obtained from dynamic modeling during the final arc propagation stage. Figure 6.25 indicates the *E-I* curve of the arc for the regions of current which are of particular interest to researchers. For higher currents, the arc gradient increases due to the increase in the arc current. This tendency may also be observed when applying alternative mathematical approaches for solving the arc heat-transfer equations [55 and 75].

The arc resistance per unit decreases with an increase in arc length, ice width and applied water conductivity, as was explained in Section 6.5.2.3. The tendency of the arc gradient to decrease with an increase in the arc current due to the preceding effect may be observed in the range of the data tested.

A regression on all the data obtained to present the dynamic *E-I* curve of the arc in the form of Ayrton's equation, will result in the following:

$$E_{arc} = 475.09I_{arc}^{-0.7098} \quad (6.10)$$

where the arc gradient, E_{arc} , is in V/cm and the arc current I_{arc} , is in A.

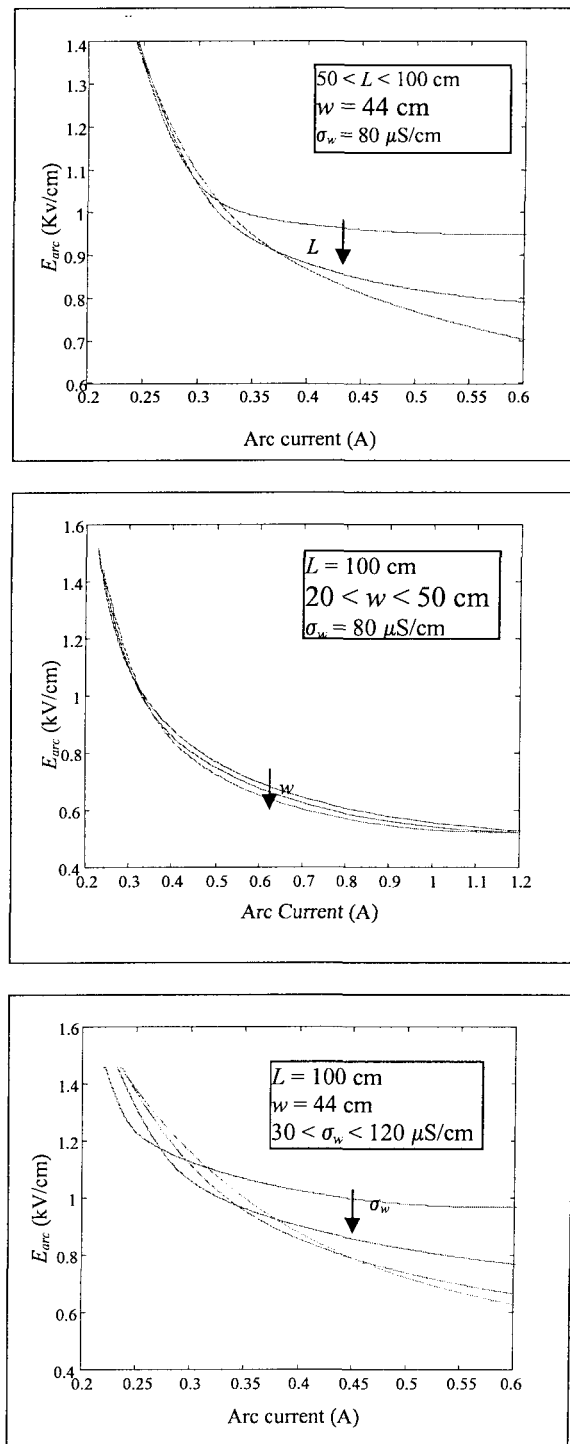


Figure 6.25 E - I arc characteristics for different simulation series.

6.5 Recapitulation of Main Points

The model presented in previous chapters was applied to the experimental results obtained previously. The heat-dissipation rate of the arc was considered to increase linearly as a function of an increase in applied voltage. In order to decrease the calculation error of the critical flashover voltage, an alternative relationship for calculating surface conductivity was found to be of greater reliability than the already established equation. The lower initial length of the arc results in lower critical voltages, thus the initial arc length was considered to be 45% of the total insulator length. A 30% variation in the propagation duration, Δt , has no significant effect on critical flashover calculation. The model predicts the critical voltage, in a satisfactory manner, for the range of the data tested. It also reflects, consistently, the effects of variation in the input test data of insulator length, applied water conductivity and ice width (or insulator diameter). Also, the arc current during the propagation stage was compared to that of the experiment, and the model was found to be adequate for predicting this current. The effects of variation on different test parameters, such as insulator length, ice width and applied water conductivity, during the arc propagation stage were also studied and discussed.

CHAPTER 7

CONCLUSIONS AND RECOMMENDATIONS

CHAPTER 7

CONCLUSIONS AND RECOMMENDATIONS

7.1 Concluding Remarks

One of the consequences of ice and snow accretion on power network equipment is a reduction in the electrical performance of high voltage insulators with the resulting power outages. The present study, carried out within the framework of CIGELE/INGIVRE at UQAC, aims at developing an AC self-consistent dynamic model with which to determine the temporal evolution throughout the propagation period of several significant parameters including current, velocity, and resistance of the arc. A number of experiments based on different insulator lengths and applied water conductivities were carried out in order to fine-tune different model parameters and to validate the performance of the model.

Visual observation of the experimental data led to formulating a hypothesis for a number of successive phenomena which lead to the flashover of ice-covered insulator surfaces. In this hypothesis, the calculation of flashover will be based on the concept that arc propagation takes place within a small fraction of time, that is to say, at the very instant when the applied voltage is close to its peak value. Thus, applied voltage during the

propagation period may be considered constant at its peak value. The initial value of the arc temperature is considered constant at 4550°K; the arc velocity is determined by a proportional factor of the arc current; and, arc resistance is calculated using the Mayr equation. The arc propagation will then take place if the arc elongation results in a higher current passing through the arc channel.

The minimum flashover voltages were obtained for two different types of insulators, involving 4 different lengths, each with three different applied water conductivities. The results obtained show that the flashover voltage decreases, the further the applied water conductivity increases. The flashover voltage per unit decreases with an increase in insulator length.

Based on experiments carried out for the specific test parameters under investigation:

- 1- The arc appears to remain stationary over a particular length before starting its propagating elongation. This length was measured and found to fall within 45-60% of the total length of the insulator independently of the initial air gap length.
- 2- The duration of the propagation period was considered to be 1.25 ms for various lengths and applied water conductivities. Flashover generally occurs when the applied voltage is in the vicinity of its peak value.
- 3- Time to flashover was measured and seems to be lower for higher applied water conductivities.

4- Due to the high speed of arc propagation, the camera speed of 1000 images per second was insufficient for measuring the arc speed with any precision during propagation.

5- An analysis of the flashover voltages obtained led to determining a particular value for the heat dissipation rate of the arc during its propagation stage under the experimental conditions tested. This value was calculated at 296.7 VA/cm for cylinders and post insulators.

As tested in the present study:-

6- The critical flashover voltage values predicted by the model respond in an inherently cohesive manner to the variation of the main affecting parameters such as applied water conductivity, insulator length and radius.

7- A higher freezing conductivity, shorter insulator length, or greater insulator diameter will each result in a lower critical flashover voltage.

8- The critical voltage per unit decreases with an increase in the insulator length. The effects of the variation in model parameters such as initial air temperature, initial arc length and propagation duration were studied and discussed.

9- The higher initial air temperatures and lower initial arc lengths each result in lower calculated critical voltages.

10- A 30% variation in propagation duration has no significant effect on the calculated critical voltage.

The critical flashover voltages obtained by the model were discussed and evaluated in the light of those obtained by other authors and an already existing static model.

Based on simulations and/or experimental results obtained during the pre-flashover stage, and when constant voltages per unit are applied:

- 11- Higher applied water conductivities and greater insulator diameters will result in higher maximum currents.
- 12- During this period, maximum current seems to remain unchanged for various insulator lengths when the applied water conductivity, ice width and applied voltage per unit are maintained constant.

Based on the simulation results alone, and in the range of the data tested, the following conclusions are valid for the propagation stage:-

- 13- Greater insulator lengths, greater insulator diameters and higher applied water conductivities result in higher arc currents which will subsequently result in higher arc velocities, lower arc resistances per unit and lastly, higher arc temperatures.
- 14- Even when the arc length extends to include the total insulator length, the arc temperature seems to be limited to values of less than 5000°K.
- 15- The arc velocity, at the end of its propagation, may attain several hundred metres per second.

16- During the propagation stage, when re-ignition is assumed to occur no longer, the arc gradient equation may be presented in the form of Ayrton's equation, for a certain range of arc currents.

7.2 Future Trends

The aim of this type of project is to establish an all-inclusive model capable of describing the entire process of surface ice formation, arc initiation and propagation, with its subsequent complete flashover of insulators. In this regard, future tendencies based on this project may include investigation and modeling of several different stages of the total phenomenon, such as ice accretion under applied voltage, water film formation and initiation of partial arcs and their transition to an established arc. Particular recommendations involving the present model may be listed as follows:

1- A primary recommendation might involve re-adjusting the model by carrying out several different series of experiments on real insulators of different lengths and diameters with a variety of applied water conductivities.

2- It is also proposed that arc temperatures be measured during the pre-flashover and propagation stages by means of appropriate equipment, and that the model results then be verified against experimental values.

3- It is also proposed that, by taking into account the different parameters involved in the ice-bulk heat transfer phenomenon, an analytical relationship be established in order to determine the temporal evolution of surface water conductivity and water film thickness during the pre-flashover stage. Such equations are of paramount importance in predicting the time-to-flashover from the moment that a white arc is established up to the instant of complete flashover. Such a study could then be used in order to determine the surface conductivity at the very moment of flashover.

4- It is also proposed that, during the pre-flashover stage, the above-mentioned equations be combined with the heat transfer equations of the arc, thereby leading to the creation of an analytical formula which would result in arc temperature calculations and to an analytical explanation for the values of maximum attainable arc lengths. The arc radius relationship as well as the re-ignition aspect would thus be covered.

5- It is also proposed that, in order to verify the values obtained from the model for arc velocity, the phenomenon be monitored using ultra-high-speed cameras filming at a rate of at least 6000 frames per second.

6- It is also proposed that, during the propagation stage, Δt , be measured using a sufficiently powerful test-set capable of delivering higher currents without the concurrent voltage drop.

7- It is also proposed that a specific study be carried out drawing a more exhaustive comparison between model and experimental results by taking the effects of source impedance into account in the model.

8- It is also proposed that a new model be created for describing arc properties as they arise during the arc propagating stage. Although the Mayr equation results in satisfactory values, it was first introduced to model arc behaviour in circuit breakers and may not therefore cover all aspects of surface flashover; also, the simplification of arc phenomena that Mayr assumed in order to establish his model (cf. Section 4.4.4), may render its application unsuitable for a propagating arc.

9- It is also proposed that heat dissipation rate, P_0 , be modified based on results from flashover tests under pollution, in order to make the model applicable to the polluted insulators. The initial arc length concept should then also be reformulated.

REFERENCES

REFERENCES

- [1] Al-Baghdadi A., "The Mechanism of Flashover on Polluted Insulators," *Thesis of Ph.D., University of Manchester, USA*, pp. 67, 1970.
- [2] Alm E., "Physical properties of Arcs in Circuit Breakers," *Trans. of the Royal Institute of Tech., Stockholm*, No. 25, p. 25, 1967.
- [3] Alston L. L. & Zoledziowski S., "Growth of discharges on polluted insulation," *Proc. of IEE*, Vol. 110, No. 7, pp. 1260-1266, July 1963.
- [4] Anjana S. & Lakshminarasimha C. S., "Computation of Flashover Voltages of Polluted Insulators Using Dynamic Arc Model," *Proc. of 6th Int. Sym. on High Voltage Eng., New Orleans, USA*, Paper No. 30.09, 1989.
- [5] Bejan A., *Heat Transfer*. John Wiley & Sons Inc., 1993.
- [6] Boehme E. W. & Obenaus F., "Pollution Flashover Tests on Insulators in the Laboratory and in Systems and the Model Concept of Creepage Path Flashover," *CIGRE*, No. 407, 1966.
- [7] Boehme E. W. & Weiner G. S., "Contamination of EHV Insulation-I, An Analytical Study," *IEEE Conf.*, Paper No. 1, pp. 66-481, 1964.
- [8] Boulos M. I., Fauchais P. & Pfender E., *Thermal Plasmas, Fundamental and Applications*. Vol. 1, New York, Plenum Press, 1994.
- [9] Boyer A. E. & Meale J. R., "Insulation Flashover under Icing Conditions on the Ontario-Hydro 500 kV Transmission Line System," *Proc. of CEA Spring Meeting, Montreal, Canada*, March 1988.
- [10] Brettschneider S., "Contribution à l'étude de l'apparition et du développement des décharges visibles à la surface de la glace," *Thesis of Ph.D. in Engineering, UQAC*, 2000.
- [11] Buchan P. G., "Electrical conductivity of insulator surface ices," *Ontario Hydro Research Division*, Report No. 89-31-k, 1989.
- [12] Cassie A. M., "Arc Rupture and Circuit Severity: A New Theory," *CIGRE Report*, No. 102, Paris, France, 1939.
- [13] Chaarani R., "Étude de l'influence des caractéristiques des isolateurs sur leurs performances électriques dans des conditions de givrage,"

Thesis of Ph.D. in Engineering, UQAC, 2003.

- [14] Charneski M. D., Gaibrois G. L. & Whitney B. F., "Flashover Tests on Artificially Iced Insulators," *IEEE Transactions on Power Apparatus & Systems*, Vol. PAS-101, No. 8, pp. 2429-2433, 1982.
- [15] Chaurasia D. C., "Scintillation Modelling for Insulator Strings Under Polluted Conditions," *High Voltage Eng. Sym., IEE Conf. Pub.*, No. 467, August 1999.
- [16] Chen X., Farzaneh M. & Zhang J., "Factors Influencing Flashover Characteristics along Ice Surfaces," *The Proc. of the 7th Int. Workshop on Atmospheric Icing of Structures, IWAIS, Chicoutimi, Canada*, pp. 77-81, June, 1996.
- [17] Chen X., "Modeling of Electrical Arc on Ice Surfaces," *Thesis of Ph.D. in Engineering, UQAC-École Polytechnique de Montréal*, 1999.
- [18] Cherney E. A., "Flashover Performance of Artificially Contaminated and Iced Long-rod Transmission Line Insulators," *IEEE Transactions on Power Apparatus and Systems*, Vol. PAS-99, No. 1, pp. 46-52, February 1980.
- [19] Chisholm W. A. *et al.*, "The Cold-Fog Test", *Proc. of IEEE/PES Winter Meeting, Baltimore, USA*, Paper No. 96 WM 099-2 PWRD, 1996.
- [20] CIGRE Task Force 33.04.09, "Influence of Ice and Snow on the Flashover Performance of outdoor insulators Part I: Effects of Ice," *ÉLECTRA*, No. 187, pp. 90-111, December 1999.
- [21] Claverie P. & Porcheron Y., "How to Choose Insulators for Polluted Areas," *IEEE Trans. on Power Apparatus and Systems*, Vol. PAS-92, No. 3, pp. 1121-1131, 1973.
- [22] Claverie P., "Predetermination of the Behavior of Polluted Insulators," *IEEE Transactions on Power Apparatus and Systems*, Vol. PAS-90, pp. 1902-1908, 1971.
- [23] Dhahbi-Megrache N., "Modélisation Dynamique des Décharges sur les Surfaces d'isolateurs Pollués sous Différentes Formes de Tension: Elaboration d'un Critère Analytique de Propagation," *Ph.D. Dissertation, Ecole Central de Lyon, France*, 1998.

- [24] Dhahbi-Megrache N. & Bérroual A., "Flashover Dynamic Model of Polluted Insulators under ac Voltage," *IEEE Trans. on Dielect. and Elec. Insul.*, Vol. 7 No. 2, pp 283-9, 2000.
- [25] Dorf R. C. & Bishop R. H., *Modern Control Systems*. 10th edition, Pearson, Prentice Hall, 2004.
- [26] Engel A. V., *Ionized Gases*. Oxford, 1965.
- [27] Farag A. S. & Cheng T. C., "Interfacial Breakdown on Contaminated Electrolytic Surfaces," *IEEE Elec. Ins. Conf.*, 1997.
- [28] Farzaneh-dehkordi J., "Experimental Study and Mathematical Modeling of Flashover of EHV Insulators Covered with Ice," Master Thesis in Engineering, UQAC, 2004.
- [29] Farzaneh M., Dallaire M. A. & Ben-Dallah M., "Essaie de tenue électrique en courant continue sur les isolateurs precontaminés et recouvert de glace," *Rapport pour Hydro Québec, Direction d'ingénierie de lignes*, Contrat No. H0924306, pp. 1-22, December 1986.
- [30] Farzaneh M. & Drapeau J. F., "AC Flashover Performance of Insulators Covered with Artificial Ice," *IEEE Trans. on Power Delivery*, Vol. 10, No 2, pp 1038-1051, April 1995.
- [31] Farzaneh M., Drapeau J.-F., Tavakoli C. & Roy M., "Laboratory Investigations and Methods for Evaluating the Flashover Performance of Outdoor Insulators on a Large Scale," *The Proc. of the 10th International Workshop on Atmospheric Icing of Structures, IWAIS 2002, Brno, Czech Republic*, pp. 6-9, June 17-20, 2002.
- [32] Farzaneh M., "Effect of Ice Thickness and Voltage Polarity on the Flashover Voltage on Ice Covered High Voltage Insulators," *Proc. of 7th Int. Symp. on High Voltage Eng., Dresden, Germany*, Vol. 4, Paper No. 43.10, pp.203-206, 1991.
- [33] Farzaneh M. *et al.*, "Electrical Performance of Ice-Covered Insulators at High Altitudes," *IEEE Tran. on Dielect. and Ele. Ins.*, Vol. 11, No. 5, pp. 870-880, Octobre 2004.
- [34] Farzaneh M. *et al.*, "Selection of Station Insulators with Respect to Ice or Snow - Part I: Technical Context and Environmental Exposure," *A Position Paper prepared by the IEEE TF on icing performance of station insulators, IEEE Transactions on Power Delivery*, ref. TPWRD-

00110-2004.

- [35] Farzaneh M. *et al.*, "Selection of Station Insulators with Respect to Ice or Snow - Part II: Methods of Selection and Options for Mitigation," *A Position Paper prepared by the IEEE TF on icing performance of station insulators, IEEE Transactions on Power Delivery*, ref. TPWRD-00111-2004.
- [36] Farzaneh M., Farzaneh-dehkordi J. & Zhang J., "Flashover Performance of EHV Station Post Insulators Covered with Ice," *IEEE Conference on Electrical Insulation and Dielectric Phenomena, 2004 Annual Report Boulder, Colorado, USA*, pp. 37-40, October 2004.
- [37] Farzaneh M., Fofana I. & Hemmatjou H., "Electrical Properties of Snow," *IEEE Conference on Electrical Insulation and Dielectric Phenomena, 2004 Annual Report, Boulder, Colorado, USA*, pp. 611-614, October 2004.
- [38] Farzaneh M., Fofana I., Tavakoli C. & Bérroual A., "A Mathematical Model of Arc Development on Ice Surfaces under DC Voltage," *Proc. of IASTED Int. Conf. on Power and Energy Systems, Rhodes, Greece*, Paper No. 337-070, July 2001.
- [39] Farzaneh M., Fofana I., Tavakoli C. & Chen X. "Dynamic Modeling of DC Arc Discharge on Ice Surfaces," *IEEE Trans. on Diel. and Elec. Ins.*, Vol. 10, No. 3, pp. 463-474, 2003.
- [40] Farzaneh M., "Ice Accretions on High-Voltage Conductors and Insulators and related phenomena", *Phil. Trans. of the Royal Society*, Vol. 358, No. 1776, pp. 297-3005, November 2000.
- [41] Farzaneh M., Kiernicki J., Chaarani R., Drapeau J. F. & Martin R., "Influence of Wet-grown Ice on the AC Flashover Performance of Ice Covered Insulators," *Proc. of 9th Int. Symp. on High Voltage Eng., Austria*, Paper No. 3176, pp.1-4, 1995.
- [42] Farzaneh M., Kiernicki J. & Dallaire M. A., "AC and DC Flashover Performance of Ice-covered Insulators during a De-icing Period," *Proc. of 5th Int. Workshop on the Atmospheric Icing of Structures, Tokyo, Japan*, Paper No. B-48, pp. 1-4, 1990.
- [43] Farzaneh M., Kiernicki J. & Drapeau J. F., "Ice accretion on energized line insulators," *Int. Offshore and Polar Eng. Conf.*, Vol. 2, No. 3, Montreal, pp. 228-233, 1992.

- [44] Farzaneh M. & Kiernicki J., "Flashover Performance of ice-covered Insulators," *Canadian Journal of Elec. and Computer Eng.*, Vol. 22, No. 3, pp. 95 - 109, July 1997.
- [45] Farzaneh M. & Kiernicki J., "Flashover Performance of IEEE Standard Insulators under Ice Conditions," *IEEE Trans. on Power Delivery*, Vol. 12, No. 4, pp. 1602-1613, October 1997.
- [46] Farzaneh M. & Kiernicki J., "Flashover Problems Caused by Ice Build-up on Insulators," *IEEE Trans. on Elec. Ins.*, Vol. EI-11, No. 2, pp. 5-17, 1995.
- [47] Farzaneh M. & Zhang J., "Behavior of DC Arc Discharge on Ice Surfaces," *Proc. of 8th Int. Workshop on the Atmospheric Icing of Structures, Iceland*, pp. 193-197, 1998.
- [48] Farzaneh M., Zhang J., Chararani R. & Fikke S. M., "Critical Conditions of AC arc propagation on Ice surfaces," *Conf. Record of the 2000 IEEE, Int. Symp. On Electrical Insulation, Anaheim, CA, USA*, pp.p211-215, April 2000.
- [49] Farzaneh M., Zhang J. & Chen X., "A laboratory study of leakage current and surface conductivity of ice samples," *Proc. Conf. on Elec. Ins. and dielec. Phenomena, Arlington, USA*, Article 9456-1, pp. 631-638, 8A-1, Oct. 1994.
- [50] Farzaneh M., Zhang J. & Chen X., "DC characteristics of Local Arc on Ice Surface," *Atmospheric Research*, Vol. 46, pp.49-56, 1998.
- [51] Farzaneh M., Zhang J. & Chen X., "Modeling of the AC Arc Discharge on Ice Surfaces," *IEEE Trans. on Power Delivery*, Vol. 12, No. 1, pp.325-338, 1997.
- [52] Farzaneh M. & Zhang J., "Modeling of DC Arc Discharge on Ice Surfaces," *IEE Proc. Generation, Transmission and Distribution*, Vol. 147, No. 2, pp. 81-86, 2000.
- [53] Fikke S. M., Hanssen J. E. & Rolfseng L., "Long Range Transported Pollution and Conductivity on Atmospheric Ice on Insulators," *IEEE Trans. on Power Delivery*, Vol. 8, No. 3, pp. 13411-1321, July 1993.
- [54] Fikke S. M., "Possible Effects of Contaminated Ice on Insulator Strength," *Proc. of 5th Int. Workshop on the Atmospheric Icing of Structures, Tokyo, Japan*, Paper No. B4-2-(1), 1990.

- [55] Finkelnburg W. & Maecker H., "Electric arcs and thermal plasmas," *Encyclopedia of Physics, Berlin: Springer*, Vol. XXII, 1956.
- [56] Fofana I. & Bérroual A., "A predictive model of the positive discharge in long air gaps under pure and oscillating impulse shapes," *J. Phys. D: Appl. Phys.*, Vol. 30, 1653-67, 1997.
- [57] Fofana I. & Bérroual A., "Predischage Models of Dielectric Liquids," *Jn. J. of Appl. Phys*, 37 (5A), Part 1, 2540-47, 1998.
- [58] Fofana I., Farzaneh M., Tavakoli C. & Bérroual A., "Dynamic modeling of flashover process on Insulator under Atmospheric Icing conditions," *Proc. of IEEE Conf. on Elec. Ins. and Dielec. Phenomena, Kitchener, Canada*, pp. 605-608, October 2001.
- [59] Fofana I., Farzaneh M & Tavakoli C., "Dynamic Modelling of DC Arc on Polluted Insulators," *12th Int. Symp. on High Voltage Engineering, Bangalore, India*, paper 5-41, Vol. 3, pp. 747-750, August 2001.
- [60] Fofana I., Farzaneh M. & Tavakoli C., "Modelling Arc Propagation Velocity on Ice-covered Surfaces," *Proc. of 10th Int. Workshop on Atmospheric Icing of Structures, Brno, Czech Republic*, pp. 1-6, June 2002.
- [61] Forest J. S., "The Performance of High Voltage Insulators in Polluted Atmospheres," *Proc. of IEEE Winter Meeting, New York*, 1969.
- [62] Francis V. J., *Fundamentals of Discharge Tube Circuits*. Methuen, London, 1948.
- [63] Gallimberti I. & Marchesi G., "Streamer corona at an insulator surface," *The 7th Int. Symp. On High Voltage Eng., Dresden, Germany*, paper 41.10, August 1991.
- [64] Ghosh P. S. & Chatterjee N., "Arc Propagation over Electrolytic Surfaces under Power Frequency Voltage," *IEEE Trans. on Dielec. and Elec. Ins.*, Vol. 3, No. 4, pp. 529-536, 1996.
- [65] Goia L. M. & Balan G., "Romanian Experience Regarding Operational Behavior of HV Oils," *Proc. 7th Int. Workshop of atmospheric Icing of Structures, Chicoutimi*, pp. 216-221, 1996.
- [66] Goldenberg H., "Approximate solution of a non-linear differential equation giving the temperature distribution in the positive column of a

- static arc," *Br. J. Appl. Phys.*, 10 No 1 47-51, January 1959.
- [67] Gopal H. G., Kumar U. & Nagbhusan G. R., "Parametric Analysis of Various Scintillation Models Used in Pollution Flashover Studies Using PSPICE," *Proc. Of the National Seminar on EHV Transmission Line Insulation held at REC Calicut*, 12-13 Dec. 1995.
- [68] Gopal S. & Rao Y. N., "On the Flashover Mechanism of Polluted Insulators," *ISPPISD, IIT, Madras*, 1983.
- [69] Guerrero T., "Étude expérimentale du contournement des isolateurs recouverts de glace sous tension impulsionnelle," maîtrise en ingénierie, UQAC, 2004.
- [70] Hampton B. F., "Flashover Mechanism of Polluted Insulation," *Proc. of IEE*, Vol. 11, No. 5, pp. 985-990, 1964.
- [71] Hara M. & Phan C. L., "Leakage Current and Flashover Performance of Iced Insulators," *IEEE Trans. on PAS*, Vol. PAS-98, No. 3, pp. 849-859, 1979.
- [72] Hara M. & Phan C. L., "A Study of the Leakage Current of H.V. Insulators under glaze and rime," *Can. Elec. Eng., J.*, Vol. 3, pp. 15-22, 1978.
- [73] Hesketh S., "General Criterion for the Prediction of Pollution Flashover," *Proc. of IEE*, Vol. 114, No. 4, pp. 531-532, 1967.
- [73] Holtzhausen J. P., "Application of a Re-ignition Pollution Flashover Model to Cap and Pin Insulator Strings," *Proc. Of the IASTED Int. Conf., POWER AND ENERGY SYSTEMS, Rhodes, Greece*, July 2001.
- [75] Hoyaux M. F., *Arc Physics*. Springer-Verlag, New York Inc., 1968.
- [76] Hydro-Québec, "Analysis of the Hydro-Québec System Blackout on April 1988," *Official Hydro-Québec Report, Montreal*, July 1988.
- [77] Hydro-Québec Committee of Experts, "January 1998 ice storm," *Report for Hydro-Québec*, 1998.
- [78] Imai I. & Ichiro, "Studies on Ice Accretion," *Researches on Snow and Ice*, No. 1, pp.35-44, 1953.

- [79] International Electrotechnical Commission (IEC), "Artificial Pollution Tests on High-voltage Insulators to be Used on AC Systems," International Standard 60507, 1991.
- [80] Ishii M. & Ohashi H., "Polarity effect in DC withstand voltages of contaminated surfaces," *IEEE Trans. on Elec. Insul.*, Vol. 23, No. 6, 1988.
- [81] Jolly D. C., "Contamination Flashover, Part I: Theoretical Aspects," *IEEE Trans.*, PAS-91, pp. 2437-2442, 1972.
- [82] Jolly D. C., Cheng T. C. & Otten D. M., "Dynamic Theory of Discharge Growth over Contaminated Insulator Surfaces," *IEEE PES Winter Power Meeting, New York, USA*, Paper, No. C74 068-3, 1974.
- [83] Kannus K., Lahti K. & Nousiainen K., "Comparisons between Experiments and Calculations of the Electrical Behavior of Ice-Covered High Voltage Insulators," *Proc. of 8th Int. Workshop on Atmospheric Icing of Structures, Iceland*, pp. 325-331, 1998.
- [84] Kannus K., "Aspect of the electrical performance of the high voltage insulator and metal Oxide surge arresters under various environmental stresses," *Tampere University of Technology, Publications 229*, 1998.
- [85] Karady G. G., Amrah F. & Sundararajan R., "Dynamic Modeling of AC Insulator Flashover Characteristics," *IEE High Voltage Eng. Symp.*, Conf. Pub. No. 467, 1999.
- [86] Kawai M., "AC Flashover Tests at Project UHV on ice-covered Insulators," *IEEE Transactions on Power Apparatus & Systems*, Vol. PAS-89, No. 8, pp. 1800-1805, Dec. 1970.
- [87] Khalifa M. M. & Morris R. M., "Performance of Line Insulators under Rime Ice," *IEEE Trans. on Power Application and Systems*, Vol. PAS-86, pp. 692-698, 1967.
- [88] Kuffel E. & Abdullah M., *High Voltage Engineering*. Pergamon Press, 1970.
- [89] Kuroiwa D., "Icing and Snow Accretion," *Monograph Series of Research, Institute of Applied Electricity, Japan*, pp. 1-30, 1958.
- [90] Larcombe P. J., Kunda W., Poots G. & Elliott J. W., "Accretion and shedding of ice on cables incorporating frees streamline theory and the joule effect," *Proc. 3rd Int. Workshop of atmospheric Icing of Structures*,

- Vancouver, pp. 389-395, 1991.
- [91] Les Renardières Group, "Double Impulse Tests of Long Air Gaps," *IEE Proc.*, vol. 133, pt. A, no. 7, pp. 395–483, October 1986.
- [92] Li Y., "Étude de l'influence de l'altitude sur les caractéristiques de l'arc électrique à la surface de glace polluée," *Thesis of Ph.D. in Engineering, UQAC*, 2002.
- [93] Li Y., Farzaneh M. & Zhang J., "Effects of Voltage Type and Polarity on Flashover Performances at Low Atmospheric Pressure on an Ice Surface," *Proc. of 8th Int. Offshore and Polar Eng. Conf., Montreal, Canada*, pp. 543-546, 1998.
- [94] Loeb L. B. & Meek J. M., "Mechanism of the Electric Spark," *Stanford University Press, California*, 1941.
- [95] Lowke J. J., Zollweg R. J. & Liebermann R. W., "Theoretical description of arcs in mercury and argon," *J. Phys. D: Appl. Phys.*, Vol. 46, No. 2, 1975.
- [96] Maecker H., "Über die Charakteristiken Zylindrischer Bögen," *Zeitschrift für Physik*, Vol. 157, pp. 1-29, 1959.
- [97] Maikopar A. S., "The Open Small Current Arc," *Elektrichestvo*, No. 2, pp. 22-25, 1965.
- [98] Matsuda H., Komuro H. & Takasu K., "Withstand Voltage Characteristics of Insulator String Covered with Snow and Ice," *IEEE Trans. on Power Delivery*, Vol. 6, No. 3, pp. 1243-1250, July 1991.
- [99] Mayr O., "Beitrag zur Theorie der Statischen und der Dynamischen Lichtbogens," *Archiv für Elektrotechnik*, Vol. 37, pp. 588-608, 1943.
- [100] Meek J. M. & Craggs J. D., *Electrical breakdown of gases*. John Wiley and Sons, New York, 1978.
- [101] Meier A. & Niggli W. M., "The Influence of Snow and Ice Deposits on Supertension Transmission Line Insulator Strings with Special Reference to High Altitude Operation," *IEEE Conference Publ.44, London, England*, pp. 386-395, Sept. 1968.
- [102] Mekhaldi A., Namane D., Bouazabia S. & Bérroual A., "Flashover of Discontinuous Pollution Layer on HV Insulators," *IEEE Trans. On Dielect.*

And Elec. Ins., Vol. 6, No. 6, 1999.

- [103] Melo O. T., Tam Y. T. & Farzaneh M., "Freezing Rain and Fog Events in Southern Ontario: Properties and Effect on EHV Transmission Systems," *Proc. of 4th Int. Workshop on Atmospheric Icing of Structures, Paris, France*, pp. 70-75, 1988.
- [104] Meteorological Service of Canada, "Ice Storm 98," *Report on Ice Storm '98*, 1998.
- [105] Näcke H., "Lichtbogenfestigkeit und Kriechstromfestigkeit von Isolierstoffen," *Dissertation, University of Berlin-Chalottenburg*, 1962.
- [106] Näcke H., "Stabilität der Fremdschichtentladungen und Theorie des Fremdschichtüberschlags," *ETZ-A*, No. 16, pp. 577-585, 1966.
- [107] Nasser E., "Contamination Flashover of Outdoor Insulation," *ETZ-A*, Vol. 93, No. 6, pp. 321-325, 1972.
- [108] Nasser E., *Fundamentals of Gaseous Ionization and Plasma Electronics*. Wiley-Interscience, New York, 1971.
- [109] Neumärker G., "Verschmutzungszustand und Kriechweg," *Monatsber. D. Deut. Akad. Wiss., Berlin*, Vol. 1, pp. 352-359, 1959.
- [110] Obenaus F., "Die Überslagspannung verschmutzter Isolatoren," *ETZ*, 56, 369, 1935.
- [111] Obenaus F., "Fremdschichtüberschlag und Kriechweglänge," *Deutsche Elektrotechnik*, Vol. 4, pp. 135-136, 1958.
- [112] Obenaus F., "The Influence of surface Coating (Dew, Fog, Salt, and Dirt) on the Flashover Voltage of Insulators," *Hescho-Mitt.*, Vol. 70, pp. 1-37, 1933.
- [113] Oguchi H. *et al.*, "Icing on Electric Wires," *Researches on Snow and Ice*, No. 1, pp.45-49, 1953.
- [114] Ortega P. *et al.*, "Performance of a 16.7 m air rod-plane gap under a negative switching impulse," *J. Phys. D: Appl. Phys.*, Vol. 27, pp. 2379-2387, 1994.
- [115] Pavlov M., Djurović S. & Kobilarov R., "Temperature Measurement of the Arc Phase of a Spark in Air," *J. Phys. D: Appl. Phys.*, Vol. 19, pp.

- 1041-1046, 1986.
- [116] Phan C. L. & Matsuo H., "Minimum Flashover Voltage of Iced Insulators," *IEEE Trans. on Electrical Insulation*, Vol. EI-18-6, pp. 605-618, 1983.
- [117] Raether M., *Electron Avalanches and Breakdown in Gases*. Butterworths, 1964.
- [118] Rahal A. M. & Huraux C., "Flashover Mechanism of High Voltage Insulators," *IEEE Trans. on Power Apparatus and Sys.*, Vol. PAS-98, No. 6 pp. 2223-2231, 1979.
- [119] Raizer Yu. P., *Gas Discharge Physics*. Springer, 1991.
- [120] Renardières Group, "Positive discharge in long air gaps at les Renardières," *Electra* No. 53, pp. 31-153, 1977.
- [121] Rizk A. M., "Analysis of Dielectric recovery with Reference to Dry-zone Arc on Polluted Insulators," *IEEE Conf. Paper, PWR, Winter Power Meeting, New York*, No. 71, C 134 1971.
- [122] Rizk A. M., "Mathematical Models for Pollution Flashover," *Electra*, Vol. 78, pp. 71-103, 1981.
- [123] Rizk A. M. & Nguyen D. H., "Digital Simulation of Source-Insulator Interaction in HVDC Pollution Tests," *IEEE Trans. On Pow. Del.*, Vol. 3, No. 1, 1988.
- [124] Roshanfekar M., "Stress Analysis of an Optical Ground Wire," *McGill University, Collaboration CIGELE-McGill*, 1999.
- [125] Sato M., Saito H., Kaga A. & Akagami H., "Fundamental Characteristics of AC Flashover on Contaminated Insulators Covered with Ice," *Japanese Journal of Applied Physics*, Vol. 28, No. 5, pp. 889-896, 1989.
- [126] Schneider H. M., "Artificial Ice Tests on Transmission Line Insulators-A Progress Report," *Proceedings of IEEE/PES Summer Meeting, San Francisco, USA*, Paper No. A75-491-1, pp. 347-353, 1975.
- [127] Singh R. R. P. & Sinha J. N., "Simulation Studies on Pollution Performance of Insulators," *Journal of the Institution of the Engineers part I, EL*, 4, Vol. 75, pp. 26-34, 1994.

- [128] Su F. & Jia Y., "Icing on Insulator String of HV Transmission Lines and Its Harmfulness," *Proc. of 3rd Int. Offshore and Polar Eng. Conf., Singapore*, pp.655-658, 1993.
- [129] Sugawara N. *et al.*, "Insulation Resistance of Transmission Line Insulators Depending on the Accretion of Ice," *Proc. of 5th Int. Workshop on Atmospheric Icing of Structures, Tokyo, Japan*, Paper No. B4-9, pp. 1-6, 1990.
- [130] Suits C. G. & Hocker J. P., "Application of heat transfer data to arc characteristics," *American Physical Society, Phys., Rev.* 55, pp. 1184-1191 1939.
- [131] Sundararajan R. & Gorur R. S., "Dynamic Arc Modeling of Pollution Flashover of Insulators under DC Voltage," *IEEE Trans. on Elec. Insul.*, Vol. 28, No. 2, 1993.
- [132] Swanson B. W., Rodit R. M. & Browne T. E., Jr. *Electrotech, Z.*, 93, pp. 375, 1972.
- [133] Swift D. A., "Flashover of Polluted Insulators: Electric Field in the Arc," *6th Int. Sym. of High Voltage Eng., New Orleans*, Paper No. 30.10, Sep 1989.
- [134] Tominiga A., "Characteristics of Power-frequency flashover on contaminated surfaces in fog," *Elec. Eng. in Japan*, Vol. 8, No 12, pp. 53-59, 1968.
- [135] Topalis F., Leontides N. & Stathopoulos I. A., "Investigation of the dielectric behavior of non-uniformly polluted insulators," *Proc. of Int. Conf. on Gas Discharges and their Applications*, Vol. 2, pp. 564-567, Swansea, September 1992
- [136] Tseng K.J. & Wang Y., "A dynamic electric arc model for electronic circuit simulation," *IEE Electronics Letters*, Vol.32, No.8, Apr 1996, pp.705-707.
- [137] Verma M. P., "Insulation Performance of DC Apparatus-housing under Pollution," *ETZ-Archive*, Vol. 5, No. 9, 1983.
- [138] Volat C., "Calcul de la distribution du potentiel du champ électrique le long des surfaces de glace recouvrant les isolateurs haute-tension et dans les intervalles d'air entre celles-ci," *Thesis of Ph.D. in Engineering, UQAC*, 2002.

- [139] Watanabe Y., "Flashover Tests of Insulators Covered with Ice or Snow," *IEEE Trans.*, Vol. PAS-97, No. 5, pp. 1788-1794, 1978.
- [140] Wareing J. B. & Bracey R. H., "Failure mechanisms in wood poles under severe conductor ice loading," *In Proc. 8th Int. Workshop of atmospheric Icing of Structures, Reykjavik*, pp. 35-41, June 1998.
- [141] Wilkins R. & Al-Baghdadi A. A. J., "Arc Propagation along an Electrolyte surface," *Proc. of IEE*, Vol. 118, No. 12, pp. 1886-1892, 1971.
- [142] Wilkins R., "Flashover Voltage of High Voltage Insulators with Uniform Surface Pollution Films," *Proc. of IEE*, Vol. 116, No. 3, pp. 457-465, 1969.
- [143] Woodson H. H. & McElroy A. J., "Insulators with Contaminated Surfaces Part II: Modeling of Discharge mechanisms," *IEEE Trans.*, Vol. PAS-89, No. 8, pp. 1858-1867, 1970.
- [144] Wu C. T. & Cheng T. C., "Formation Mechanisms of Clean Zones during the Surface Flashover of Contaminated Insulators," *IEEE Trans. on Electrical Insulation*, Vol. EI-13, No. 3, pp. 149-156, June 1978.
- [145] Zarudi M. Y., *Izv. Sibirs. Iodel, AN USSR, Seriya Tekhnich. Nauke*, No. 3, 1967.
- [146] Zhang J. & Farzaneh M., "Computation of AC Critical Flashover Voltage of Insulators Covered with Ice," *Proc. of 1998 Int. Conf. on Power System Technology, Beijing, China*, Vol. 1, pp. 524-528, August, 1998.
- [147] Zhang J. & Farzaneh M., "Propagation of AC and DC Arcs on Ice Surfaces," *IEEE Trans. on Dielectrics and Electrical Ins.*, Vol. 7, No. 2, pp. 269-276, 2000.
- [148] Zhang J. & Farzaneh M., "Propagation of DC Arc on Ice Surfaces," *Proc. of 8th Int. Offshore and Polar Eng. Conf., Montreal, Canada*, pp. 547-550, 1998.
- [149] Zhang J., Guerrero T. & Farzaneh M., "Experimental Study on the Flashover Performance of Ice-covered Insulators under Impulse Voltage Ice," *IEEE Conference on Electrical Insulation and Dielectric Phenomena*, 2004 Annual Report, Boulder, Colorado, USA, pp. 635-638, October 2004.

- [150] Zhicheng G. & Renyu Z., "Calculation of dc and ac Flashover Voltage of polluted Insulators," *IEEE Trans. On Electrical Insulation*, Vol. 25, No. 4, August 1990.